NF-1583.03

NONPROPRIETARY VERSION

METHODS OF PRESTO-B

A THREE-DIMENSIONAL, LWR CORE SIMULATION CODE

TOPICAL REPORT

FEBRUARY 1983

CP&L

Carolina Power & Light Company

METHODS OF PRESTO-B
A THREE-DIMENSIONAL, BWR CORE SIMULATION CODE

S. Børresen
L. Moberg
J. Rasmussen*

* Institute for Energy Technology, Kjeller, Norway

NONPROPRIETARY VERSION

TOPICAL REPORT

Prepared by

SCANDPOWER INC

4853 Cordell Avenue
Bethesda, Maryland 20014

20 January 1983

Reviewed by :

A.L. Wallace

Approved by :

T.O. Sauar
Assistant Director

DISCLAIMER OF RESPONSIBILITY

This document was prepared by SCANDPOWER Incorporated on behalf of Carolina Power & Light Company. This document is believed to be completely true and accurate to the best of our knowledge and information. It is authorized for use specifically by Carolina Power & Light Company, SCANDPOWER Incorporated, and/or the appropriate subdivisions within the Nuclear Regulatory Commission only.

With regard to any unauthorized use whatsoever, Carolina Power & Light Company, SCANDPOWER Incorporated, and their officers, directors, agents, and employees assume no liability nor make any warranty or representation with regard to the contents of this document or its accuracy or completeness.

Proprietary information of SCANDPOWER Incorporated is indicated by "bars" drawn in the margin of the text of this report.

ABSTRACT

This report describes the methods of the PRESTO-B computer code and the basis for confidence provided by comparison with measured data and higher order methods. PRESTO-B is a three-dimensional BWR nodal core simulator, describing the coupled neutronic and thermal-hydraulic phenomena under specified operating conditions. The code can be used for detailed core analysis, fuel management, reload design, operations support, or generation of safety-related core parameters.

VOLUME 2

METHODS OF PRESTO-B, A THREE-DIMENSIONAL BWR CORE SIMULATION CODE

C O N T E N T S

Page

1. INTRODUCTION

This report describes the methods of PRESTO-B and provides documentation on its basic and general verification. It has been prepared for Carolina Power & Light Company, in support of their submittal to the US NRC to establish reload design capability for the Brunswick steam electric plants, Units 1 and 2. A detailed evaluation of the code performance for the specific plants considered is given in a supplementary report.

The code was developed by Scandpower A/S (ScP), in cooperation with the Institute for Energy Technology (I.F.E), Kjeller, Norway. PRESTO-B is intended for application by BWR Utilites in performing various core analysis tasks, including :

- Multicycle Fuel Management Analysis
- Reload Core Design Analysis
- Core-Follow Calculation
- Current Cycle Operations Support Calculations.

PRESTO-B is part of the ScP Fuel Management System (FMS) code package, and is usually run with lattice data generated with the code RECORD. RECORD is described in a report complimentary to this report. PRESTO-B has also been successfully run with lattice data generated by codes other than RECORD (e.g., CASMO). The code is written in FORTRAN IV and has been implemented on the following computers :

CDC - CYBER 74, 175, 176, 170

CDC - 7600

IBM - 370

UNIVAC - 1110

NCR - 8450

2. SUMMARY OF MODELING AND CODE PERFORMANCE

PRESTO-B is a three-dimensional BWR core simulator with integrated neutronics and thermal-hydraulics models. The neutronics model of PRESTO is based on an approximation of two-group diffusion theory, utilizing a special coarse mesh prescription originally developed for this code (Ref. 1). The thermal-hydraulics model is a steady-state version of the hydrodynamics model developed for the RAMONA codes (Ref. 2).

The BWR core is modeled as a three-dimensional array of near cubical nodes, each having homogenized internal properties. The nodal structure coincides with the fuel assembly array, horizontally, and with an axial subdivision giving approximate cubical shape.

The neutronic properties of a node are described by a set of conventional, two-group, homogenized macroscopic cross-section data, represented as polynomials in fuel exposure, exposure-weighted void and instantaneous void. The thermal-hydraulic properties are described by geometric data such as in-channel flow area, hydraulic diameter, etc. Hydraulic throttling is described by pressure loss coefficients.

Simulation of the reactor operation may include the following reactor conditions :

- cold subcritical
- cold critical
- hot, zero power critical
- hot, operating steady-state
- hot, operating - transient Xenon
- hot, operating - fuel burnup increment

The following special calculational modes are also available :

- Haling burnup calculation
- Criticality search calculation on flow or power

- One stuck-rod shutdown margin calculation
- Reflector albedo generation

Each reactor state point is specified by giving the following data as input :

- total thermal power
- total coolant flow rate
- core inlet subcooling (or feedwater enthalpy)
- control rod insertion pattern

Consistent, three-dimensional distributions of power and steam void are then determined by iteration between the neutronics and the thermal-hydraulics models. Efficient numerical solution methods are employed to ensure fast calculation. The following local effects are accounted for in calculating the nodal power distribution :

- instantaneous void (hydraulics feedback)
- fuel exposure
- exposure-weighted void
- control rod insertion
- equilibrium or transient Xenon concentration
- Samarium concentration
- fuel temperature (Doppler)
- control rod history
- control rod depletion

The following simulated core performance data are derived on the basis of the calculated distributions :

- Evaluation of margins to various thermal limits (Maximum Linear Heat Generation Rate, Fraction of Limiting Power Density, Fraction of Average Planar Power with respect to Emergency Core Cooling Design Limits, Minimum Critical Heat Flux Ratios, and various power peaking factors.

- Predicted in-core detector readings (LPRM and TIP)

The code may determine the development of the reactor power level with time in a Xe-transient period, or determine the total coolant flow rate required to keep the power level constant during the period. Local power ramp rates are also evaluated under simulated operating transients.

Cycle length estimates for a complete reactor cycle, or for remaining parts of a current cycle, may be performed.

Fuel assemblies are individually labeled, allowing easy simulation of core reloading, including options for

- insertion of new fuel
- fuel shuffling
- reinsertion of fuel from an earlier operating period
- discharge of spent fuel to a simulated fuel storage

An extensive evaluation program has been carried out to verify the code, both against reference calculations and against special data, such as BWR gamma scan data and measured void loop data. In addition, the accumulated experience gained in application of the code since 1971 has yielded a large number of comparisons with reactor data, such as TIP traces, comparisons with other codes, and with process computer results.

The special diffusion theory approximation of PRESTO has been independently evaluated by comparison with fine mesh diffusion theory benchmarks (Ref. 3). In summary, the following results were obtained :

Case	Eigenvalue % Diff.	Bundle Power STD Dev. (%)
2-D	0.28	0.63
3-D	0.33	0.65

The thermal-hydraulics model of PRESTO-B has been verified against the FRIGG void loop data (Ref. 4). The standard deviation (RMS) in per cent void between calculated and measured voids was 2.1%, which is almost

within the experimental uncertainty of 2.0%. The detailed results of the benchmark calculations are presented in Chapter 11.

Gamma scan data, measured following EOC-1 of the Edwin I. Hatch BWR (Ref. 12), has been used to qualify the combined thermal-hydraulics and neutronics core models of PRESTO.

Comparisons between calculated and measured La-140 distributions were performed for :

- Bundlewise axial distributions
- Bundlewise average (radial) distributions
- Pin-wise axial distributions
- Bundles adjacent to partially inserted control rods
- Bundles in the core boundary versus those in the interior of the core

The total standard deviation between calculated and measured nodal La-140 distributions was 6.4 per cent.

The total standard deviation in the bundlewise comparison was 2.5 per cent.

An overview of the results, showing plots of the bundlewise axial distributions for all bundles in a complete core octant, is presented in Section 11.3.

In general, very good agreement was obtained between calculated and measured La-140 distributions. This demonstrates the accuracy in results of the coupled neutronics and thermal hydraulics models of PRESTO.

3. CORE DESCRIPTION

A BWR core is made up of a number of fuel assemblies arranged in a regular lattice grid. The fuel assembly array constitutes a physical subdivision of the core, which is maintained in the simulator model. Each assembly is further subdivided axially, usually 24 or 25 axial segments. The geometrically identical unit cells thus obtained are called nodes. The water-gaps associated with each fuel assembly are included in the node.

The main nodal variables (such as power density, void fraction, etc.) calculated by PRESTO, represent average values within the node.

3.1 Core Geometry

The geometric shape of the core is described in a Cartesian coordinate system with integer coordinate values (I, J, K), as shown in Figure 3.1.

The I, J coordinates for the nodes along the core periphery are given as input, thus defining the core shape. Each fuel assembly location is identified by its coordinates or, equivalently, by a channel number.

The core model may describe the entire, physical core, or a fraction of the core, depending on core symmetry assumption. 1/8, 1/4 or 1/2-core models may be represented, in addition to the full core representation. Various symmetry options based on either rotational or reflective symmetry are available.

The physical size of the core is determined by the nodal dimensions specified in input, together with the definition of the core periphery and number of axial nodes.

3.2 Fuel Designation

Fuel assembly images are "loaded" into the core by specifying the fuel assembly identification number corresponding to each channel.

The fuel assembly identifications are 5 or 6-digit integer numbers, iijkkk, where :

ii = fuel type designation

j = identifier for fuel batch number or core quadrant

kkk = identifier for individual assemblies

Data characterizing the state of the fuel (i.e., exposure, exposure-weighted void and other nodal arrays) are stored on a data file maintained by PRESTO. The data are labeled by the associated fuel assembly number, thus allowing complete freedom for simulation of fuel shuffling, discharge and reinsertion. Core reload simulation simply consists of redefining the relationship between core location and fuel assembly identification.

3.3 Nuclear Data Assignment

A nuclear data library, consisting of precalculated group constants and other data characteristic for each type of fuel design is made available to PRESTO on an input data file (so-called POLGEN file). Each unique data set on the file is identified by a nuclear parameter set number.

The correspondence between the nuclear data sets and fuel assembly types is established by input data relating fuel type identification to nuclear parameter set number. In the case of fuel designs with axially zoned burnable poison or axially varying enrichment, each axial zone is related to a specific nuclear parameter set.

3.4 Control Rod Designation

Control rods are labeled by individual identification numbers and with the locations specified through the input data.

For BWR cruciform rods, each rod usually controls the four surrounding assemblies.

The model allows shuffling and replacement of control rods (since control rod depletion is monitored by PRESTO).

3.5 Hydraulics Data Assignment

General data needed for the thermal-hydraulics model are given in the form of a set of library data on input cards.

Data describing the in-channel flow area, heated perimeter and hydraulic diameter are given separately for each fuel type and will thus enable the simulation of mixed (i.e., 7 x 7 and 8 x 8 fuel) cores.

Since BWR cores usually feature coolant flow restrictions for channels near the core periphery, each such hydraulic throttling zone is labeled by a unique index and characterized by specified core inlet and outlet pressure loss coefficients.

The thermo-hydraulics parameters are thus represented as either general data characteristic for the whole core, fuel type-dependent data or as data related to the core location.

3.6 Spacer Grid Locations

The axial location of the fuel spacer grids are specified in order to account for the neutronic effect of the spacers.

3.7 In-Core Detector Locations

Two types of in-core detectors are included in the PRESTO model :

- Fixed (LPRM) detectors
- Travelling (TIP) detectors.

LPRMs and TIPs are assumed to be located inside detector tubes (strings), positioned adjacent to the corner (narrow-narrow gap) of selected fuel assemblies. Thus each string will be surrounded by four fuel assemblies.

Detector string locations are specified by defining the four channels surrounding each detector.

The axial locations of the fixed detectors are specified by the elevation of the detector centerline for each of the four detectors in a string.

3.8 Radial Core Regions

The core may be subdivided into a number of radial regions for the purpose of output editing of volume averaged quanties like void, power, etc.

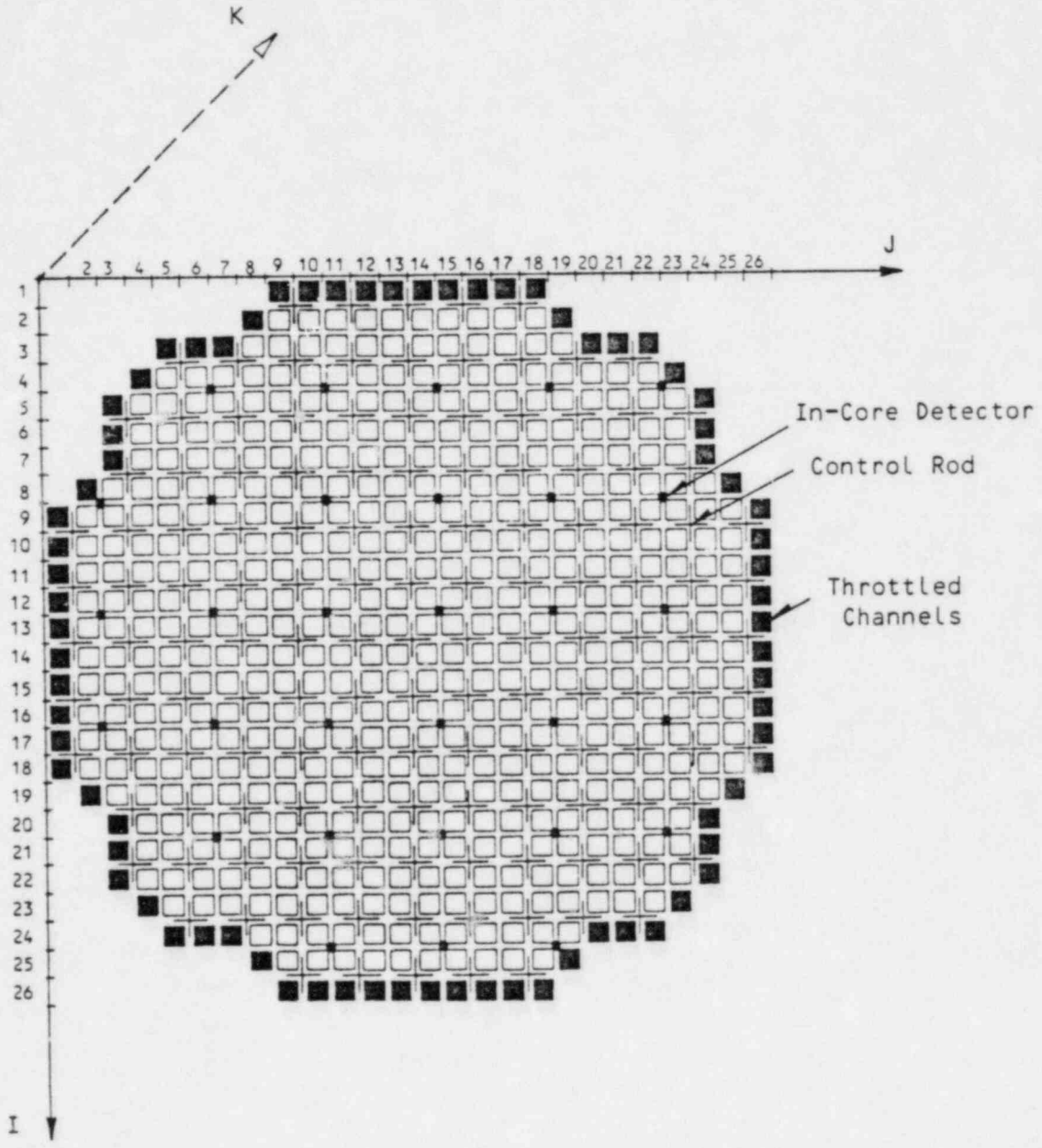

FIGURE 3.1 Basic Coordinate System for Core Description

4. REPRESENTATION OF NUCLEAR DATA

4.1 Polynomial Representation of Two-Group Data

Basic, two-group, assembly averaged cross-section data and peaking factors are assumed available from RECORD or from a corresponding lattice physics code. These basic parameters must be generated under the following conditions :

- The power density must correspond to the core average nodal power at rated total core power.

- The fuel temperature is the core average effective Doppler temperature for unexposed fuel at rated total core power.

- The Xenon and Samarium isotopic concentrations must correspond to the equilibrium concentrations at rated power, at any core burnup. Equilibrium concentrations are also assumed at zero burnup.

- The moderator temperature used in RECORD must correspond to the saturation temperature at rated core pressure.

- The basic cross-sections must be generated as functions of burnup and given in discrete burnup points (about 20 points), covering the range from zero to the expected maximum nodal burnup. Separate burnup calculations must be performed for three void fractions (i.e., 0, .40, .70), and for each type of fuel assembly cross-section (segment) encountered in the core. (If axially zoned fuel is used, one fuel assembly type may contain several cross-section types.)

The basic cross-section data sets are input to PRESTO in the form of polynomial coefficients generated by the auxiliary program POLGEN.

POLGEN subdivides the burnup range into intervals, each consisting of five burnup points. Fourth order polynomials are laid through the given points. Polynomial coefficients are thus given for each interval, each void fraction (exposure-weighted) and for each fuel segment type.

A basic cross-section for an arbitrary node in PRESTO is calculated by first locating the exposure interval of the node, then evaluating the cross-section at the actual nodal exposure-weighted void, using a second order interpolation between the three void values used in the RECORD cross-section generation.

The basic cross-sections are thus functions (g) of two parameters, exposure (E) and exposure-weighted void (α_x). Instantaneous void (α) is accounted for by additional polynomial fits (f), as follows :

(4.1)

2,3

where

Normally, when the difference between α and α_x is small, the exposure influence on the instantaneous void dependence may be neglected, and the functional dependence can be determined at zero burnup :

(4.2)

2,3

(4.3)

The simplified model (Eq. 4.3) is available as an option in PRESTO-B.

4.2 Xenon Feedback Effect

4.2.1 Steady-State Xenon Model

Deviations in local equilibrium Xenon concentrations from the average equilibrium concentration at rated power are accounted for in evaluating the nodal cross-sections. Xenon influences the group constants both by direct neutron absorption and by distorting the thermal neutron spectrum. These effects may be taken into account by modification of the basic thermal group absorption and fission cross-sections :

(4.4)

(4.5)

(4.6)

(4.7)

2,3

2,3

(4.8)

Q = Actual full core thermal power

Q^r = Rated full core thermal power

P^{rel} = Normalized (nodal) power density (core average = 1.0)

r = Conditions at rated power density

∞ = Conditions at infinite power density

The coefficients a_1, a_2 and a_3 are evaluated on the basis of RECORD results for no Xenon condition, rated power equilibrium Xenon condition, and an additional calculation at off-rated condition.

4.2.2 Transient Xenon Model

For calculations where the local Xenon concentrations may differ from equilibrium, a cross-section correction based directly on the nodal Xenon number density is applied :

(4.9)

(4.10)

2,3

where

X = Nodal Xenon number density

σ_x = Effective microscopic absorption cross-section for Xenon

κ_x = Coefficient describing the influence of Xenon on the thermal neutron spectrum

η_f = Coefficient describing the influence of Xenon on the fission cross-section due to spectrum hardening

σ_x and κ_x are evaluated as functions of void fraction α, and Xenon density :

(4.11)

(4.12)

2,3

The coefficients C_1 through C_5 and η_f may be evaluated on the basis of RECORD calculations.

4.3 Doppler Feedback Effect

The Doppler broadening of the cross-section resonance peaks with increasing fuel temperature causes increased epithermal neutron absorption and reduced resonance escape probability. This effect is accounted for in PRESTO through the following correlations :

(4.13)

(4.14)

2,3

The nodal average fuel temperature is obtained from a correlation of nodal power according to Eq. 6.30 which is described in Section 6.

4.4 Samarium Effect

The basic cross-section data input to PRESTO, in the form of POLGEN polynomials, are assumed to contain the effect of equilibrium Sm-149 also at zero burnup.

The following nodal correction is performed in PRESTO to account for deviations from equilibrium concentration of Sm-149 :

(4.15)

(4.16)

(4.17)

The average number density of Sm-149 for each fuel type is tracked in PRESTO whenever a burnup step or a time step calculation is performed. The initial concentration of Sm-149 is automatically set to zero for all

2,3

fresh fuel. Pseudo time steps at zero power may be included to simulate Pm decay and Sm buildup during periods of shut down.

4.5 Control Rod Model

4.5.1 Control Rod Reactivity Effect

The 2-group constants enter PRESTO's coupling equation through the nodal quantity $\bar{s}_i$, defined by Equation 5.4 :

$$\bar{s}_i = \left(\frac{k_\infty}{\lambda} - 1 \right) (\Sigma_{a1} + \Sigma_{r1}) \tag{4.18}$$

$$k_\infty = \frac{1}{\Sigma_{a1} + \Sigma_{r1}} \left(\nu\Sigma_{f1} + \frac{\Sigma_{r1} \cdot \nu\Sigma_{f2}}{\Sigma_{a2}} \right) \tag{4.19}$$

Therefore, correct representation of control rod insertion is assured if the influence on k_∞ and $(\Sigma_{a1} + \Sigma_{r1})$ is modeled properly. The influence of control rod insertion on the fast group diffusion coefficient (see Eqs. 5.8 and 5.14) is generally negligible. It is also observed (RECORD) that the sum $\Sigma_{a1} + \Sigma_{r1}$ is almost unaffected by control rod insertions. Hence, it is sufficient to model control rod insertion by its influence on k_∞. This is done by adding a control rod correction term, $\Delta\Sigma_{a2}$, to the thermal group absorption cross-section. In this way, the thermal group flux (Eq. 5.24) will be modified due to control rod absorption.

The following expression is used to evaluate $\Delta\Sigma_{a2}$:

(4.20)

where

k_∞^c = k_∞ - control rod inserted (RECORD calc.)

This expression is obtained by requiring the controlled k_∞ (obtained by adding $\Delta\Sigma_{a2}$ to Σ_{a2} and solving Equation 4.19 for $\Delta\Sigma_{a2}$) to agree with a reference, controlled k_∞ (RECORD).

The control rod correction term, $\Delta\Sigma_{a2}$, is represented as a polynomial fit where the following effects are taken into account :

- Void in the adjacent channel
- Fuel burnup in the adjacent assembly
- Depletion of the boron absorber
- Moderator condition (cold or hot)
- Partial insertion of a control rod into a node.

In addition, the effect of control rod insertion on the local power peaking factor and the effect of the control rod history on the group constants (through spectrum hardening and increased Pu production) in the adjacent fuel are taken into account. This is described in detail below. The basic expression for $\Delta\Sigma_{a2}$ is :

(4.21)

(4.22)

2,3

b_5 = fitted constant

h_4 = multiplier accounting for 4-bundle homogenization effects.

The following term accounts for the effect of undepleted control rods (subscript o) in fully controlled nodes :

$$\Delta\Sigma^{o}_{a2} = b_2(E) + b_3(E) \cdot \alpha + b_4(E) \cdot \alpha^2 \qquad (4.23)$$

E = fuel burnup

α = in-channel void fraction

The functions b_2, b_3 and b_4 are second order polynomials in E.

4.5.2 Control Rod Depletion

The term $C_{RC} \cdot B \cdot f(\Sigma)$ of Equation 4.21 accounts for a reduction in the rod worth due to depletion of the Boron absorber (B^{10}). Detailed analysis of Boron depletion for BWR control rods (rodded blade rods) have shown that the rod worth, Δk, decreases linearly with increasing burnup :

$$\Delta k(B) = \Delta k(0) - C_{RC} \cdot B \qquad (4.24)$$

B = burnup obtained in the adjacent fuel during the periods of control rod insertion

C_{RC} = fitted constant (different for cold and hot condition)

$f(\Sigma)$ of Equation 4.21 is a function of the 2-group constants converting the reduction $C_{RC} \cdot B$ in k_∞ into a corresponding reduction in Σ_{a2}.

The content of B^{10} in each segment of the control rod, given in per cent of the initial B^{10} content is :

$$N_{B^{10}} = 100 - C_3 \cdot B + C_4 \cdot B^2 \qquad (4.25)$$

where

C_3 and C_4 are fitted constants

Constants for the control rod depletion model have been derived for BWR rodded blade control rods by detailed calculation of the B^{10} depletion using the codes RECORD and THERMOS. These constants are assumed to be generic for GE-type rodded blades.

4.5.3 Control Rod History Effect

Control rod history effects on the nodal 2-group constants are accounted for by means of a model derived on the basis of a large number of RECORD calculations. This model allows the nodal Σ_{a2} and $\nu\Sigma_{f2}$ to increase (second order polynomial) due to increased Pu production in periods when the control rod is inserted; whereas, a corresponding decrease (exponential decay) of the excess quantity accounts for burnup in periods when the control rod is withdrawn.

4.5.4 Control Rod Model for Cold Condition

For cold condition analysis, where all or nearly all control rods are inserted, the basic group constants as input to PRESTO (POLGEN-File) are assumed to contain the effect of the control rod.

For uncontrolled nodes, a quantity $\Delta\Sigma_{a2}$, evaluated as by Equation 4.20 replacing k_∞^c with the uncontrolled k_∞, is subtracted. Control rod depletion and control rod history effects are applied as described above.

4.6 Cross-Section Model at Reduced Moderator Temperature

The hot operating condition, two-group data set is applicable for analysis of reactor conditions ranging from hot, near zero power to hot full power. Separate data sets are required for analyses of zero power states at reduced moderator temperature. The polynomial representation described in Section 4.1 is applied at each moderator

temperature (i.e., cold condition), thus the group constants are functions of exposure (E) and exposure-weighted void (α_x). Each low temperature cross-section set is assumed generated by branch-off RECORD calculations based on the isotopic composition file generated in the corresponding hot condition RECORD calculation. The branch-off calculation is performed under the following assumptions :

- The power density is set to zero.
- The fuel temperature is the same as the moderator temperature (i.e., $20^{\circ}C$ for cold cases).
- The Xenon and Iodine concentrations are set to zero.
- The Sm concentrations are kept unchanged (from the hot case).
- The control rod is inserted in cold condition (see §4.5.4).

4.7 Spacer Representation

Neutron absorption in spacer grids is accounted for by adding an exposure and void dependent correction term to the thermal group absorption cross-section in nodes defined as spacer nodes. The effect of the spacer on the flux and power distributions is thus smeared out over the nodal volume. The following form of the spacer correction term is used :

(4.26)

where b_5 through b_9 are fitted constants.

The magnitude of $\Delta\Sigma_{a2}^{SP}$ may be obtained by separate RECORD calculations with spacer material included, followed by a one-dimensional diffusion calculation (MD-1) to perform the axial homogenization over the nodal volume.

5. NEUTRON DIFFUSION MODEL

5.1 Derivation of Equations for Calculation of Two-Group Flux Distributions and Eigenvalue

The neutronic equations of PRESTO are derived as an approximation to coarse mesh diffusion theory (Reference 1). A constant planar mesh width (h) is assumed. The axial mesh width (k) is usually equal to the planar mesh width for BWRs (cubical nodes). The method is derived for non-cubical nodes as well; however, the cubical node (k=h) formulation is described first :

A central mesh point finite difference formulation is used for the fast flux (ϕ) equation (Reference 1) :

$$a_{ii}\phi_i - \sum_{6j} a_{ij}\phi_j = \bar{s}_i \cdot \bar{\phi}_i \cdot h^3 \tag{5.1}$$

where

$$a_{ij} = h \frac{2D_iD_j}{D_i+D_j} \tag{5.2}$$

$$a_{ii} = \sum_{6j} a_{ij} \tag{5.3}$$

i and j are nodal indices. The summation is over the six nearest nodes j surrounding node i (4 planar and 2 axial neighbor nodes). $\bar{s}_i$ is a function of the 2-group nodal macroscopic cross-sections and the eigenvalue λ :

$$\bar{s}_i = \frac{1}{\lambda}\left(\nu\Sigma_{f1} + \nu\Sigma_{f2}\frac{\Sigma_{r1}}{\Sigma_{a2}}F\right) - \Sigma_{a1} - \Sigma_{r1} \tag{5.4}$$

where

F = nodal thermal spectrum index. (See Eq. 5.18.)

(Standard 2-group notation is used for the 2-group constants.)

The following approximation is used to simplify Equation 5.1 :

$$\frac{2D_i D_j}{D_i+D_j} \approx \sqrt{D_i} \cdot \sqrt{D_j} \tag{5.5}$$

(See Reference 1 for discussion of accuracy of this approximation.)

Equation 5.1 is then reduced to :

$$P_i \psi_i - \sum_{6j} \psi_j = - q_i \bar{\psi}_i \tag{5.6}$$

where

$$\psi_i = \phi_i \sqrt{D_i} \quad , \tag{5.7}$$

$$P_i = \frac{1}{\sqrt{D_i}} \cdot \sum_{6j} \sqrt{D_j} \quad , \tag{5.8}$$

and

$$q_i = - \frac{\bar{s}_i}{D_i} h^2 \tag{5.9}$$

Further, the nodal average flux $\bar{\phi}_i$ is expressed as an interpolation between the mesh point flux ϕ_i and the six nodal interface flux values ϕ_{ij} (on the interfaces between the node considered and its six nearest neighbors) :

$$\bar{\phi}_i = b\phi_i + \frac{1-b}{6} \sum_{6j} \phi_{ij} \tag{5.10}$$

where b is a fitted constant.

The interface fluxes may be expressed as :

$$\phi_{ij} = \frac{\psi_i}{2\sqrt{D_j}} + \frac{\psi_j}{2\sqrt{D_i}} \tag{5.11}$$

giving

$$\bar{\psi}_i = (b + cr_i)\psi_i + c \sum_{6j} \psi_j \tag{5.12}$$

with

$$c = \frac{1-b}{12} \tag{5.13}$$

and

$$r_i = \sqrt{D_i} \sum_{6j} \frac{1}{\sqrt{D_j}} \tag{5.14}$$

Introducing Equation 5.12 into Equation 5.6 gives :

$$Q_i \psi_i = \sum_{6j} \psi_j \tag{5.15}$$

with

$$Q_i = \frac{P_i + q_i (b + cr_i)}{1 - cq_i} \tag{5.16}$$

Equation 5.15 is the fundamental nodal coupling equation, as applied in PRESTO. All nuclear constants are contained in a single vector, Q_i, thus Equation 5.15 lends itself to uncomplicated computer representation.

The eigenvalue λ, entering Equation 5.4, must be found simultaneously with Equation 5.15. This is achieved by iterative methods (starting from a guess of λ=1.0); λ is calculated as

$$\lambda = \frac{\text{Total neutron production}}{\text{Total neutron absorption + neutron leakage from core boundary}} \tag{5.17}$$

The nodal average thermal flux distribution, $\bar{\phi}_2$, is required for calculation of the nodal power density (Equation 7.1) and for the thermal spectrum index entering Equation 5.4 :

$$F_i = \frac{\bar{\phi}_{2i}}{\bar{\phi}^{as}_{2i}} \tag{5.18}$$

where $\bar{\phi}^{as}_{2i}$ is the average asymptotic flux defined as :

$$\bar{\phi}^{as}_{2i} = \frac{\Sigma_{r1}}{\Sigma_{a2}} \cdot \bar{\phi}_{1i} \tag{5.19}$$

Two optional models are available for calculation of $\bar{\phi}_2$ in PRESTO-B :

Option 1.

The node average thermal flux is calculated by analogy with Equation 5.10 and assuming asymptotic conditions (Equation 5.19) in the node midpoint :

$$\bar{\phi}_2 = b_2 \phi^{as}_{2i} + \frac{1 - b_2}{6} \sum_{6j} \phi^{as}_{2ij} \tag{5.20}$$

Under this option, the non-asymptotic thermal flux (Equation 5.20) is only used in the calculation of the nodal power, whereas the spectrum index F is assumed asymptotic :

$$F = 1 \tag{5.21}$$

Option 2.

The node average thermal flux is found from the thermal group neutron balance equation integrated over the nodal volume :

$$\bar{\phi}_2 = \phi_{2i}^{as} - \frac{L_2}{\Sigma_{a_2}} \tag{5.22}$$

where L_2 is the net leakage of thermal neutrons per unit volume. L_2 is calculated using the same finite difference approximation as for the fast group flux, optionally modified by a thermal group gradient correction factor, a_2 :

(5.23)

(5.24)

Under this option, the non-asymptotic thermal flux is recalculated in each eigenvalue iteration and used to calculate the spectrum index entering Equation 5.4 and to calculate the nodal power.

Option 1 usually gives sufficient accuracy in hot condition applications, whereas calculations involving larger flux gradients, such as cold, single rod out cases, require the method under Option 2.

For noncubical nodes, the constant $R = h^2 / k^2$ is introduced as a multiplier on all axial neighbor node terms in the nodal summations, as shown in Reference 1. k is the vertical mesh width. Equation 5.15 is then modified to :

$$Q_i \Psi_i = \sum_{4j\text{-planar}} \Psi_j + R \sum_{2j\text{-axial}} \Psi_j \tag{5.25}$$

The constants b and c are expressed in terms of a new constant, a (with a=b for cubical nodes) :

$$b = 3a \frac{1}{3a+(1-a)(R+2)} \tag{5.26}$$

$$c = \frac{1-a}{4} \frac{1}{3a+(1-a)(R+2)} \tag{5.27}$$

Corresponding expressions are employed for the thermal group constant b_2 of Equation 5.20.

Numerous comparisons with fine mesh diffusion theory results for typical BWR configurations have shown that a ≈ 0 is close to optimum for both hot, voided condition and cold condition cases. Correspondingly, b_2 = 0 (Option 1) or a_2 = 0 (Option 2) is recommended for the thermal flux model. Cold cases using thermal flux Option 2 may require a slightly negative value of a_2 (i.e. -0.5).

Examples of comparisons of PRESTO with reference diffusion theory solutions are provided in Section 11.1. These results are the primary basis for evaluation of the constants a and a_2.

5.2 Reflector Treatment

Equation 5.15 is solved subject to precalculated boundary conditions on the core reflector interface. For nodes facing the reflector, Equation 5.8 is modified to :

$$P_i = \frac{1}{\sqrt{D_i}} \sum_{j=1}^{6-n} \sqrt{D_j} + B_i \tag{5.28}$$

A constant reflector diffusion coefficient is used for "reflector nodes" in Equation 5.14.

The boundary condition B_i may be expressed as :

$$B_i = \frac{n \cdot h}{\lambda_i^{eff}} \tag{5.29}$$

where

n = number of "missing neighbor" nodes

λ_i^{eff} = effective extrapolation length into the reflector for the group 1 flux, node i.

Equation 5.28 accounts for fast neutron leakage into the reflector. Adequate reflector treatment also requires modeling of thermal neutron return from the reflector. In PRESTO, the net thermal neutrons impinging on the core from the reflector are assumed to be completely absorbed in the periphery nodes. The increased thermal flux in the boundary nodes is described by :

$$\bar{\phi}_2 = \frac{\Sigma_{r1} + S_i}{\Sigma_{a2}} \cdot \bar{\phi}_1 \tag{5.30}$$

The "albedo" source term, S_i, may be written as :

$$S_i = \frac{n}{h} \cdot \frac{\beta_i}{\lambda_i^{eff}} \cdot D_i \tag{5.31}$$

where the albedo β is defined by :

$$\beta_i = \frac{J_1}{J_2} \tag{5.32}$$

J_1 and J_2 are the fast group and thermal group net currents at the core reflector interface.

The albedo source term is added to the removal cross-section in Equations 5.4 and 5.19 and Equations 5.20, 5.22 are replaced by $\bar{\Phi}_2 = \Phi_{2i}$ for all nodes treated as boundary nodes.

The reflector parameters B_i and S_i are determined from a reference, two-group, fine mesh diffusion theory solution for the flux distributions in a 2-D horizontal core cross-section (side reflector) and from a 1-D solution in the axial direction for the top and bottom reflectors. Evaluation of (B_i, S_i) is performed by the subroutine ALBMO in PRESTO.

B_i is determined by inserting the reference nodal fluxes into the nodal coupling equation and the solution for P_i , B_i is then found from Equation 5.28. Equation 5.30 is solved for S_i, using the reference fast to thermal group flux ratio.

The found values of (B_i, S_i) are applied in a 2-D (or 1-D) PRESTO calculation using the same nodal cross-sections as in the fine mesh calculation.

A set of nodal correction factors, $PCORR_i$, modifying the original B_i-values, is determined in an iterative way by requiring improved agreement in the overall power distribution (checking the power in the center of the core as well as on the periphery).

The side reflector boundary conditions are strictly only applicable at the axial elevation where the fine mesh, 2-D calculation was performed. Calculations performed at different axial elevations (bottom, mid and top of core) have shown that these parameters are slightly void-dependent. The following linear correlation has been developed on the basis of such calculations to account for the variation in void content along the channel :

$$B_{i,k} = B_i + C \cdot n_i (D_{ik} - \bar{D}) \qquad (5.33)$$

$B_{i,k}$ = boundary condition, channel i axial node k (3-D)

B_i = corresponding boundary condition at reference elevation (2-D)

C = constant (normal value = -0.067)

n_i = number of missing neighbor nodes, channel i

$D_{i,k}$ = fast group diffusion coefficient, channel i, node k

$\overline{D}$ = reference level average fast group diffusion coefficient

The method for calculation of reflector boundary conditions is automated in PRESTO. Thus, the following procedure is followed (2-D calc.) :

1) Select option for Sigma-file generation -
   run 3-D PRESTO case -
   save Sigma-file for core midplane

2) Run fine-mesh code (MD-2 or PDQ-7)
   using cross-sections from Sigma-file

3) Select ALBMO option -
   run PRESTO case to generate albedoes and
   perform checking and adjustment against fine mesh, 2-D power
   distribution

6. THERMAL-HYDRAULICS MODEL

The large variations in coolant density in a BWR have a significant effect on the calculation of reactivity and power distributions. Also of some importance, is the influence of the fuel temperature (Doppler effect). Therefore, the thermal-hydraulic analysis may be considered of equal importance as the neutronics analysis in a BWR core simulator.

The average void content (or coolant density) in each volume associated with a neutronic node is needed to account for the void feedback. This void distribution is calculated, given the nodal power distribution, total core mass flow and core inlet subcooling. In PRESTO, the interior of each flow box (fuel channel) represents one flow path, and the flow leakage outside the boxes is represented by one single bypass flow path. The flow in each such channel is one-dimensional and is discretized axially into sections of the same size as the neutronic nodes; i.e., each fuel assembly is divided into 24 or 25 axial sections. The flow distribution among the channels is dependent on the flow resistance in each individual channel, and is a function of geometry, channel power, axial power shape, coolant density, etc. Obviously, the coolant conditions are, in turn, dependent on the flow through the channel. The flow rate in each channel and the bypass flow are determined from the requirement of equal pressure drop over all the parallel flow paths.

The void distribution in each channel is calculated from the mass and energy balance equations, together with correlations for steam slip, heat transfer and evaporation/condensation rate, which are valid for thermo-dynamic nonequilibrium conditions.

An average fuel temperature in each node is required to account for the Doppler effect. PRESTO-B uses a linear correlation between nodal power and effective Doppler temperature.

6.1 System Heat Balance

The reactor system, as described in PRESTO-B is illustrated in Figure 6.1.

The energy and mass balance equations may be written as :

$$\begin{bmatrix}\text{Energy flowing}\\ \text{into the system}\end{bmatrix} + \begin{bmatrix}\text{Energy added to the}\\ \text{fluid in the system}\end{bmatrix} = \begin{bmatrix}\text{Energy flowing out}\\ \text{of the system}\end{bmatrix}$$

$$\begin{bmatrix}\text{Total mass flowing}\\ \text{into the system}\end{bmatrix} = \begin{bmatrix}\text{Total mass flowing}\\ \text{out of the system}\end{bmatrix}$$

Reactor vessel energy balance :

$$w_{fw}h_{fw} + w_{cr}h_{cr} + Q_{th} - Q_{rad} + Q_p - Q_{cl} = w_S\{h_f^{SD} + (1 - f_{cm})h_{fg}^{SD}\} \quad (6.1)$$

Vessel mass balance :

$$w_{fw} + w_{cr} = w_S \quad (6.2)$$

Downcomer energy balance :

$$w_{fw}h_{fw} + w_{cr}h_{cr} + w_{DC}h_f^{SD} + f_{cu}w_Th_{fg}^{SD} + Q_p - Q_{cl} = w_Th_{in} \quad (6.3)$$

Downcomer mass balance :

$$w_{fw} + w_{cr} + w_{DC} = w_T \quad (6.4)$$

Reactor core energy balance :

$$w_Th_{in} + Q_{TH} = w_Th_f^c + X_g w_Th_{fg}^c \quad (6.5)$$

where :

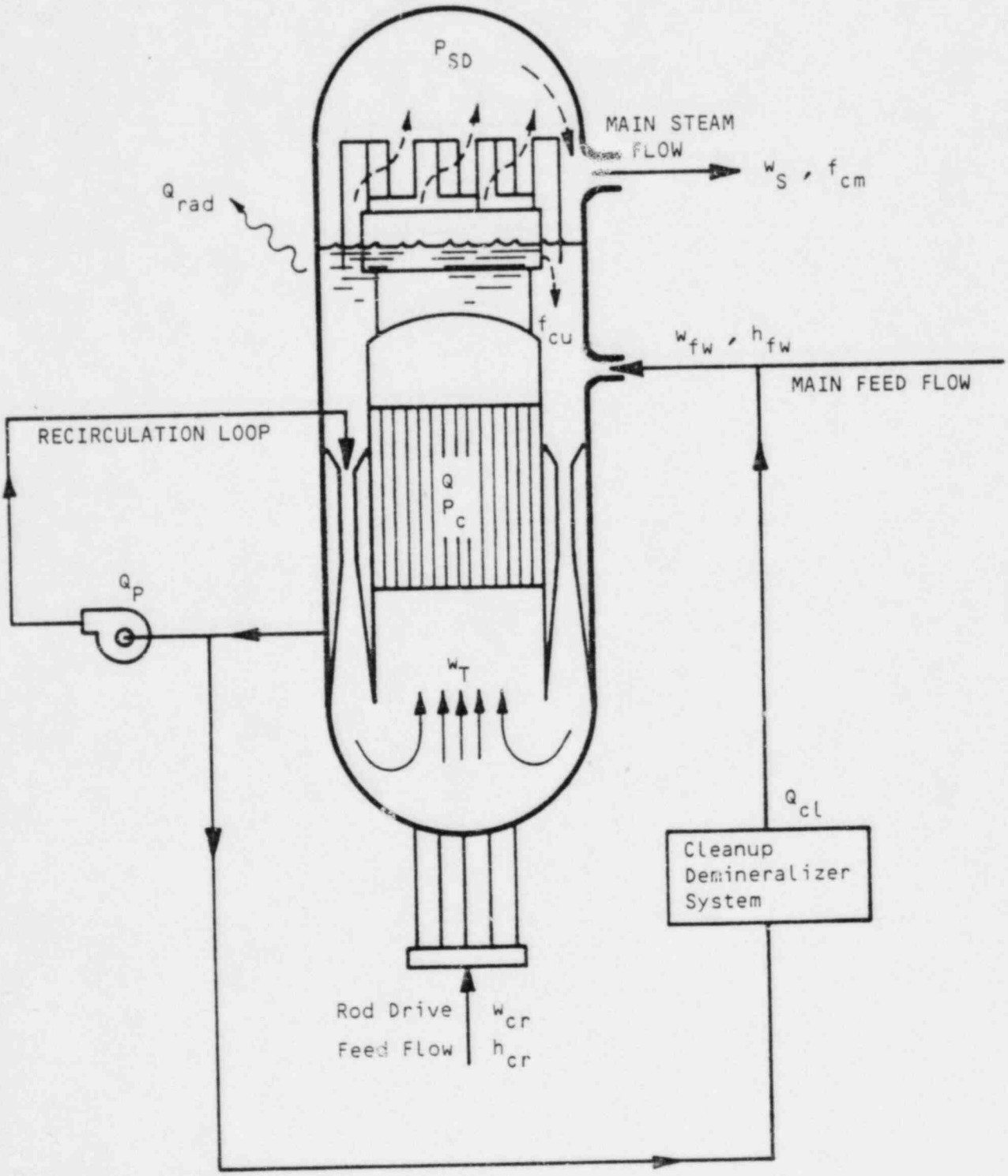

FIGURE 6.1 Reactor System with Heat and Flow Components, as Modelled in PRESTO

Q_{th} = core thermal power

Q_{rad} = radiative heat loss

Q_{p} = recirculation pump heat

Q_{cl} = cleanup demineralizer system heat removal

h_{fw} = feedwater enthalpy

h_{cr} = control rod drive flow enthalpy

h_{fg}^{SD} = heat of evaporation at steam dome pressure

h_{fg}^{c} = heat of evaporation at core pressure

h_{f}^{SD} = saturated water enthalpy at steam dome pressure

h_{f}^{c} = saturated water enthalpy at core pressure

h_{in} = water enthalpy at the core inlet

h_{cr} = control rod drive flow enthalpy

w_{T} = total core mass flow

w_{fw} = feedwater flow

w_{cr} = control rod drive flow

w_{S} = steam flow

w_{DC} = downcomer inlet mass flow

f_{cu} = steam carry-under fraction into downcomer

f_{cm} = liquid carry-over fraction into steam lines

X_{g} = core exit steam quality

The heat balance equations (6.1 - 6.5) are derived under the assumption of a constant pressure, P_{SD}, valid for the steam dome and the downcomers and another pressure, P_{c}, valid for the core region. The thermodynamic properties (h_{f}^{SD}, h_{f}^{c}, h_{fg}^{SD}, h_{fg}^{c}) are evaluated at the corresponding pressures, using a steam table function internal to PRESTO-B.

Equations 6.1 - 6.4 are combined to eliminate the variables w_{fw}, w_{S}, w_{DC} and to calculate the core inlet enthalpy :

$$h_{in} = h_f^{SD} + f_{cu} h_{fg}^{SD} - \frac{(Q-Q_{rad})(h_f^{SD}-h_{fw}) - (Q_p - Q_{cl} + w_{cr} h_{cr} - w_{cr} h_{fw})(1-f_{cm}) h_{fg}^{SD}}{w_T \{h_f^{SD} + (1-f_{cm}) h_{fg}^{SD} - h_{fw}\}} \quad (6.6)$$

The core inlet enthalpy is used in the calculation of flow and void conditions in the core, as will be outlined in sections 6.2 and 6.3.

The main components going into the heat balance equations are the core power (Q_{th}), the total flow (w_T) and the feedwater enthalpy (h_{fw}), which all have to be provided as input data. Of second order importance are the parameters Q_p, Q_{cl}, w_{cr}, h_{cr}, f_{cm} and f_{cu} also specified as input. The steam dome and core pressures may be given directly as input (in which case $P_c = P_{SD}$) or may be calculated by the code (cf. Section 10.5).

As an alternative to calculating the core inlet enthalpy from the feedwater enthalpy, etc., the core inlet subcooling may be specified directly as input.

6.2 Basic Models and Equations for Void Calculation

The thermal-hydraulics model is specially designed to describe the coolant conditions in a BWR under power generating conditions. It was originally developed at the Institute for Energy Technology, Kjeller, Norway (Ref. 2). The prime source of experimental data used for verification of the model is the FRIGG Loop Experiments (Refs. 4 and 5) on both 36-rod and 64-rod, full-scale geometries. The basic model has also been applied in the transient codes RAMONA and NORA (Refs. 6 and 7).

Details on the model are given below :

6.2.1 Mass Balance

The mass balance for section i is given by :

$$\text{Steam :} \quad w_{gi} - w_{gi+1} + \psi_i = 0$$

$$\text{Water :} \quad w_{fi} - w_{fi+1} - \psi_i = 0 \qquad (6.7)$$

with

w_{gi} = steam flow into section i

w_{fi} = liquid flow into section i

ψ_i = evaporation rate in section i
(correlation for ψ_i given below)

6.2.2 Energy Balance

The energy balance for section i is given by :

$$w_{gi}\, e_{gi} + w_{fi}\, e_{fi} - w_{gi+1}\, e_{gi+1} - w_{fi+1}\, e_{fi+1} + Q_i = 0 \qquad (6.8)$$

with

Q_i = heat flux rate into section i

e_{fi}, e_{gi} = specific energy (index f for fluid and g for steam)

The steam temperature is assumed constant and equal to the saturation temperature. The water temperature in section i is determined by

$$T_{fi} = T_o + e_{fi}/C_{vi} \qquad (6.9)$$

with

T_o = a reference temperature

C_{vi} = specific heat of water

6.2.3 Momentum Balance

The momentum equation can be written as

$$-\frac{\partial p}{\partial z} = +\frac{\partial u}{\partial z} + \frac{\partial F}{\partial z} + g\left[(1-\alpha)\rho_f + \alpha \cdot \rho_g\right] \qquad (6.10)$$

acceleration, restriction — friction — static acceleration

with

p	=	pressure
u	=	momentum flow
g	=	constant for gravitational acceleration
α	=	void
ρ_f	=	water density
ρ_g	=	steam density
F	=	friction
z	=	elevation coordinate

The momentum flow is given by

$$u = (1-\alpha)\rho_f v_f^2 + \alpha\rho_g v_g^2 \qquad (6.11)$$

with

v_f	=	water velocity
v_g	=	steam velocity

Integrating Equation (6.10) from z_1 to z_2 yields :

$$-(p_2 - P_1) =$$

$$(u_2 - u_1) + (F_2 - F_1) + \left[g\rho_f (z_2 - z_1) - g(\rho_f - \rho_g) \cdot \int_{z_1}^{z_2} \alpha \, dz \right] \qquad (6.12)$$

acceleration restriction — friction — static head

The pressure drop over a restriction (i.e., spacer, channel inlet and outlet) is modelled by

$$\Delta p' = - K \cdot u \qquad (6.13)$$

with

K = loss coefficient

The momentum equation is, in PRESTO-B, applied in the integrated form, Equation 6.12, combined with Equation (6.13).

6.2.4 Two-Phase Flow Friction

The pressure loss due to friction is calculated using a single-phase friction factor, based on Weisback's formula and a two-phase friction multiplier, described by the Becker correlation (Ref. 8).

The friction loss is given by :

$$\frac{\partial F}{\partial z} = f \cdot R_k \cdot \frac{w \cdot |w|}{A^2 \cdot \rho_f^2} \qquad (6.14)$$

with single-phase friction factor (Weisbach's formula) :

$$f = \frac{G_1}{2D_h Re^{G_2}} \qquad (6.15)$$

and two-phase friction multiplier (Becker correlation) :

$$R_K = 1 + A_F \cdot \left(\frac{X}{p}\right)^{0.96} \qquad (6.16)$$

where

A	=	flow area
ρ_f	=	liquid density
w	=	total mass flow
D_h	=	hydraulic diameter
Re	=	Reynold's number
X	=	steam quality
p	=	pressure
G_1, G_2, A_F	=	empirical constants given in Table 6.1

The calculation of Reynold's number, Re, is based on total mass flux G and liquid properties

$$Re = \frac{G \cdot D_h}{\mu_f} = \frac{V_{f,in} \cdot D_h \cdot \rho_f}{\mu_f}$$

where

μ_f = dynamic viscosity

$G = w/A$

6.2.5 Slip Correlation

To account for differences in cross-section averaged steam and water velocities, a modified Bankoff slip correlation is applied.

The steam velocity is given by :

$$v_g = S \cdot v_f + v_o \tag{6.17}$$

where

$$S = \frac{1-\alpha}{B-\alpha} \tag{6.18}$$

with

v_g = steam velocity

v_f = water velocity

v_o = bubble rise velocity

α = void fraction

B is a flow dependent parameter given by the following empirical correlation :

(6.19)

At very high voids, the Bankoff slip correlation is modified to better describe the flow under annular flow conditions. Therefore, above a certain cutoff void, α_c , Equation 6.18 is replaced by

(6.20)

(6.21)

6.2.6 Boiling Model

The boiling model describes evaporation at the heated cladding surface as well as bulk flashing/condensation. The surface term is based on a mechanistic approach, describing the formation of void bubbles and the "pumping" effect from the bubbles leaving the wall. This describes the process, when first the formation of a steam bubble pushes hot wate out from the hot boundary layer into the colder bulk fluid, and then, how the steam bubble detaches from the wall and the occupied volume is refilled with colder water. For details, see Ref. 2.

Steam Generation on the Heated Surface :

$$\psi_{SF} = \frac{Q_B}{h_{fg} + C_p (T_g - T_f) \frac{\rho_f}{\rho_g} + (T_{CA} - T_g) \left(\frac{\rho_f}{\rho_g} - 1\right) \frac{C_p}{2}} \qquad (6.22)$$

Flashing/Condensation in Bulk Fluid :

$$\psi_B = f_1(\alpha) \cdot \left[(T_f - T_g) + \kappa \cdot |T_f - T_g| \right]$$

$$f_1(\alpha) = R_0 + R_1 \alpha \ (1-\alpha) \qquad (6.23)$$

where

T_f = water temperature

T_g = steam temperature

T_{CA} = cladding surface temperature

h_{fg} = heat of evaporation

C_p = spec. heat capacity of water

ρ_f = density of water

ρ_g = density of steam

Q_B = heat flux to the coolant (under boiling conditions)

R_0, R_1, K = correlation coefficients given in Table 6.1

α = void fraction

The surface evaporation term (6.22) applies only under heated surface boiling conditions. If no boiling occurs on the surface, it is set equal to zero, $\psi_{SF} = 0$.

The two evaporation terms are additive to give the total evaporation rate

$$\psi = \psi_{SF} + \psi_B \tag{6.24}$$

6.2.7 Heat Transfer from Fuel to Coolant

The heat transfer from the cladding surface to the coolant is described by Jens-Lotte's Correlation for boiling heat transfer and by the Colburn Correlation for nonboiling heat transfer.

Boiling Heat Transfer :

$$Q_B = A_S \left[K_B (T_{CA} - T_S)\right]^4 \tag{6.25}$$

with

$$K_B = 1.266\ e^{+1.61 \cdot 10^{-7} p}$$

Non-Boiling Heat Transfer :

$$Q_{NB} = A_S \cdot K_{NB} \ (T_{CA} - T_f) \qquad (6.26)$$

with

$$K_{NB} = 0.023 \ \frac{|\rho_f v_{in}|^{0.8} \ C_p^{0.4} \ \lambda_f^{0.6}}{D_c^{0.2} \ \eta_f^{0.4}} \qquad (6.27)$$

and

A_S = heated surface area

T_{CA} = cladding surface temperature

T_f = water temperature

T_S = saturation temperature of coolant

p = pressure

v_{in} = core inlet water velocity

C_p = specific heat capacity of water

λ_f = thermal conductivity of water

η_f = viscosity of water

D_c = hydraulic diameter

Under steady-state conditions, the heat flux, Q, from the cladding surface to the coolant is given directly by the power production in the fuel. By setting $Q_B = Q$ and $Q_{NB} = Q$, and applying Equations (6.25) and (6.26), respectively, two different values on the cladding temperature, T_{CA}, can be evaluated. The minimum value,

$$T_{CA} = \text{Min}\left[T_{CA}^{(6.18)}, T_{CA}^{(6.19)}\right] \qquad (6.28)$$

will be utilized.

Or, expressed differently, of the two heat transfer correlations, Equation (6.25) and Equation (6.26), the one giving the maximum heat flux will always be selected and used for calculating the surface temperature.

6.2.8 Heat Source Distribution

The energy produced in the fission process is mainly conducted as heat through the fuel into the coolant. However, a small part is deposited directly in the coolant by means of neutron slowing down and gamma heati

$$\begin{aligned} Q_{cond} &= Q_{fiss} \cdot (1-\delta_1) \\ Q_{in\text{-}chn} &= Q_{fiss} \cdot (1-\delta_2) \end{aligned} \qquad (6.29)$$

with

Q_{fiss} = power produced by fission

Q_{cond} = power conducted through the cladding into the coolant

$Q_{in\text{-}chn}$ = total power absorbed in the in-channel coolant

δ_1, δ_2 = constants given in Table 6.1

The total power absorbed in the bypass channel is given by

$$Q_{bypass} = Q_{fiss} \cdot \delta_2$$

Optionally, the bypass heat generation rate in the interchannel volumes, may be assigned different values depending on whether or not a control rod is inserted.

6.2.9 Fuel Temperature Model

The temperature distribution in a fuel pin is primarily a function of power density and gap conductance. The latter varies strongly with irradiation due to pellet expansion, cracking and fission gas release. The dominating effect, especially for unpressurized BWR fuel, is the decrease in gap conductance due to the fission gas release into the gap. The buildup of crud on the clad surface may significantly affect the heat transfer properties and thus the fuel temperature.

These burnup effects of the fuel are typically very difficult to predict since they cannot be correlated solely to the accumulated irradiation but are also very much dependent on the operating history of the fuel.

Due to resonance self-shielding effects, the volumetric average fuel temperature can not be used directly as the parameter describing the Doppler effect. Instead, an effective Doppler temperature, averaged over the fuel pin with a higher weight on the outer regions of the pin, has to be utilized.

Fortunately, the Doppler effect is of relatively small importance in static BWR analyses, and the temperature calculation can be considerably simplified. Roughly estimated, the Doppler reactivity effect is of one order of magnitude less than the void reactivity effect for a given power perturbation at operating BWR conditions. The influence on the power distribution is also much less from the Doppler effect than that from the void effects.

PRESTO-B correlates the effective Doppler temperature to the power density. Burnup-dependent terms are included to account for, mainly, the variation of gap conductance with exposure :

$$T_f = T_f^o + C_{DOP} \cdot (P - P_{Ref}) \qquad (6.30)$$

$$T_f^o = d_1 + d_2 E + d_3 E^2$$

$$C_{DOP} = (T_f^o - d_5)/P_{Ref}$$

with

T_f = actual Doppler temperature

T_f^o = Doppler temperature at rated power density

P = actual power density

P_{Ref} = rated power density

E = fuel exposure

d_1, d_2, d_3, d_5 = input parameters

The parameters d_1, d_2, d_3 and d_5 have to be determined from independent fuel temperature calculations, and are specified individually for each fuel type. A rule of thumb for estimating the effective Doppler temprature is to reduce the volumetric average fuel temperature by 10 - 15% at rated power conditions.

6.3 Calculational Procedure

The calculation of the coolant conditions in all the parallel channels can be visualized as a two-step procedure :

1) calculation of flow distribution
2) calculation of axial void distribution

However, the first step, the flow calculation, is dependent on the results of the second step, the void distribution in the channel. Numerically, the complete problem can be solved by, e.g., iteration between the two steps.

The calculational method applied in PRESTO-B is based on the following observation :

> The pressure drop over a channel, which will determine the flow, is not so much dependent on the detailed void distribution in the channel, but can be calculated with relatively good accuracy, knowing the elevation of the bulk boiling boundary and the total steam production in the channel.

To reduce the computing time, PRESTO-B uses a special procedure with a simplified void model for the calculation of the flow distribution. Once the flow is determined, however, the void distribution in the channel is calculated with the detailed void model.

6.3.1 Calculation of Flow Distribution

For a specified total core flow rate, each individual channel flow is determined by equalizing the pressure drops across all flow paths. The channel flow, or equivalently, the channel inlet velocity, v_{in}, is related to the pressure drop by the following relationship

$$\Delta P = A \cdot v_{in}^2 + B\, v_{in} + C \qquad (6.31)$$

which is solved iteratively for all channels.

The constants A, B and C can be evaluated by integrating the momentum balance equation (Eq. 6.12) over the height of the channel, and combining it with the expressions for friction (Eq. 6.14), acceleration and restriction losses (Eq. 6.13).

(6.32)

with

K_{in}, K_{out} = Restriction loss coefficients at channel inlet and outlet, respectively

u_{in}, u_{out} = Momentum flow at channel inlet and outlet, respectively

$F_{out} - F_{in}$ = Friction forces integrated over the channel

g = gravity acceleration constant

ρ_f, ρ_g = density for water and steam, respectively

ℓ = channel height

α = void fraction

This formulation assumes restriction losses at the inlet and the outlet of the channel only, which then should also include the effect of the spacers.

Equation (6.32) will require information on steam quality, slip and void locally throughout the channel. For these parameters, the following approximations are made :

- the slip has a constant value, S.
- the steam quality varies linearly between zero at the bulk boiling boundary and X_{exit} at the core exit. The bulk boiling boundary, as well as the exit quality are calculated assuming thermodynamic equilibrium :

(6.33)

(6.34)

(6.35)

The void distribution is now given by

$$\alpha(z) = \frac{X(z)}{X(z) + \left[1-X(z)\right] \cdot S \cdot \frac{\rho_g}{\rho_f}} \qquad (6.36)$$

Introducing Equations (6.35) and (6.36), together with the expression for the momentum flow, Equation (6.11), and the friction correlation, Equation (6.14) into Equation (6.32) will yield :

(6.37)

5

The exponent, , within the integral is now approximated by 1 and the expression within the bracket (containing the logarithm) is approximated by a second order Taylor expansion around a given point v_{in}^{o}.

Equation (6.37) then takes the quadratic form associated with Equation (6.31) and the inlet velocity can be calculated, given the pressure drop. In the iteration process, several channels are first lumped together into larger groups. After a few iterations, the problem is solved for individual channels until the pressure drop over all channels is equalized.

6.3.2 Calculation of Void Distribution

The detailed void calculation starts after the flow calculation, described in §6.3.1 above, is finished. There is no return path from the void calculation to the flow calculation.

The mass and energy balance equations (Eqs. 6.7 and 6.8), are applied to each section in the channel, and are combined with the boiling model (Eqs. 6.22 and 6.23); the slip model (Eq. 6.17) and the heat transfer models (Eqs. 6.25 and 6.26). All material thermo-dynamic properties are assumed constant in the reactor core and corresponding to the specified system pressure.

The inlet mass flow and temperatures for both steam and water are known from the solution in the previous section. The set of equations may then be condensed to

$$\psi = f(T_f, \alpha)$$

$$T_f = g(\psi)$$

$$\alpha = h(\psi)$$

or alternatively,

$$\psi = f\left[g(\psi), h(\psi)\right] = F(\psi) \qquad (6.38)$$

Equation (6.29) is solved by an iteration procedure.

The results of the calculations are the flows, temperatures and void fractions on the volume interfaces. The mean void fraction in section i, given by

$$\bar{\alpha}_i = \frac{\alpha_i + \alpha_{i+1}}{2} \qquad (6.39)$$

where

α_i = void fraction on the inlet to section i

is being used as the feedback parameter to the neutronics solution.

6.3.3 Treatment of Void in the Bypass Channel

In the flow and void calculations outlined above, the bypass flow is modelled as one flow channel, representing all flow paths not encountering any heat conduction from the fuel pins. The nuclear cross-sections are normally generated with no void in the inter-channel flow area or in the internal water holes, so any void appearing in the bypass flow channel will therefore have no nuclear feedback.

As an option, PRESTO-B may calculate the bypass void fraction individually for each fuel assembly, and by adding this void volume to the in-channel void for that bundle, account for the nuclear feedback from the bypass void. These calculations include the following simplifications :

- the single (lumped) bypass channel flow is distributed between the fuel channels, accounting for interchannel area differences and the presence of control rods

- the heat generation rate is affected by inserted control rods

- the axial void distribution is calculated in the individual bypass flow volumes assuming a homogeneous equilibrium model with constant flow

- the calculated bypass void is spread out over the corresponding in-channel flow area to yield an effective in-channel moderator density.

TABLE 6.1 Thermal Hydraulic Model Parameters

PARAMETER	ACRONYM	EQUATION NO.	RECOMMENDED VALUE
Two-Phase Friction Coefficient	A_F	(6.16)	2400.
Fanning Friction Factor	G_1	(6.15)	0.22
	G_2	(6.15)	0.2
Slip Coefficients	B_1	(6.19)	
	B_2	(6.19)	
	v_1	(6.19)	
	v_2	(6.19)	
	v_c	(6.17)	
	δD	(6.21)	
Boiling Model Coefficients	R_ℓ	(6.23)	
	R_1	(6.23)	
	K	(6.23)	
Direct Heat Fractions	δ_1	(6.29)	
	δ_2	(6.29)	

2,3

7. POWER DISTRIBUTION AND FUEL DEPLETION CALCULATION

7.1 Nodal Power Distribution

The relative nodal power is calculated on the basis of the nodal two-group flux distributions :

$$P^{rel} = C(\Sigma_{f1} \cdot \bar{\Phi}_1 + \Sigma_{f2} \cdot \bar{\Phi}_2) \tag{7.1}$$

where C is a normalization constant such that :

$$\left(\sum_{n=1}^{NMAX} P_n^{rel} \cdot V_n \Big/ \sum_{n=1}^{NMAX} V_n \right) = 1.0 \tag{7.2}$$

where

NMAX = number of nodes

V_n = nodal volume

The nodal average linear heat generation rate (APLHGR) is calculated in W/cm as follows :

$$APLHGR = \frac{Q_{TH} \cdot Q_{COND}}{N_{TOT} \cdot N_p(I) \cdot D_z} \cdot P^{rel} \tag{7.3}$$

where

Q_{TH} = full core thermal power (w)

Q_{COND} = fraction of power conducted through cladding (~96%)

N_{TOT} = total number of nodes in a full core

$N_p(I)$ = number of fuel pins - depends on fuel type (I)

D_z = nodal height (cm)

The nodal maximum linear heat generation (MLHGR) rate is calculated as :

$$MLHGR = APLHGR \cdot P_{pin} \tag{7.4}$$

P_{pin} is the relative pin-power peaking factor in the node :

$$P_{pin} = P_I(E, \alpha_x, \alpha)\left[1 + C(I) \cdot C_f\right] \tag{7.5}$$

with

$P_I(E, \alpha_x, \alpha)$ = peaking factor, Fuel Type I (obtained from RECORD), represented as polynomial fit in fuel exposure (E), exposure-weighted void (α_x) and void (α) in the same way as the basic cross-sections (see Eq. 4.1).

$C(I)$ = factor accounting for modification of peaking factor for rodded nodes, Fuel Type I

C_f = effective nodal control fraction

The following formula is used to account for 3-D effects near the tip of a control rod :

$C_f = 1.0$ if $X \geq 1.0$

$C_f = X$ if $0 < X < 1$

$C_f = 0$ if $X \leq 0$

with

$$X = (T_p - k + 1)/2 \tag{7.6}$$

where

T_p is the control rod insertion depth (nodes)

k is the axial node index (starting from K=1 for the bottom node)

7.2 Stepwise Burnup Calculation

After calculation of the steady-state power distribution, the calculation may optionally continue with a so-called burnup step calculation. A new steady-state calculation may, again optionally, take place upon completion of the burnup step calculation. In this way, core-follow or predictive analysis may be performed through the operating cycle. The following are involved in a burnup step calculation :

- The nodal fuel exposure and exposure-weighted void distributions are integrated through the step.

- The fuel type dependent average Sm-149 and Pm-149 concentrations are integrated through the step.

- The nodal concentration of one (Ba-140) or two fission product isotopes (used for γ-scanning) is integrated through the step.

The nodal exposure distribution E^n at the end of Burnup Step n is calculated as :

$$E^n = E^{n-1} + \Delta E^m \cdot \bar{P} \frac{\bar{\rho}}{\rho} \qquad (7.7)$$

where

ΔE^n = Length of Burnup Step n (MWD/TU)

ρ = Nodal, homogenized Uranium density (g/cm^3) provided as input data for each fuel type (for fresh fuel)

$\bar{\rho}$ = Core average nodal homogenized Uranium density (g/cm^3)

$\bar{P}$ = Nodal relative power averaged over time through Step n

Normally, $\bar{P}$ is taken as the beginning of step relative power distribution; however, optionally the following formula may be used :

$$\bar{P} = P^n \cdot R_c + P^{n+1} (1-R_c) \qquad (7.8)$$

where R_c is an input constant (i.e., 0.5).

Since P^{n+1} depends on E^n, an iterative solution is employed. The exposure-weighted void distribution is calculated as follows :

$$\alpha_x^n = \frac{V_x^n}{E^n} \tag{7.9}$$

with

$$V_x^n = V_x^{n-1} + \alpha^n \cdot \Delta E^n \tag{7.10}$$

7.3 Cycle Burnup (Haling) Calculation

Let $\overline{P}$ of Equation 7.7 represent the average power distribution over an operating cycle, ΔE^n the cycle length in MWD/TU, and E^{n-1} the beginning of cycle exposure distribution. The end-of-cycle power distribution, P^n, will then be a function of the end-of-cycle exposure distribution, E^n, and the end-of-cycle operating condition. The following relationship is assumed :

$$\overline{P} = F_i \cdot P^n \tag{7.11}$$

where

F_i is a fuel type (i) dependent correction factor

(normally : $F_i = 1.0$ for all i)

Starting from a guess for $P^n (= P^{n-1})$, a first estimate of E^n is calculated from Equation 7.7. With this exposure distribution, a new P^n distribution may be calculated. The iteration is continued until certain convergence criteria on E^n are satisfied. The resulting exposure distribution, E^n, represents the end-of-cycle state which would be obtained with a cycle average power distribution $\overline{P}$ related to the end-of-cycle distribution P^n through Equation 7.11. The correction factor F_i may be used to account for known power sharing characteristics among different fuel types.

The cycle length ΔE^n may either be input or calculated by the code from a given end-of-cycle k_{eff}-value :

$$\Delta E_j^n = \left(\frac{\partial k}{\partial E}\right)^{-1} \left(k_{eff}^{EOC} - k_{eff,j}\right) \qquad (7.12)$$

where

$\left(\frac{\partial k}{\partial E}\right)^{-1}$ = given (input) coefficient $\approx \left(\frac{\partial k_\infty}{\partial E}\right)^{-1}$

j = iteration index

Haling calculations may be performed for one, two or three-dimensional problems.

7.4 Integration of Sm-149 and Ba-140 Concentrations

Certain fission product isotopes are tracked as functions of time in a simulated reactor operation. The fuel type average concentrations Pm-149 and Sm-149 are followed to account for the influence of nonequilibrium Sm-149 on the calculated k_{eff} (the influence on the power distribution is negligible). Equations are given in Appendix A2.

The nodal concentrations of Ba-140 and of one additional isotope (User specified) are treated to enable direct comparisons with distributions measured by γ-scanning of exposed fuel.

Each fission product concentration is integrated through one or more time steps per burnup step. Each time step is characterized by its length in days and by the reactor total power.

The equations for integration of the γ-scan isotopes are given in Appendix A3.

8. PREDICTION OF CORE PERFORMANCE PARAMETERS

8.1 Model for TIP and LPRM Calculation

Fixed, in-core, local power monitors (LPRMs) and travelling, in-core probes (TIPs) may be included in the PRESTO core simulation. The instrument tubes (TIP strings) are assumed to be located in the watergaps between the fuel assemblies, each string being surrounded by four assemblies. The string locations are specified by giving the channel numbers for each of these four assemblies. TIP strings located outside the modeled core fraction (if not full core model) may be included by folding into symmetric positions within the modeled fraction. Four LPRMs are assumed to be located at different axial elevations (Levels A, B, C and D) within each string. The axial height (cm) of each detector level is specified as input. The calculated TIP or LPRM signal, at a given axial height, is a function of the local conditions in each of the four assemblies surrounding the string :

$$T_k = \frac{1}{4} \sum_{i=1}^{4} m_{k,i} \cdot P_{k,i} \qquad (8.1)$$

where

T_k = calculated signal, axial node k

$m_{k,i}$ = instrument factor, axial node k, assy. no. i

$P_{k,i}$ = relative nodal power, axial node k, assy. no. i

The instrument factor (m-factor) is obtained by interpolation in data given as input for various values of fuel exposure and exposure-weighted void. The m-factors are also given for both control-rod-in and control-rod-out conditions.

The m-factor is defined as the signal generated per unit nodal power. Such m-factors are calculated in RECORD. The normalization of the m-factors is irrelevant; however, it is recommended to use values around unity.

The calculated TIP signal is obtained from Equation 8.1 with k = 1, 2, ... KMAX. The calculated LPRM signal at a given axial level is obtained by interpolation between the two nearest (axially) axial nodes of the TIP calculation.

Measured TIP data may be provided as input for comparison between calculation and measurement.

The total area under all measured curves is calculated and compared to the total area under the corresponding calculated curves. The measured TIP values are then normalized, using the ratio of calculated-to-measured total area as a normalization factor. Thus, the ratio of calculated-to-measured area for each curve (after normalization) serves as a comparison between the calculated and measured radial power distribution.

The difference between calculation and measurement in each of the KMAX points for each string is used to calculate the statistical standard deviation (RMS). Standard deviations are also calculated for each string, for each of four axial core regions (KMAX divided into four equal regions), and for "rodded" and "unrodded" regions, separately.

The calculated LPRMs are normalized to an average value of 100 · CALPRM, where CALPRM is a User-specified (input) calibration constant. LPRMs are printed out in a special map format, similar to the usual BWR process computer format. The LPRM map format may be specified as a full-core map, even if only a core fractional (e.g., 1/4-core) model is used. TIP strings located outside the modeled fraction will then be shown in their real positions.

Results of TIP calculations and comparisons between calculated and measured TIPs may be plotted as lineprinter plots by PRESTO, or plotted externally by the TIPPLOT Program.

Measured LPRM readings may be provided as input data. Whenever such data is input, the ratio of measured-to-calculated signal of each detector is calculated and stored for use in subsequent runs.

Predicted LPRM readings at time points where no measured readings are given are defined as :

$$ESTPRM(I,K) = COFPRM(I,K) \cdot PLPRM(I,K) \qquad (8.2)$$

where

ESTPRM(I,K) = predicted LPRM reading, String I, Level K

PLPRM(I,K) = calculated LPRM signal, String I, Level K

COFPRM(I,K) = ratio of measured-to-calculated signal, String I, Level K, from last time point with measured data

These predictions represent best-estimate predictions of expected LPRM readings and are recommended for use in reactor operations support applications.

8.2 Calculation of Margins to Thermal Limits - BWR

8.2.1 Critical Heat Flux Ratio (CHFR)

The critical heat flux, which is the value of the heat flux at the onset of nucleate boiling, is calculated for each node by applying the Hench-Levy Correlation (Ref. 9). The flow quality and the mass flow rate, as calculated in the thermal-hydraulics module, are input to the correlation equations.

Subsequently, the critical heat flux ratio is found as the ratio between the critical heat flux (Q_c) and the maximum actual cladding heat flux (Q_m) within each node :

$$CHFR = Q_c/Q_m \qquad (8.3)$$

with

$$Q_m = \frac{Q_{TH} \cdot \delta_1}{A_{S,TOT}} \cdot P^{rel} \cdot P_{pin} \qquad (8.4)$$

where

Q_{TH} = Total core thermal power (w)

δ_1 = Fraction of power appearing as heat transferred through cladding

$A_{S,TOT}$ = Total heated surface area (cm)

P^{rel} = Nodal relative power (see Eq. 7.1)

P_{pin} = Pin-power peaking factor within node (see Eq. 7.5)

8.2.2 Fraction of Limiting Power Density (FLPD)

A linear power density, considered as limiting with respect to vital fuel performance parameters, such as clad integrity, may be given as input to PRESTO. Different values may be given for each fuel type.

The ratio between the actual maximum linear heat generation rate (MLHGR), as calculated by Equation 7.4, and the corresponding limiting value (HGRLIM) is calculated for each node :

$$FLPD = \frac{MLHGR}{HGRLIM} \qquad (8.5)$$

8.2.3 ECCS - Fuel Heat Storage Limit

Fuel type and exposure-dependent values of average linear heat generation rates (EXPECC), considered as limiting with respect to the LOCA behaviour, may be given as input to PRESTO.

The ratio between the actual average linear heat rate (APLHGR) and the limiting value is calculated for each node :

$$ECCSR = \frac{APLHGR}{EXPECC} \qquad (8.6)$$

APLHGR is calculated by Equation 7.3.

8.2.4 Thermal Limits Summary Table

The 12 most limiting positions in the core with respect to maximum linear heat generation rate and the three limiting ratios described above, are compiled and edited in a special output table for User convenience.

9. XENON DYNAMICS MODEL

Reactor operations involving slow transients, such as reactor startups, power cycling and control rod pattern exchange maneuvers, may be simulated with PRESTO-B, using the Xenon transient, multi-time-step mode of calculation. Under conditions involving transients in local or global power, the local Xe concentration will be out of balance with its predecessor I-135.

Since Xe has a strong influence on the local neutronics properties as described in 4.2.2, both reactivity and power distribution will be influenced under transient Xe conditions.

The time-dependent nodal Xe concentration is calculated in PRESTO, starting from a state of equilibrium or from Xe-free conditions.

Analytic solutions of the differential equation for the time-dependent I and Xe nodal concentration equations are used to find the concentrations at time $t + \Delta t$, starting from the concentrations at time t. The assumption of constant local power and neutronic properties during the time step Δt is assumed. The equations, as programmed in PRESTO-B, are given in Appendix A1.

The reactor operating period to be simulated is described by the User by specifying the reactor operating data (power, flow, subcooling and rod pattern), characterizing the reactor state for a number of time points through the period. A 3-D converged power-void calculation is obtained at each time point. The interval between two successive time points is subdivided into a User-specified number of substeps for the purpose of Xe-integration.

The relative power distribution as calculated at time point i is used for the interval i to $i + 1$; however, the total reactor power and, thereby, the absolute nodal power values are adjusted at each substep, as illustrated in Figure 9.1.

Criticality search options on reactor power level or coolant flow rate may be exercised in the Xe-dynamics mode of calculation. The calculation at each time point will then include an outer iteration to determine the power level (or flow rate) required to maintain a given, critical k_{eff} value. The iteration is terminated by a convergence criterion, which is a factor of 2 larger than the k_{eff}-criterion applied within the power-void loop.

Also included under the Xe-transient option is a calculation of the maximum rate of change of nodal power density with time (maximum power ramp rate), and recording of the core location where the maximum ramp rate occurs. The search for the maximum ramp rate is limited to nodes where the power exceeds a User-specified limit. This feature allows User to compare simulated ramp rates with limits recommended for fuel integrity protection.

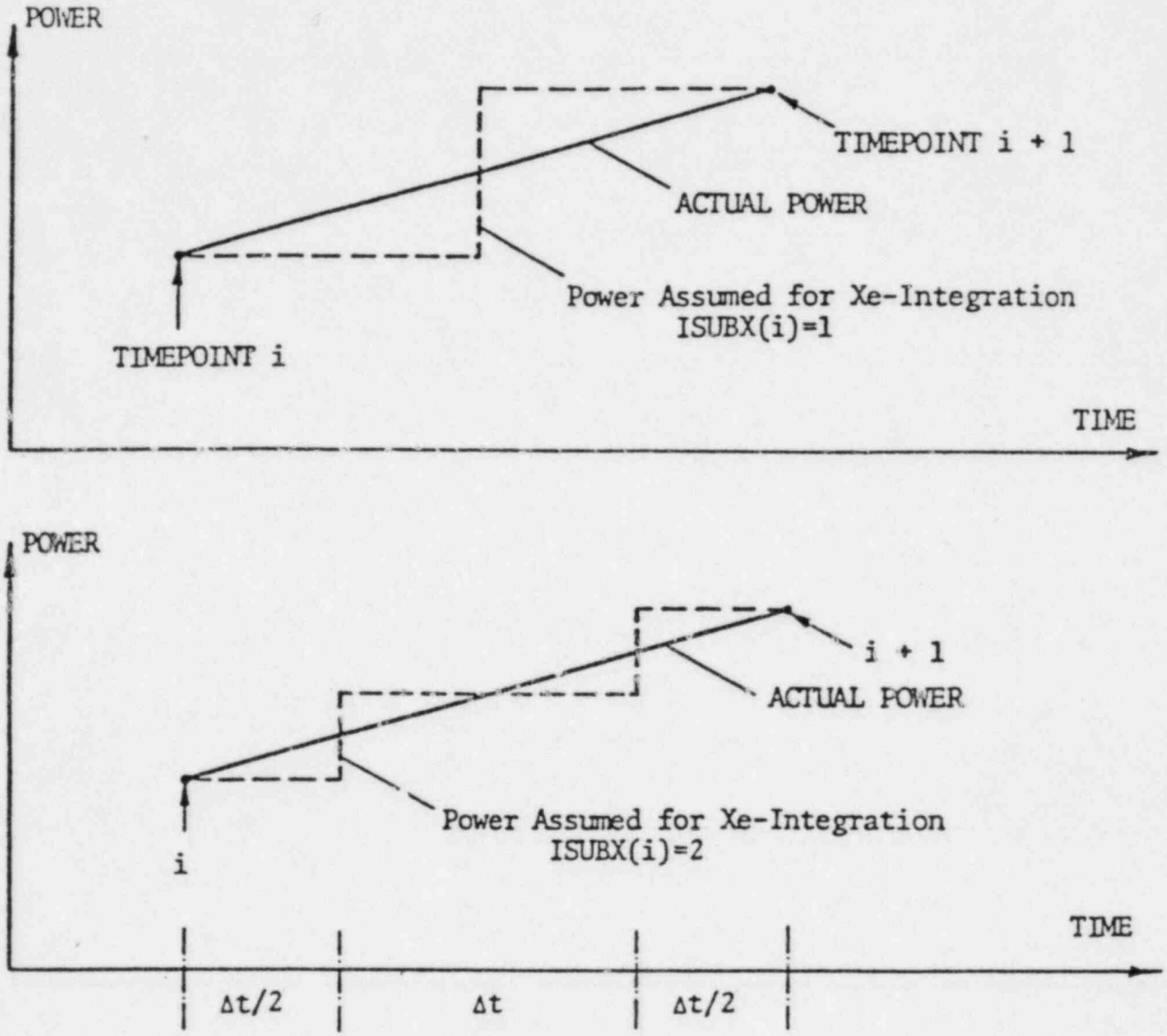

FIGURE 9.1 Illustration of Substeps Used for Xe-Integration Between Each Statepoint Calculation (i)

10. AUXILIARY FUNCTIONS INCORPORATED IN PRESTO-B

A number of auxiliary functions are built into PRESTO-B to aid the User in performing specific analytical tasks. The underlying methods are not described in this report.

10.1 Critical Control Rod Pattern Search Option

A search option is available, where the insertion of certain User-defined control rods is determined in an iterative way, to obtain a feasible rod pattern with otherwise given reactor operating data. The rod pattern is considered feasible when the calculated k_{eff} is close to a given target value. The method normally produces acceptable power distributions, however, the User may perform a manual correction to further improve the solution. The critical rod search algorithm in PRESTO-B is based on and similar to that described in Reference 10.

10.2 Shutdown Margin Evaluation

Performing a cold condition analysis with all control rods fully inserted, the User may select an option that performs a "stuck rod priority selection". The control rods are sorted according to expected rod worth, using a simplified perturbation theory method or a method based on flux-weighted, average k_{∞}-values for the four bundles adjacent to each control rod. The code may also be set to pull single control rods according to the priority list, and perform a series of criticality calculations to determine the single stuck rod shutdown margin.

10.3 Core Reload Analysis Features

All fuel assemblies involved in the PRESTO-B Model are kept on a separate data file and updated as to the fuel history parameters in each PRESTO-B calculation. Fuel assemblies from the file may be "loaded" in any core location, enabling easy simulation of fuel shuffling and reinsertion. Fresh fuel, which may be added, will automatically be included on the fuel file. Fuel that has been

discharged from the core will remain on the file until it is deliberately deleted by the User. A number of User aids, in the form of special checking and editing routines, are available in PRESTO-B to facilitate reload simulation.

10.4 Fuel Discharge Priority List

An option is provided for guiding the User in selecting fuel assemblies to be discharged at the end of an operating period. All fuel in the core is sorted according to certain criteria (a combination of reactivity and burnup) and a discharge priority table is printed in the output.

10.5 Functional Relationships between Heat Balance Components

The User normally provides the process data entering the heat balance calculations outlined in Section 6.1.

However, as an option, plant specific functional relationships may be specified in order to facilitate predictive calculations or perturbation studies where process data are not available.

The following system functions are defined :

Steam dome pressure vs. steam flow :

$$P_{SD} = P_{syst} + C_1\left(\frac{W_S}{W_{S_{rat}}} - 1\right) + C_2\left(\frac{W_S}{W_{S_{rat}}} - 1\right)^2 \qquad (10.1)$$

Core pressure vs. core exit flow conditions :

$$P_C = P_{SD} + C_3 \cdot \rho_x + C_4 \cdot \frac{W_T^2}{\rho_x} \qquad (10.2)$$

Pump heat vs. total core flow :

$$Q_p = C_5 + C_6 \cdot w_T + C_7 \cdot w_T^2 + C_8 \cdot w_T^3 \qquad (10.3)$$

Bypass flow fraction vs. total core flow :

$$f_B = C_9 + C_{10} \cdot \left(\frac{w_T}{w_T^{rat}} - 1\right) + C_{11} \cdot \left(\frac{w_T}{w_T^{rat}} - 1\right)^2 \qquad (10.4)$$

Feedwater enthalpy vs. steam load :

$$h_{fw} = f^{TABLE} \cdot \left(\frac{w_S}{w_S^{rat}}\right) \qquad (10.5)$$

where

P_{SD} = steam dome pressure

P_C = core pressure

P_{syst} = "system" pressure

w_S = steam flow

w_S^{rat} = rated steam flow

ρ_x = density at core exit

w_T = total core mass flow

Q_p = pump heat

w_B = bypass flow

h_{fw} = feedwater enthalpy

$C_1 \ldots C_{11}$ = input constants

f^{TABLE} = input data table

11. CODE QUALIFICATION

11.1 Fine Mesh Diffusion Theory Benchmarks

A benchmark problem for 3-D neutronics code evaluation, originally developed by the Danish Atomic Energy Commission, is described in Reference 3. Specifications for this problem, also referred to as the IAEA 3-D Benchmark, are provided in Figure 11.1. Several fine mesh solutions have been published in Reference 3. At the moment, the most accurate solution is considered to be the so-called "VENTURE-extrapolated". This was produced by extrapolating to an infinite number of mesh points, based on solutions with increasingly finer mesh :

1 - 17 x 17 x 19 mesh

2 - 34 x 34 x 38 mesh

3 - 68 x 68 x 76 mesh

4 - 102 x 102 x 114 mesh

5 - Extrapolated

The VENTURE-extrapolated solution is taken as the reference in this report.

Solutions for the corresponding 2-D problem (core midplane of the 3-D problem) have also been produced with many different codes. The current reference is an ultra-fine mesh PDQ solution, also published in Reference 3.

PRESTO results for the 2-D and the 3-D problems are given below. Option 1 for the thermal flux calculation was used. (See Section 5.1.)

An overview of the calculations performed is given in Table 11.1. Mesh widths of 20 cm and 10 cm were used and the 3-D problem was run with both cubical and strongly noncubical nodes.

Results are given in the following Figures :

Figure 11.2 2-D Bundle Power, 20 x 20 cm nodes
Figure 11.3 2-D Bundle Power, 10 x 10 cm nodes
Figure 11.4 3-D Bundle Power, 20 x 20 x 20 cm nodes
Figure 11.5 3-D Bundle Power, 10 x 10 x 20 cm nodes
Figure 11.6 Axial Power, Partly Rodded Bundle, 20 x 20 x 20 cm nodes
Figure 11.7 Power Along X-Axis, Core Midplane, 20 x 20 x 20 cm nodes

A series of 2-D benchmark results of four-bundle power sharing and eigenvalues were generated for six different, typical BWR configurations as shown in Figure 11-8.

Two bundle enrichments and three void fractions were employed. A control blade was inserted adjacent to one of the four bundles in three cases.

The reference data were generated by RECORD/MD-2 5-group diffusion theory solutions, with zero current boundary conditions, and with exactly the same, detailed geometrical representation of fuel pin cells, watergaps and control rods as in RECORD.

PRESTO results were generated using both Option 1 and Option 2 for the thermal flux representation. (See Section 5.1.)

Results are given in Figure 11.8. The following statistical data were obtained :

Model	Standard Deviation (PR - REF)	
	Nodal Power	Eigenvalue
Option 1	$\pm$1.6%	+.00040$\pm$.00114
Option 2	$\pm$1.2%	-.00030$\pm$.00066

Excellent agreement in both nodal power and eigenvalue was obtained with Option 2 (more detailed thermal flux model); however, the results for Option 1 are fully acceptable.

These results are the primary basis for evaluation of the gradient correction factors of the PRESTO neutronics model.

11.2 Qualification of Hydraulics Model

The FRIGG void loop experimental data (Ref. 4) were analyzed with the thermal-hydraulics model of PRESTO. The measurements were performed on a full-scale coolant loop with an electrically heated fuel assembly mockup. The operating conditions of the experiment are listed in Table 11.2. The range of the parameters characterizing the operating conditions are given in Table 11.3. The PRESTO hydraulics model parameters used are listed in Table 11.4. Results showing calculated and measured axial void profiles for 31 different experimental conditions are shown in Figures 11.9 - 11.39. The overall standard deviation, RMS, of the difference between calculated and measured void, in per cent void, was 2.1%. This quantity was defined as :

$$RMS = \left[\frac{1}{N-1} \sum_{i=1}^{N} (X_i - \bar{X})^2 \right]^{\frac{1}{2}} \qquad (11.1)$$

with

$$X = \alpha_{calc} - \alpha_{meas} \quad (\%)$$

N = Number of points

The number of points N was 243, and the total mean deviation $\bar{X}$ was 0.58% void.

The experimental standard deviation determined from calibration measurements with a plexiglass mockup was 2.0% in void.

The overall correlation between calculated and measured void is illustrated in Figure 11.40.

11.3 Comparison with Gamma Scan Data for EOC-1 of HATCH-1

An analysis of the HATCH-1 EOC-1 gamma scan data was performed by Scandpower as part of a general benchmarking effort of PRESTO-B, using

RECORD lattice physics data. The work was funded by members of the European FMS User Group, the Institute for Energy Technology, Norway, and Scandpower A/S, Norway.

The HATCH gamma scan data represents a valuable data base for evaluation of the ability of a code system like RECORD/PRESTO to predict complicated BWR power shapes. In particular, detailed measurements of the influence of partially inserted control rods on the power distribution in adjacent fuel were carried out. Thus, predictions of the important power shaping aspect of BWR control rods may be evaluated.

Since the measurement covered a complete core octant, relative bundle power comparisons may also be carried out. Comparisons of rodded versus unrodded bundles and core periphery versus core interior bundles are also of special interest.

Design and operating data for Cycle 1 of HATCH-1 are given in EPRI Report NP-562 (Ref. 11).

The results of the measurements, as well as the gamma scan technique and the data acquisition system, are described in EPRI Report NP-511 (Ref. 12).

11.3.1 The Gamma Scan Measurements

Gamma scan measurements of 106 bundles of the initial HATCH-1 BWR core were performed by General Electric at EOC-1, in a program jointly sponsored by EPRI and G.E.

The 106 gamma scanned bundles are shown in Figure 11.41. Seventy-five of these comprise a complete octant of the core. The additional 31 bundles are located in four-bundle cells, around real or psuedo instrument locations symmetric to those in the octant. These cells were chosen to evaluate any real asymmetry in the core.

All 106 bundles were measured at a minimum of 12 axial positions, as shown in Table 11.5, which correspond to the midpoints of the odd

numbered PRESTO-B nodes. Partially controlled bundles were measured at additional positions in the vicinity of the control blade tip.

Six bundles were measured at 24 or 27 axial elevations to obtain a detailed profile of the axial La-140 shape. Four of these, located at positions 14-08/14-09/15-08/15-09, Figure 11.41, were disassembled for single-rod scanning, to obtain local power distribution measurements.

The uncertainty in the measurements was determined from repeated measurements of the standard bundle. The total uncertainty in nodal La-140 concentration, quoted in Reference 12, is 1.7%. This value includes the uncertainty associated with representing the activity of a node by the average of the four corner count rates, as well as single measurement reproducibility.

11.3.2 Simulation of the Cycle-1 Operation

Reactor operation through the first cycle was simulated with PRESTO-B, with the objective of predicting the EOC La-140 distribution for comparison with the corresponding measured distribution.

The calculation was carried out using 33 burnup steps, as shown in Table 11.6. Operating data, characterizing each step, were obtained from EPRI Report NP-562 (Ref. 11).

All core dimensional data and core-specific thermal hydraulic parameters required for the PRESTO-B core model were obtained from the mentioned EPRI report.

A complete nuclear cross-section data bank was generated with RECORD, based on the published fuel design data.

The data bank consisted of the following :

> Two-group macroscopic cross-sections, diffusion coefficients pin-power peaking factors as functions of burnup, exposure-weighted void and instantaneous void (see Section 4.1).

A perturbed cross-section set, assuming 15% void in the water gaps at 70% in-channel void. (No water gap voidage at 0% and 40% in-channel void.)

Coefficients for the influence of control rods, Xenon, Doppler, and Samarium models in PRESTO-B account for differential effects relative to the corresponding equilibrium values. The control rod and spacer grid effects are included as additive terms to the thermal group-absorption cross-section

The perturbed data set was used to account for a slight water gap voidage caused by plugging of the bypass flow holes in the core support plate. This data set was used after the core-average burnup had reached 4000 MWD/TU, approximately corresponding to the time when the bypass plugging was performed. The reactivity effect of the assumed water gap void fraction (15%) was 0.8% in Δk at 70% in-channel void.

A 1/4-core symmetric core model was set up to generate the reflector boundary conditions at EOC-1. First, an approximate EOC condition was obtained by running through the 33 burnup steps with a 1/4-core model, using typical BWR reflector boundary conditions. Then, the ALBMO procedure (an option with PRESTO-B) was used to generate a specific set of boundary conditions for the EOC condition. The latter data was not significantly different from the data used in the 33 burnup steps. These 33 burnup steps were then recalculated, using a 1/2-core model, with the specific reflector data derived as explained above.

The 1/2-core model was used to enable exact representation of all control rod patterns associated with each of the burnup steps.

The nodal distribution of Ba-140 was automatically tracked through the 33 burnup steps and the EOC distribution was saved on a file for comparison with the corresponding experimental La-140 distribution.

Detailed simulation, using an option in PRESTO-B where each burnup step is further subdivided into time steps, was performed for the last three months of operation to ensure proper integration of the Ba-140 nodal concentration distribution. The reactor total power was given for each

time step, closely resembling the actual power history; thus accounting for, e.g., Ba-140 decay during periods of shutdown within the time period of a burnup step. The following steps were applied :

BURNUP STEP NO.	STEP LENGTH (MWD/TU)	NO. DAYS	NUMBER TIME STEPS
28	377	24	13
29	427	23	8
30	54	4	3
31	236	29	9
32	191	12	5
33	89	5	3

Comparisons with plant data, such as the process computer core-average axial power distribution, were performed at some points during the simulation of the operating history, to make sure the power distribution was reasonably accurately represented. Some examples of such comparisons are shown in Figures 11.42 and 11.43.

Plots of calculated k_{eff} and core-average void fraction versus core-average exposure through Cycle 1 are shown in Figure 11.44. The reactor power level and control density are also shown.

The cycle-average k_{eff} was 0.99715, with a standard deviation of 0.00246. The EOC value was 0.99621.

11.3.3 Comparison of Calculated and Measured La-140 Distributions

The time between reactor shutdown and the actual measurement was sufficient to justify the assumption that the measured La-140 intensities were in equilibrium with the corresponding Ba-140 concentrations. Thus, the two distributions would be proportionate.

In order to compare calculated and measured data, normalization was performed as follows :

$$\frac{1}{N} \cdot \sum_{\text{octant}} P_{calc} = 1 \qquad (11.2)$$

A normalization factor, c, was defined for the measured data :

$$\frac{c}{N} \cdot \sum_{\text{octant}} P_{meas} = 1 \qquad (11.3)$$

The nodal standard deviation (σ) was found from the following expression :

$$\sigma = \left[\frac{1}{N} \sum_{\text{octant}} \left(P_{calc}(I,J,K) - c \cdot P_{meas}(I,J,K) \right)^2 \right]^{\frac{1}{2}} \qquad (11.4)$$

where

I,J,K = coordinates of nodes with measured data

N = total number of data points

c = normalization factor

The standard deviation thus calculated was 6.4%. Separating controlled and uncontrolled nodes, the following result was obtained :

TYPE NODE	NO. DATA POINTS	STANDARD DEVIATION (%)
Controlled	182	6.4
Uncontrolled	828	6.5
TOTAL	1010	6.4

An overview of the plots, comparing measured and calculated data, is shown in Figure 11.45. Individual bundle plots are shown in Figures 11.46 through 11.54. These plots are shown for all six bundles measured with at least 24 axial points (Figures 11.46 - 11.50) and for typical distributions of the following categories :

- Unrodded, core-interior bundle (Fig. 11.51)
- Bundle with deep control rod insertion (Fig. 11.52)
- Bundle with shallow control rod insertion (Fig. 11.53)
- Unrodded, core-periphery bundle (Fig. 11.54)

Bundlewise ratios between calculated and measured, axially integrated curves are shown in Figure 11.55. This representation illustrates the average radial, or bundle power, comparison. The total standard deviation in the bundlewise comparison was 2.5% (75 bundles). Three bundles (Nos. 251, 514, 487) showed uncorrelated deviations of about 10%. Excluding these three bundles, the standard deviation in the bundlewise comparison was 1.8% (72 bundles). The average bundle power ratio and the bundlewise standard deviation was calculated for each of the following groups of bundles :

	NO. BUNDLES	AVERAGE RATIO	STANDARD DEVIATION (%)
Rodded Bundles	22	1.012	1.8
Unrodded Bundles	53	0.995	2.7
Core Periphery Bundles	10	1.026	3.3
Core Interior Bundles	65	0.996	2.3
TOTAL	75	1.000	2.5

Excluding the three "bad" bundles, the following results were obtained :

	NO. BUNDLES	AVERAGE RATIO	STANDARD DEVIATION (%)
Rodded Bundles	22	1.012	1.8
Unrodded Bundles	50	0.992	1.8
Core Periphery Bundles	8	1.005	1.0
Core Interior Bundles	64	0.997	1.9
TOTAL	72	0.998	1.8

Comparisons of calculated and measured axial pin-wise La-140 distribution were performed for four different fuel pins (the narrow-narrow and wide-wide corner pins of Assembly Nos. 373 and 393).

The calculated pin-wise axial distributions were obtained by multiplying the nodal distributions calculated by PRESTO with pin-to-node power-peaking factors obtained from the RECORD Data Bank. Peaking factors for each axial node were calculated by interpolating to the nodal exposure and exposure-weighted void among the values tabulated in the data bank. Different sets of peaking factors were used for the rodded and the unrodded condition. Results are shown in Figures 11.56 and 11.57.

Calculated and measured curves were normalized separately for each pin.

In general, the pin-wise axial shapes are well reproduced. Especially the ratio between the power levels in the "rodded" and "unrodded" portions of the pins are in excellent agreement.

11.3.4 Discussion of Results

NODAL COMPARISONS :

An overview of the nodal gamma scan comparison is presented in Figure 11.45. The total standard deviation was 6.4%, including 1010 data points of the measured core octant.

In general, very good agreement was obtained in comparing calculated and measured axial La-140 shapes. Although not shown in the Figure, it was found that the calculated La-140 distribution agreed well with the calculated EOC power distribution. Thus, the conclusions drawn are valid for the power distribution as well.

The discrepancies seen may be grouped into two categories, as follows :

- In the center region of the core, where the power distribution is relatively flat, the calculation shows a tendency to double hump, while the measurement shows a depression of the "bottom hump". This is probably due to inaccuracies in the calculated EOC exposure distribution resulting from approximations in power distribution modelling throughout the cycle.

- A slight overprediction of the power-peak is observed for some of the sharply top-peaked distributions in the outer region of the core. This phenomenon does not correlate with control rod insertion, and is probably also related to exposure distribution inaccuracies.

The following observations and conclusions are made :

- The influence of partially inserted control rods (both deep and shallow insertion) on the axial power distribution in surrounding fuel assemblies is very well predicted by PRESTO. This is true for the four assemblies immediately adjacent to the control blade, as well as for those located in the next "ring" away from the blade. Both power shape and the rodded-to-unrodded power step are in good agreement with measurements.

- The axial power shape in the throttled periphery bundles (Fig. 11.45) is as good as in the unthrottled assemblies.

BUNDLEWISE COMPARISONS :

A comparison of axially integrated distributions (ratios of calculation-

to-measurement) is shown in Figure 11.55. These results are directly applicable for evaluation of PRESTO's bundle power prediction.

The following observations and conclusions are made :

- The general agreement between calculated and measured "bundle power" is quite good. The standard deviation was 2.5%, with all bundles included, and 1.8% with 3 of the 75 bundles excluded from the comparison.

- There are no systematic radial tilts.

- Periphery bundle power is calculated with the same precision as core-interior bundles.

- Rodded bundle powers are in good agreement with measurements (average ratio 1.012).

- Errors of about 10% in the ratio of calculation-to-measurement occur in three different, uncorrelated positions : Bundle Nos. 487, 251 and 514. The reason for this is unexplained.

PIN-WISE, AXIAL DISTRIBUTION COMPARISONS :

Comparisons of calculated and measured distributions along the W-W corner pin and the N-N corner pin of two partially rodded (deep and shallow rod insertions) assemblies are shown in Figures 11.56 and 11.57.

The following observations are made :

- The axial power shape along the W-W corner rod is very well predicted. Especially the power increase from the "rodded" to the "unrodded" positions of the pin is in almost exact agreement with measurements.

- The calculated axial power shape along the N-N corner rod is also in reasonably good agreement with measurements.

- Figure 11.57 shows that the "long distance" effect (power depression ending at 90 inches elevation) of the control blade inserted to Notch 14 in a diagonally neighboring assembly, is underpredicted in the N-N corner and overpredicted in the W-W corner. This is as should be expected, since the N-N corner is closer to the next control blade.

- The results shown in Figures 11.56 and 11.57 are of interest both for evaluation of the model used in PRESTO for calculation of local maximum pin-power (max. LHGR), and for evaluation of models used for calculation of power shocks associated with control rod movements.

- Control rod withdrawal power shocks are most important for pins adjacent to the rod blade. As seen in the Figures, power shocks seen by the W-W corner pin are very well predicted by the RECORD / PRESTO "overlay" method.

11.4 Comparisons with BWR Operating Data

A list of BWR operating cycles analyzed with PRESTO since its initial development in 1971 is given in Table 11.7.

Lattice data calculated by RECORD were used in all cases, except as indicated in the Table.

Although the basic assumptions of the FMS - RECORD / PRESTO Model remain valid, a number of detailed developments and improvements have been continuously implemented. Thus, a statistical treatment of the accumulated data would not reflect the current status of obtainable accuracy. However, an overview of the experience during the ten year period is given in Reference 13. Applications of PRESTO are reported in References 14 through 19.

Comparisons with BWR operating data have included :

- calculated and measured TIP traces
- calculated and measured LPRM readings

- detector-inferred (process computer) power distributions
- process computer fuel exposure distributions
- predicted and actual critical control rod patterns and analysis of cold, critical cores
- reactivity - core lifetime predictions with actual data
- special gamma scan data for power distribution and exposure distribution evaluation

An extensive analysis of the past operating cycles of CP&L's Brunswick BWRs is presented in a separate report. Examples of results obtained from other reactors are given in the following :

D O D E W A A R D, G.E. BWR-1, 163 MWth (Netherlands)

The first two operating cycles of this natural circulation, small BWR were analyzed with early versions of RECORD / PRESTO during 1971. Satisfactory results were obtained. Examples of TIP-comparisons are shown in Figure 11.58 (Ref. 14).

M Ü H L E B E R G, G.E. BWR, 950 MWth (Switzerland)

The first three cycles were analyzed by Scandpower (Ref. 15). The remaining cycles have been analyzed for core-follow and operations support by the Utility (Cycles 4, 5, 6 and 7). Gamma scan comparisons have been performed as part of the qualification of the code (Refs. 16 and 17). Examples of TIP-comparisons and gamma scan results are shown in Figures 11.59 and 11.60.

B A R S E B Ä C K, ASEA-ATOM BWR, 1700 MWth (Sweden)

Cycle 1 core-follow calculations and Cycle 4 startup analysis performed with PRESTO. Results unpublished.

B R U N S B Ü T T E L, KWU BWR, 2300 MWth (Germany)

Cycle 1 core-follow calculations, including detailed Xe-dynamics simulation of a number of operational transients, were performed. Examples

of TIP-comparisons are shown in Figure 11.61. Results unpublished.

P H I L I P P S B U R G, KWU BWR, 2300 MWth (Germany)

Cycle 1 core-follow calculations performed by the Utility. Gamma scan comparisons performed at about 4000 MWD/TU. Results unpublished.

S A N T A M A R I A de G A R O Ñ A, G.E. BWR, 1380 MWth (Spain)

Cycles 7, 8 and 9 core-follow and operations support performed by Utility in extensive applications. Example of TIP-comparisons are shown in Figure 11.62.

F O R S M A R K - 1, ASEA-ATOM BWR, 2700 MWth (Sweden)

Cycle 1 core modelling and core-follow analysis performed by Scandpower. Results unpublished.

Q U A D _ C I T I E S _ - _ 2, G.E. BWR, 2400 MWth (U.S.A.)

Cycles 1 and 2 analyzed with RECORD / PRESTO by Scandpower, as part of a fuel performance evaluation study for EPRI (Ref. 18). Examples of TIP-comparisons are shown in Figures 11.63 and 11.64.

H A T C H - 1, G.E. BWR, 2400 MWth (U.S.A.)

Cycle 1 core-follow and gamma scan comparison performed by Scandpower. See §11.3.

F I T Z P A T R I C K - 1, G.E. BWR, 2400 MWth (U.S.A.)

Cycle 1 and part of Cycle 2 core-follow performed by the Utility. Results unpublished.

TABLE 11.1 PRESTO 2-D and 3-D Benchmark Runs - Overview

CASE NO.	NO. DIMENSIONS	NODAL DIMENSIONS (cm)	WEIGHT f.*		NO.NODES (Core Fract.)	CPU (sec) CDC CYBER-74	$\left(\frac{k_{eff}}{k_{eff}^{REF}} - 1\right)100$	BUNDLE POWER	
			a_1	a_2				STD.DEV. (%)	MAX.DEV. (%)
02-01	2	20x20	0.0	0.4	52 (1/4-Core)	4.64	0.40	0.93	2.3
02-02	2	10x10	0.0	0.0	94 (1/8-Core)	7.90	0.28	0.63	1.9
03-01	3	20x20x20	0.0	0.4	884 (1/4-Core)	18.02	0.40	1.16	2.6
03-02	3	10x10x20	0.0	0.2	1598 (1/8-Core)	57.90	0.33	0.65	1.3

**See §5.1 for def. of a_1 and a_2. (Recommended values of a_1 and a_2 for BWR applications (mesh width ~15 x 15 x 15 cm) are $a_1 = 0.0$, $a_2 = 0.0 - 0.2$).*

TABLE 11.2 Frigg Loop Operating Data

CASE NO.	POWER	FLOW	SUBCOOLING
001	low	intermediate	low
2	"	low	"
3	"	"	"
4	intermediate	"	"
5	"	"	"
6	"	"	"
7	"	intermediate	"
8	"	"	"
9	"	"	"
10	"	high	"
11	"	"	"
12	high	"	"
13	"	"	"
14	"	intermediate	"
15	"	"	"
16	low	low	intermediate
17	"	"	"
18	intermediate	"	"
19	"	"	"
20	high	"	"
21	intermediate	intermediate	"
22	"	"	"
23	high	"	"
24	"	"	"
25	intermediate	high	"
26	high	"	"
27	intermediate	intermediate	high
28	high	"	"
29	low	low	"
39	intermediate	intermediate	low
40	high	low	"

TABLE 11.3 FRIGG Loop Operating Data

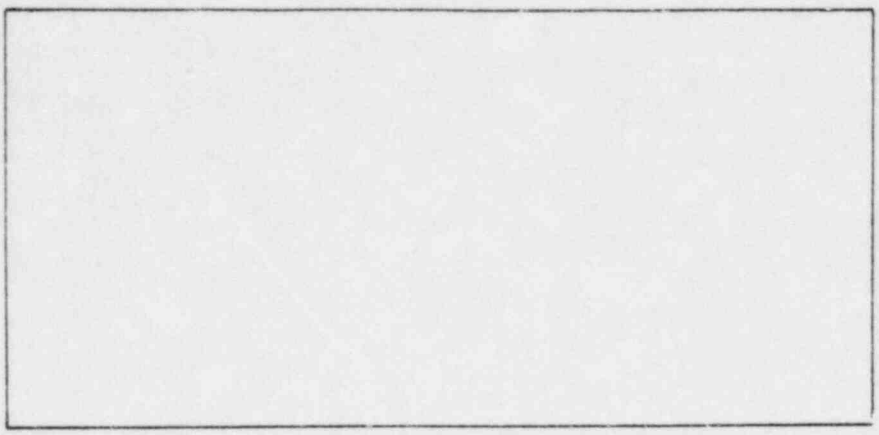

2,3

TABLE 11.4 PRESTO Hydraulics Model Parameters

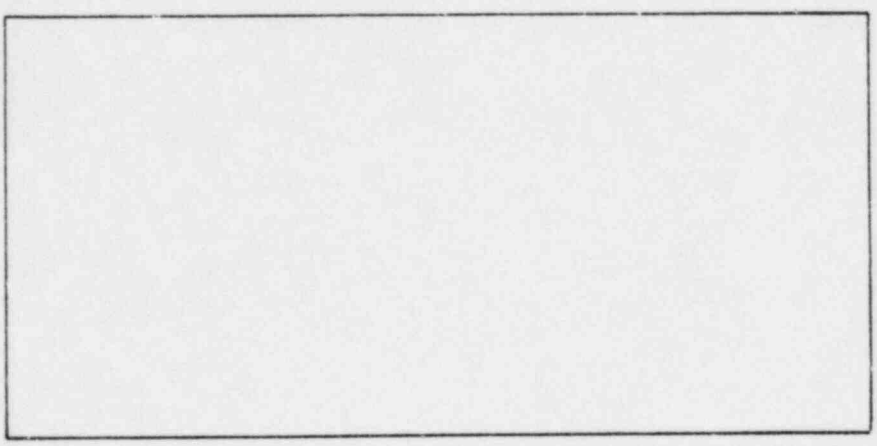

4

TABLE 11.5 Gamma Scan Measurement Positions

MEASUREMENT[1] ELEVATION	CORRESPOND. PRESTO NODE	MEASUREMENT LOCATIONS		
		24-NODE SCANS	12-NODE SCANS	14-NODE[3] SCANS
141	24	X		
135	23	X	X	X
129	22	X		
123	21	X	X	X
117	20	X		
111	19	X	X	X
106[2]	18	X		
97[2]	17	X	X	X
93	16	X		X
87	15	X	X	X
82[2]	14	X		X
75	13	X	X	X
69	12	X		
63	11	X	X	X
57	10	X		
51	9	X	X	X
45	8	X		
37[2]	7	X	X	X
33	6	X		
27	5	X	X	X
21	4	X		
15	3	X	X	X
9	2	X		
3	1	X	X	X

[1] *Distance in inches above bottom of active fuel.*

[2] *Measurement position moved from center of axial node to avoid spacer.*

[3] *Example for a bundle with blade inserted to Notch 20. Extra measurements are added in the vicinity of control blade tips.*

TABLE 11.6 Operation Data Used in PRESTO Analysis of HATCH-1, Cycle 1

RUN IDENT.	BURNUP STEP NO.	BURNUP EOS (MWD/TU)	DATE EOS	DATA SET NO. *	C-ROD SEQ.	POWER (%)	CORE INLET SUBCOOL (ws/kg)	TOTAL CORE FLOW (kg/s)	CONTROL DENSITY (%)
PR-HA-89	1	308.6	75/02/13	1	A	60	53721.	6400.8	11.0
-90	2	493.8	75/03/05	2	B	75	45117.	10370.	8.1
-91	3	702.1	75/03/28	3	A	50	79536.	4347.	9.4
-92	4	1040.5	75/05/06	3	A	50	79536.	4347.	9.4
-93	5	1281.9	75/05/24	4	A	90	55582.	8568.	7.1
-94	6	1631.3	75/06/13	4	A	90	55582.	8568.	7.1
-95	7	2013.8	75/07/10	5	A	80	61163.	7157.	9.2
-96	8	2583.7	75/08/26	6	B	96	49070.	9929.	9.0
-97	9	3116.1	75/09/25	7	B	86	55814.	8404.	10.2
-98	10	3646.3	75/10/24	8	B	86	60000.	7673.	10.9
-99	11	3948.3	75/12/30	8	B	86	60000.	7673.	10.9
-106	12	4157.7	76/01/13	9	B	80	54187.	8102.	13.7
-107	13	4204.0	76/01/18	9	B	80	54187.	8102.	13.7
-108	14	4319.7	76/01/25	10	A	76	42093.	9891.	16.5
-109	15	4685.7	76/02/18	10	A	76	42093.	9891.	16.5
-110	16	5024.1	76/03/11	11	A	79	45582.	9337.	17.0
-111	17	5300.8	76/04/25	12	A	80	48373.	8996.	17.0
-112	18	5793.5	76/05/25	13	B	86	48605.	9261.	16.9
-113	19	6276.3	76/07/05	13	B	86	48605.	9261.	16.9
-114	20	6592.7	76/07/22	14	A	83	56977.	7862.	17.5
-115	21	6979.6	76/08/13	15	A	93	50698.	9488.	17.5
-116	22	7161.5	76/08/23	15	A	93	50698.	9488.	17.5
-117	23	7618.9	76/09/16	16	B	92	48605.	9878.	19.2
-118	24	8059.8	76/10/12	16	B	92	48605.	9878.	19.2
-119	25	8432.4	76/11/03	17	B	87	48838.	9551.	19.2
-120	26	8938.4	76/11/24	18	B	84	45117.	9891.	19.2
-121	27	9025.5	76/12/05	18	B	84	45117.	9891.	19.2
-122	28	9402.5	76/12/29	19	A	92	47907.	9853.	15.6
-123	29	9829.1	77/01/21	20	A	87	46512.	9916.	15.6
-124	30	9883.1	77/01/25	21	A	88	51861.	8984.	15.2
-125	31	10119.0	77/02/23	21	A	88	51861.	8984.	15.2
-126	32	10310.8	77/03/07	22	A	91	47907.	9904.	15.2
-127	33	10399.0	77/03/12	23	A	87	47442.	9727.	15.2

*Corresponds to notation in Reference 11.

TABLE 11.7 Operating BWR's Analyzed with PRESTO

REACTOR	OPERATING CYCLE ANALYZED	ANALYSIS PERFORMED BY	TIP COMPARISONS MADE	GAMMA SCAN ANALYZED	COLD CONDITION ANALYZED
DODEWAARD	1,2	ScP	Yes		
MÜHLEBERG	1,2,3,4,5	ScP/Utility	Yes	Yes	Yes
BARSEBÄCK	1	ScP	Yes		Yes
BRUNSBÜTTEL	1	ScP	Yes		Yes
PHILIPPSBURG	1	Utility	Yes	Yes	
SANTA MARIA de GARONÑA	7,8,9	ScP/Utility	Yes		Yes
FORSMARK-1	1	ScP*	Yes		Yes
QUAD CITIES-2	1,2	ScP	Yes		
BRUNSWICK-1	1,2,3	Utility	Yes		Yes
BRUNSWICK-2	1,2,3,4	Utility	Yes		Yes
HATCH-1	1	ScP	Yes	Yes	
FITZPATRICK	1,2	Utility*			

**Lattice data provided by Utility (CASMO)*

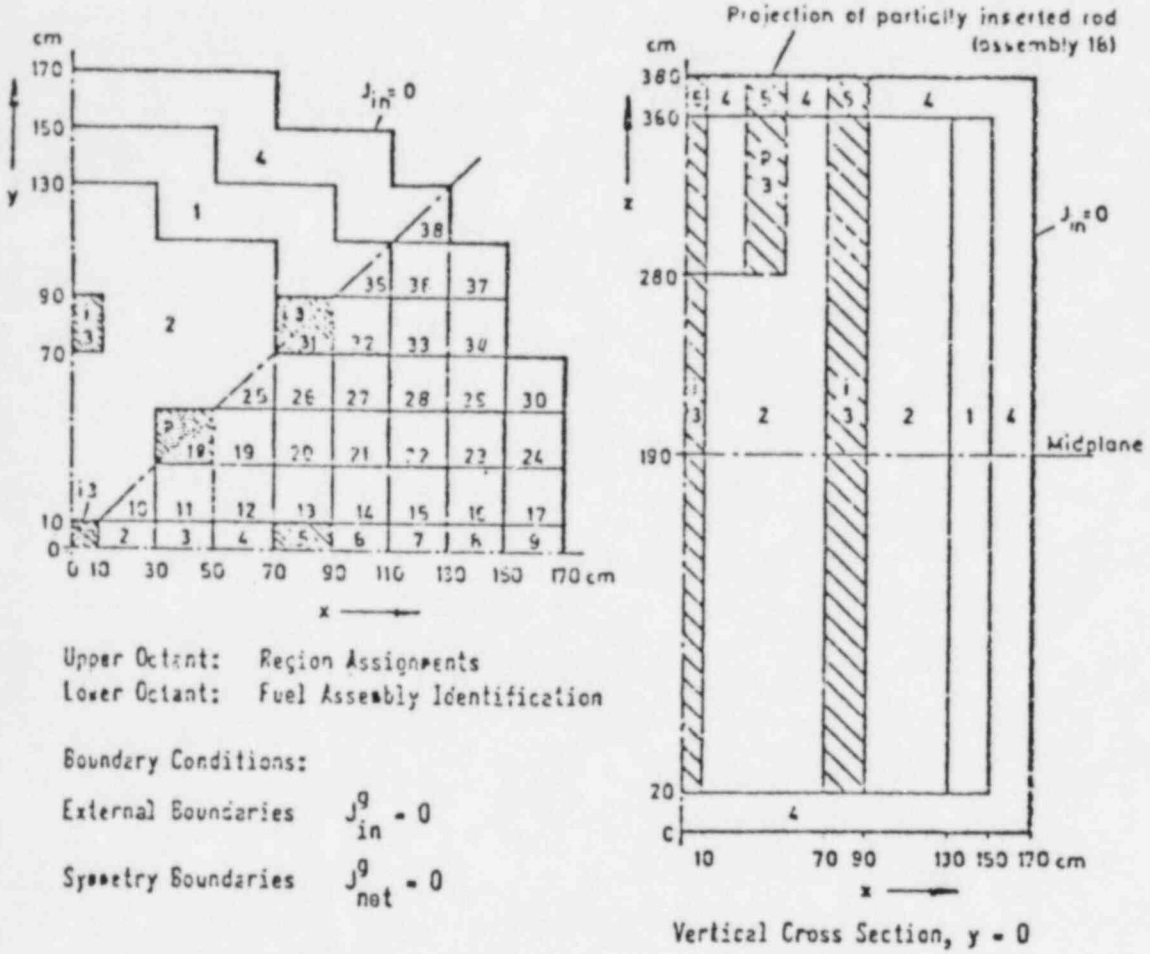

Upper Octant: Region Assignments
Lower Octant: Fuel Assembly Identification

Boundary Conditions:

External Boundaries $J_{in}^g = 0$

Symmetry Boundaries $J_{net}^g = 0$

Vertical Cross Section, y = 0

Group Constants for 3D IAEA Benchmark Problem

Region	D_1	D_2	Σ_{r1}	Σ_{a1}	Σ_{a2}	$\nu_2\Sigma_{f2}$	
1	1.5	0.4	0.02	0.01	0.08	0.135	Fuel 1
2	1.5	0.4	0.02	0.01	0.085	0.135	Fuel 2
3	1.5	0.4	0.02	0.01	0.13	0.135	Fuel 2 + Rod
4	2.0	0.3	0.04	0	0.01	0	Reflector
5	2.0	0.3	0.04	0	0.055	0	Refl. + Rod

$\chi_1 = 1.0$, $\chi_2 = 0.0$, $\nu_1\Sigma_{f1} = 0$ all regions

Note: 2D IAEA Benchmark Problem represents midplane z = 190 cm with constant axial buckling $B_z^2 = 0.8 \times 10^{-4}$ for all regions and energy groups

FIGURE 11.1 Benchmark Problem Specifications for 3-D and 2-D Core Neutronics Neutronics Model Verification.

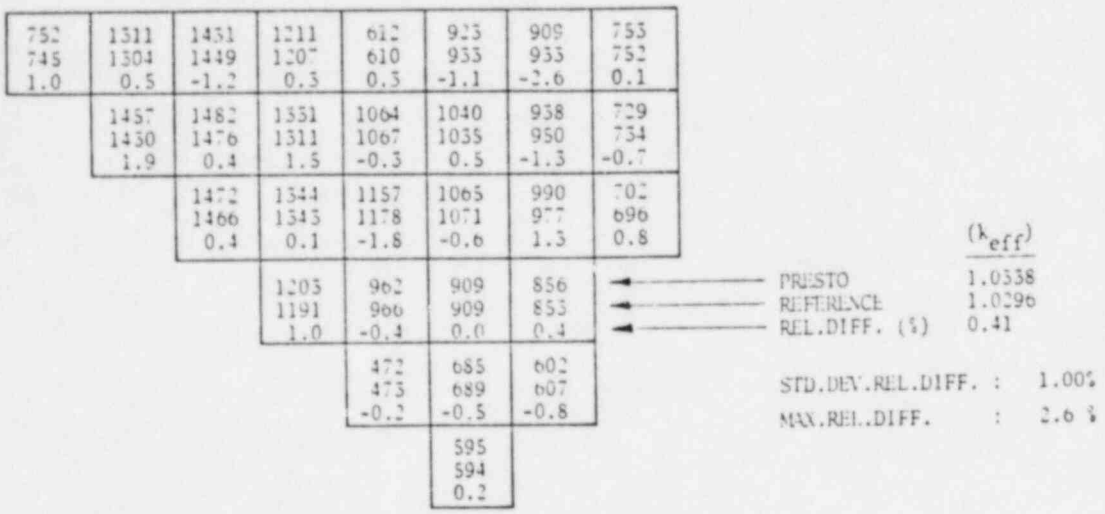

FIGURE 11.2 PRESTO 2-D IAEA Benchmark Comparison. Node Size: 20 x 20 cm
Relative Bundle Power

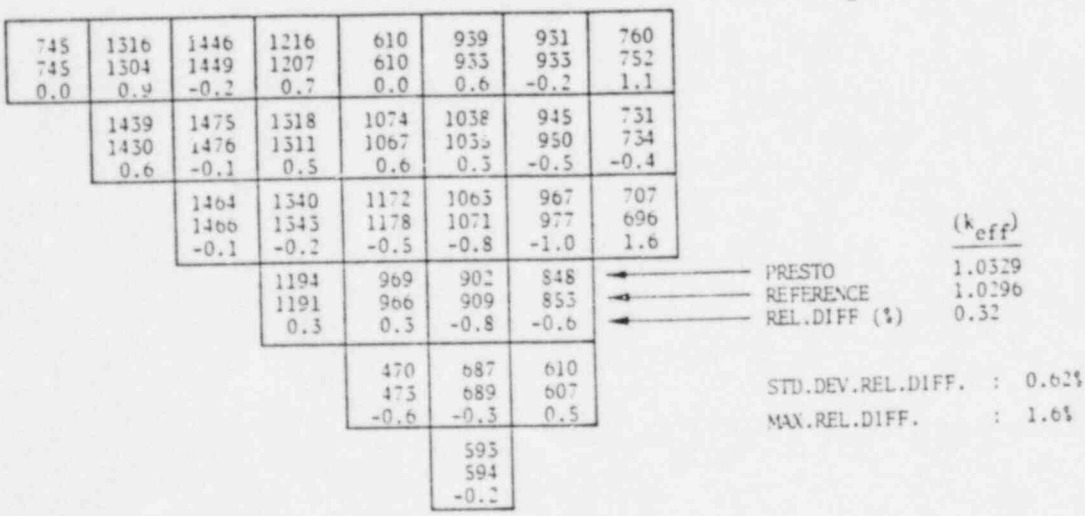

FIGURE 11.3 PRESTO 2-D IAEA Benchmark Comparison. Node Size: 10 x 10 cm
Relative Bundle Power

733 729 0.5	1282 1281 0.1	1396 1422 -1.8	1193 1193 0.0	609 610 -0.2	940 953 -1.4	933 959 -2.8	777 777 0.0
	1420 1397 1.6	1432 1432 0.0	1307 1291 1.2	1065 1072 -0.6	1057 1055 0.2	962 976 -1.5	751 757 -0.8
		1367 1368 -0.1	1309 1311 -0.2	1155 1181 -2.2	1081 1089 -0.7	1014 1000 1.4	722 711 1.5
			1189 1178 0.9	965 972 -0.7	924 923 0.1	877 866 1.3	
				475 476 -0.2	700 700 0.0	617 611 1.0	
					609 597 2.0		

	(k_{eff})
PRESTO	1.03521
REFERENCE	1.02903
REL.DIFF. (%)	0.40

STD.DEV.REL.DIFF. : 1.17%

MAX.DEV.REL.DIFF. : 2.8 %

FIGURE 11.4 PRESTO 3-D IAEA Benchmark Comparison, Node Size: 20 x 20 x 20 cm
Relative Bundle Power

727 729 -0.3	1275 1281 -0.5	1404 1422 -1.3	1191 1193 -0.2	612 610 0.3	959 953 0.6	962 959 0.3	782 777 0.6
	1390 1397 -0.5	1418 1432 -1.0	1287 1291 -0.3	1072 1072 0	1059 1055 0.4	979 976 0.3	753 757 -0.5
		1356 1368 -0.9	1302 1311 -0.7	1173 1181 -0.7	1088 1089 -0.1	1001 1000 0.1	715 711 0.6
			1178 1178 0.0	975 972 0.3	927 923 0.4	866 866 0.0	
				482 476 1.3	709 700 1.2	617 611 1.0	
					593 597 -0.7		

	k_{eff}
PRESTO	1.03238
REFERENCE	1.02903
REL.DIFF (%)	1.33

STD.DEV.REL.DIFF. : 0.65%

MAX.REL.DIFF. : 1.3 %

FIGURE 11.5 PRESTO 3-D IAEA Benchmark Comparison. Node Size: 10 x 20 x 20 cm
Relative Bundle Power

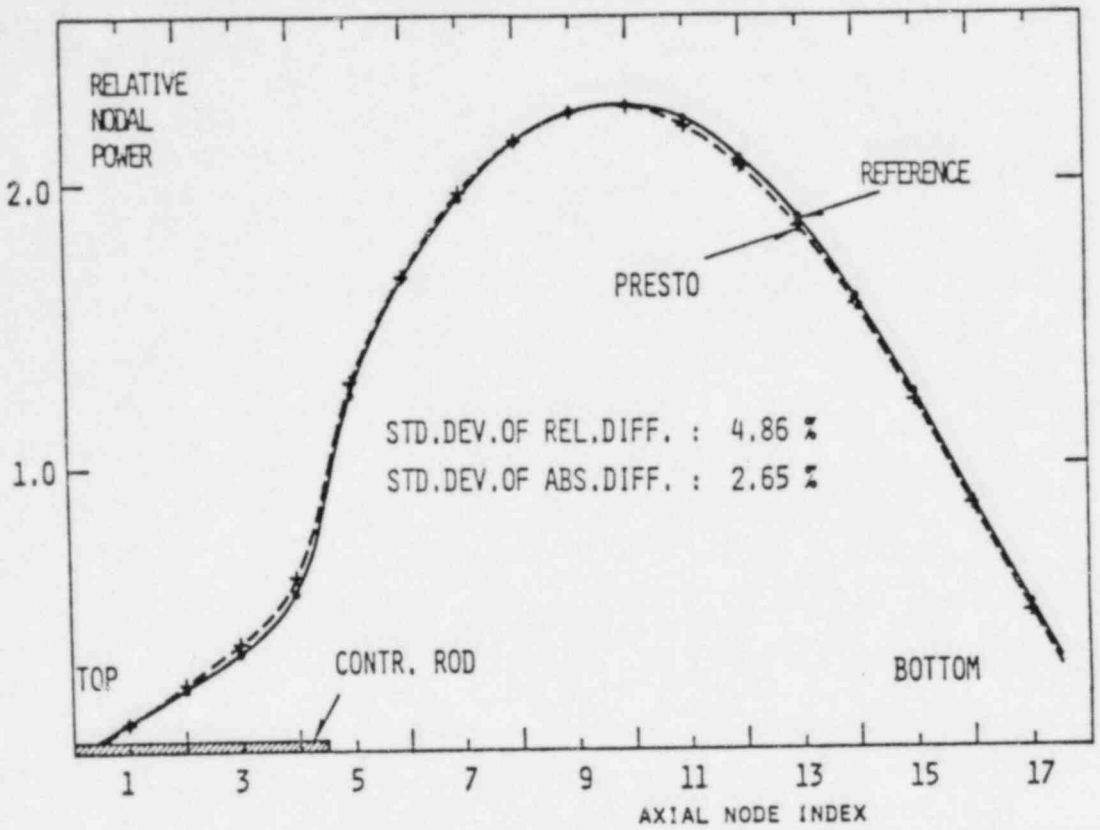

FIGURE 11.6 PRESTO 3-D IAEA BENCHMARK COMPARISON. NODE SIZE : 20 x 20 x 20 CM
AXIAL POWER DISTRIBUTION - THIRD BUNDLE ON DIAGONAL (X,Y)=(3,3)

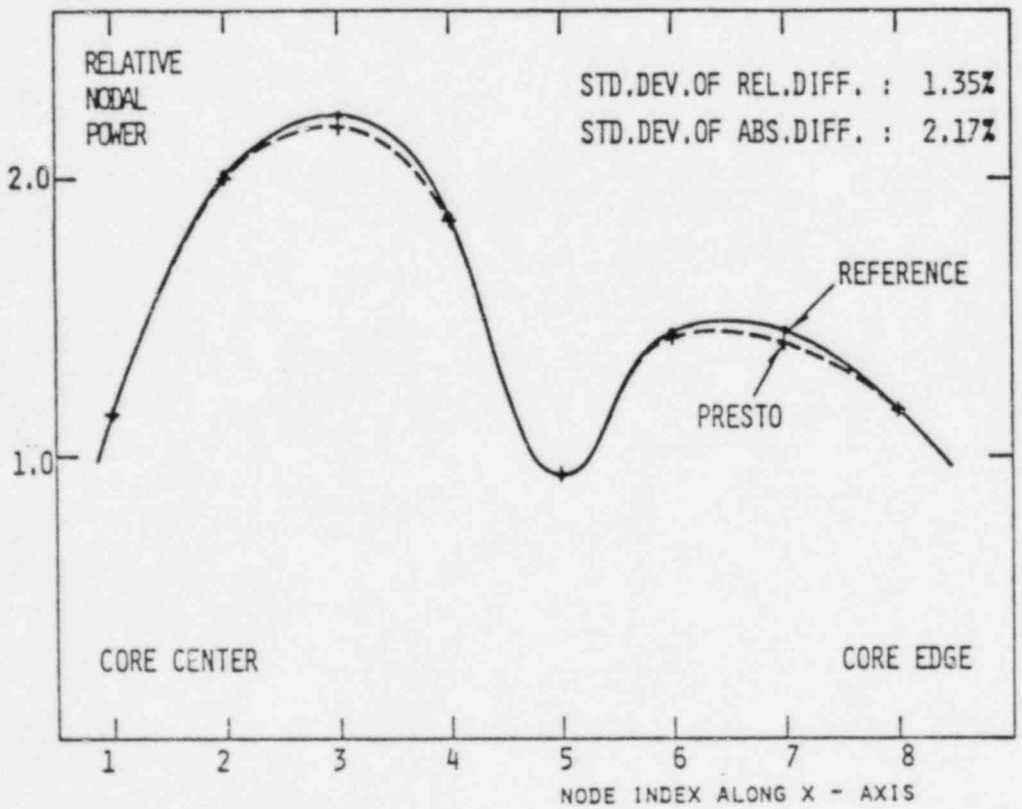

FIGURE 11.7 PRESTO 3-D IAEA BENCHMARK COMPARISON. NODE SIZE : 20 x 20 x 20 CM
RADIAL POWER ALONG X-AXIS AT CORE MIDPLANE (K= 9)

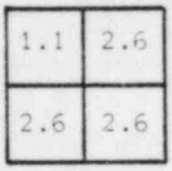

Bundle enrichment (%)

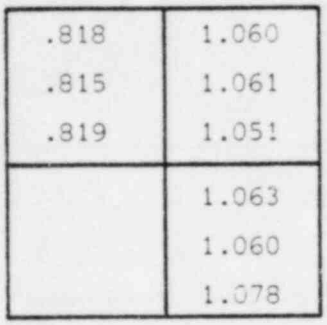

0% VOID

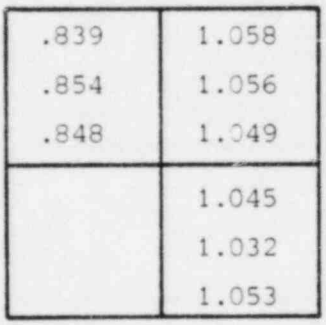

REF
OPT1
OPT2

40% VOID

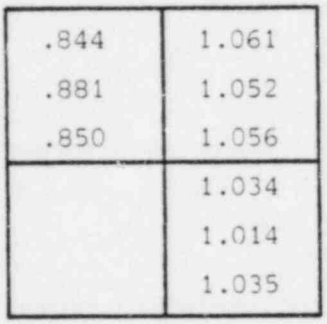

80% VOID

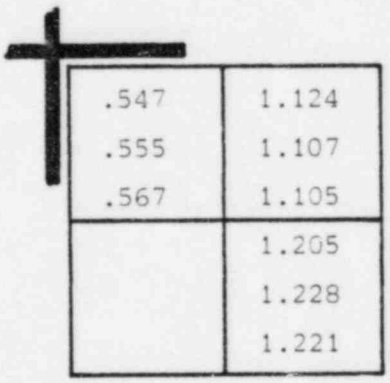

40% VOID

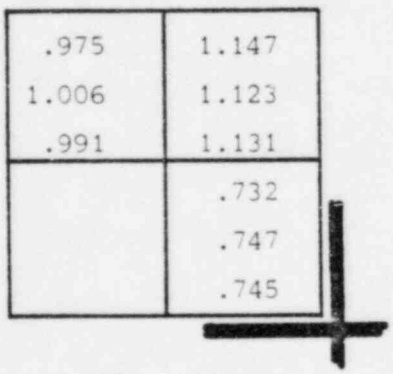

40% VOID

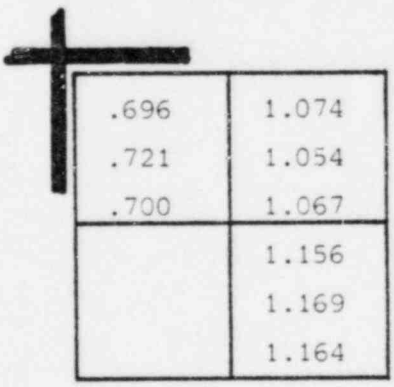

40% VOID,
ALL 2.6% enrichment

REF = RECORD/MD-2, 5-group, explicit

OPT1 = PRESTO, Model Option 1, $a_1 = a_2 = 0$

OPT2 = PRESTO, Model Option 2, $a_1 = a_2 = 0$

FIGURE 11.8 Comparison of PRESTO 4-bundle power sharing calculations with 5-group explicit (RECORD MD/2) benchmark results.

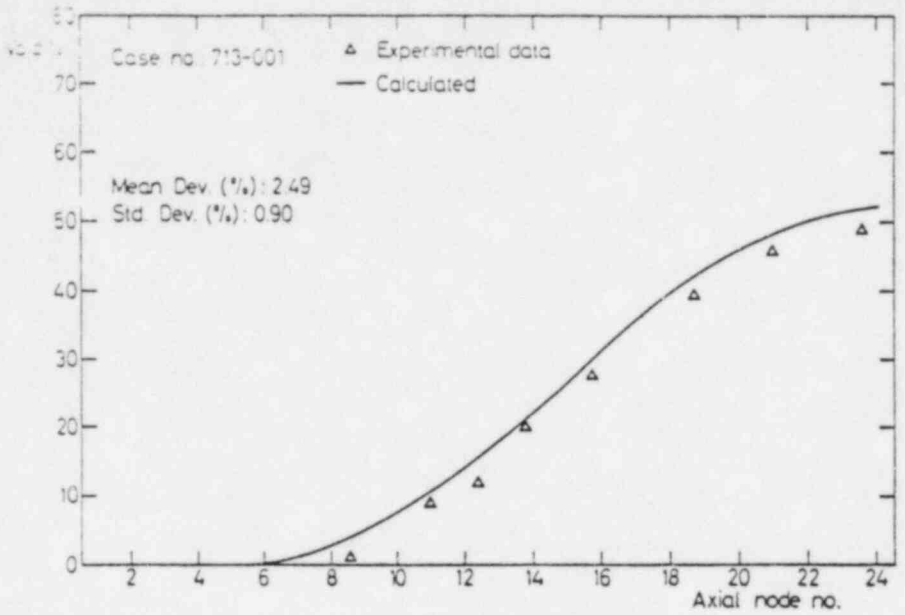

FIGURE 11.9

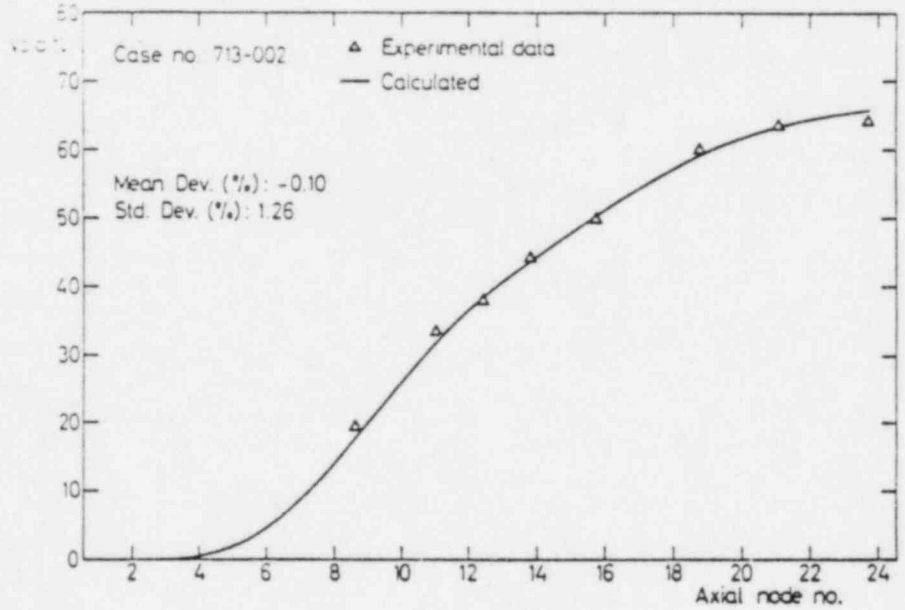

FIGURE 11.10

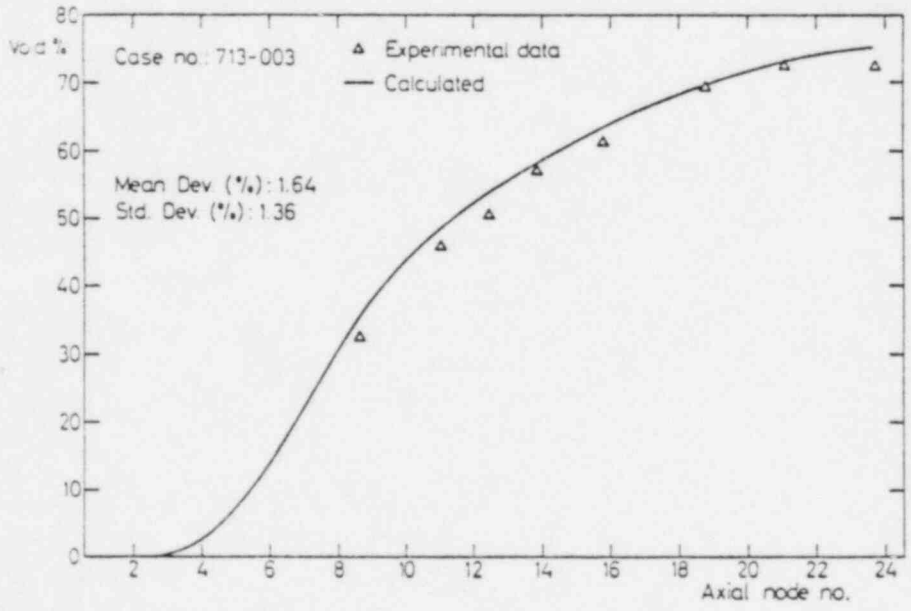

FIGURE 11.11

Comparison of Calculated and Measured Axial Void Distributions

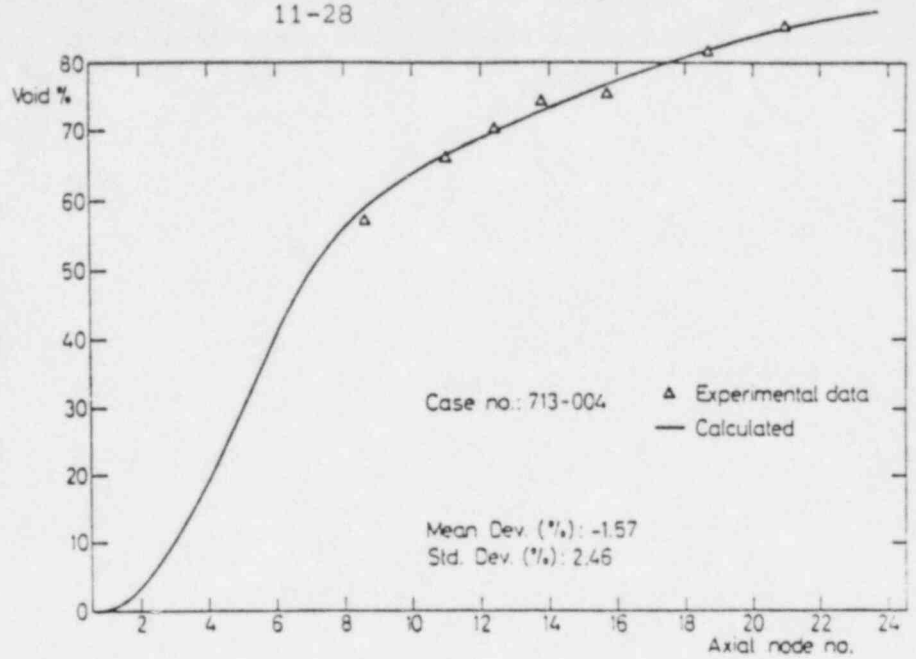

FIGURE 11.12

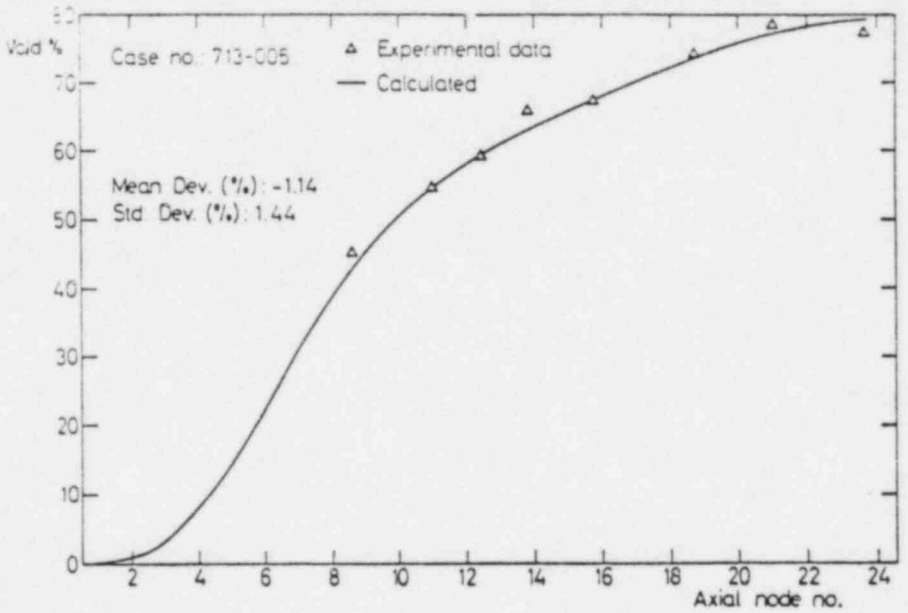

FIGURE 11.13

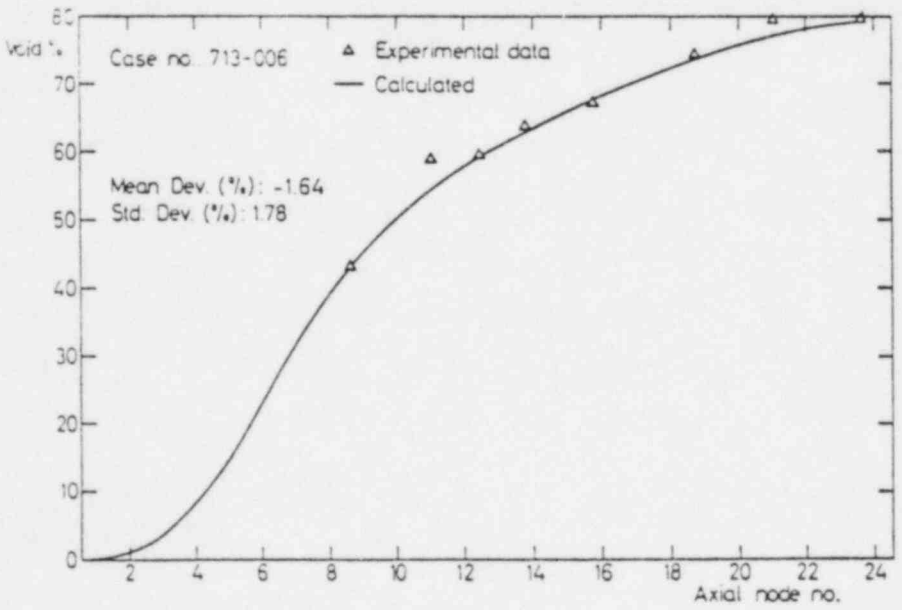

FIGURE 11.14

Comparison of Calculated and Measured Axial Void Distributions

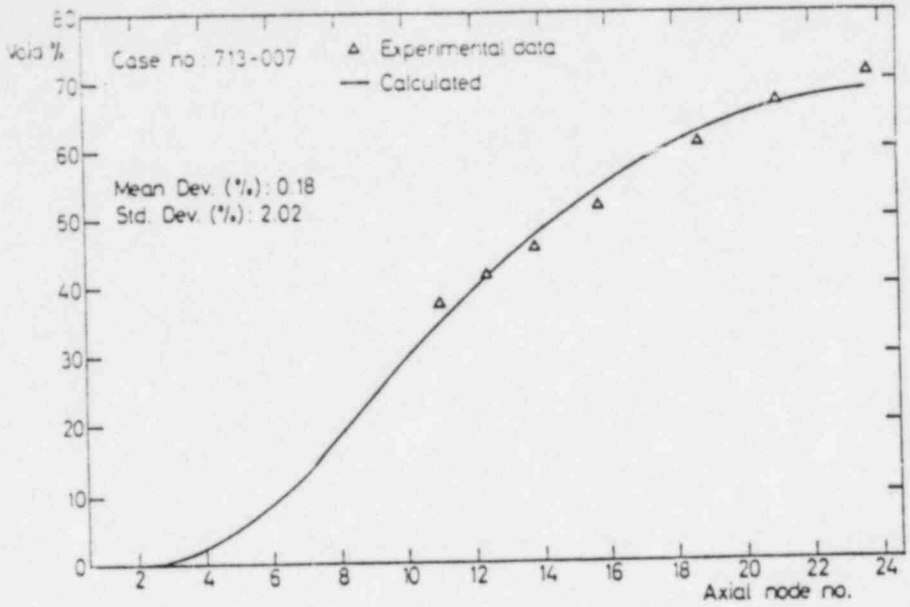

FIGURE 11.15

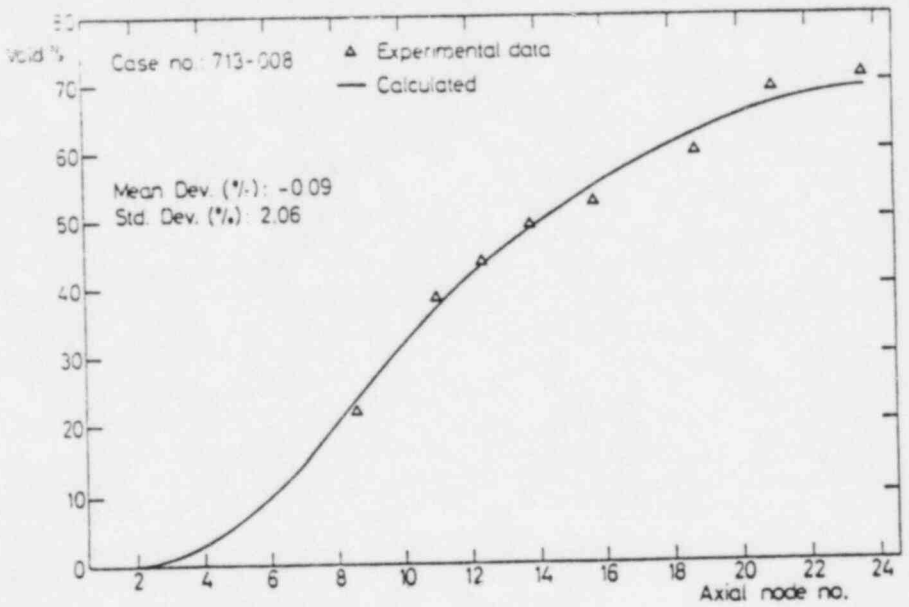

FIGURE 11.16

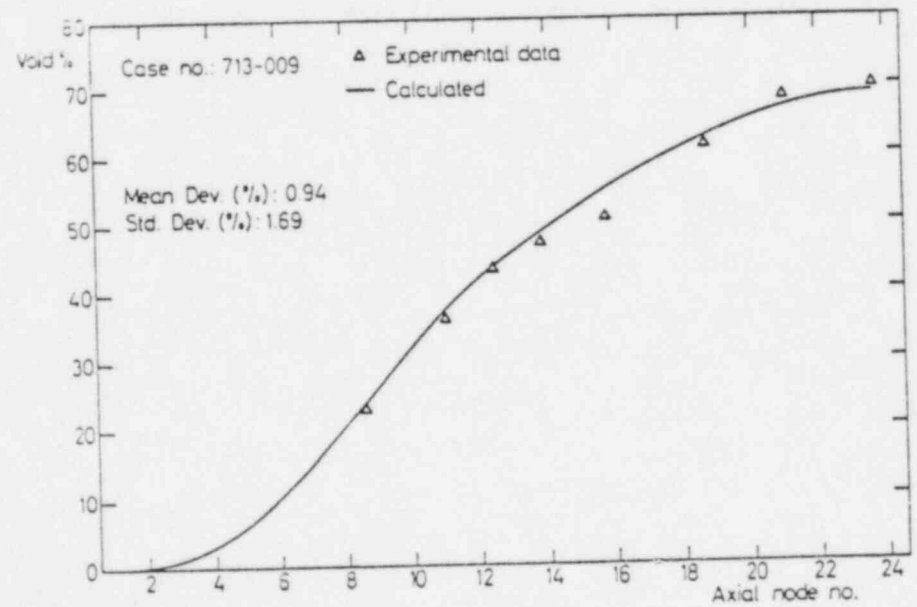

FIGURE 11.17

Comparison of Calculated and Measured Axial Void Distributions

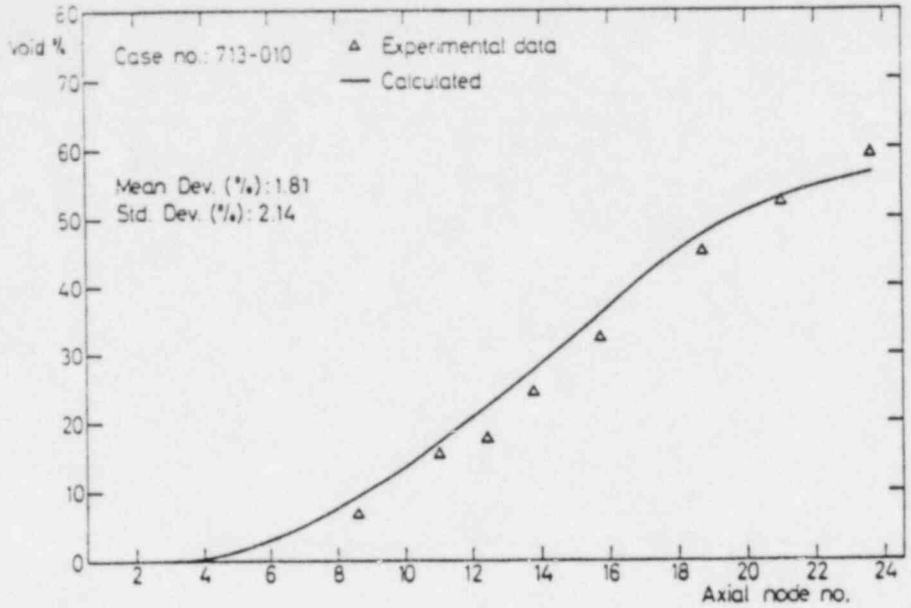

FIGURE 11.18

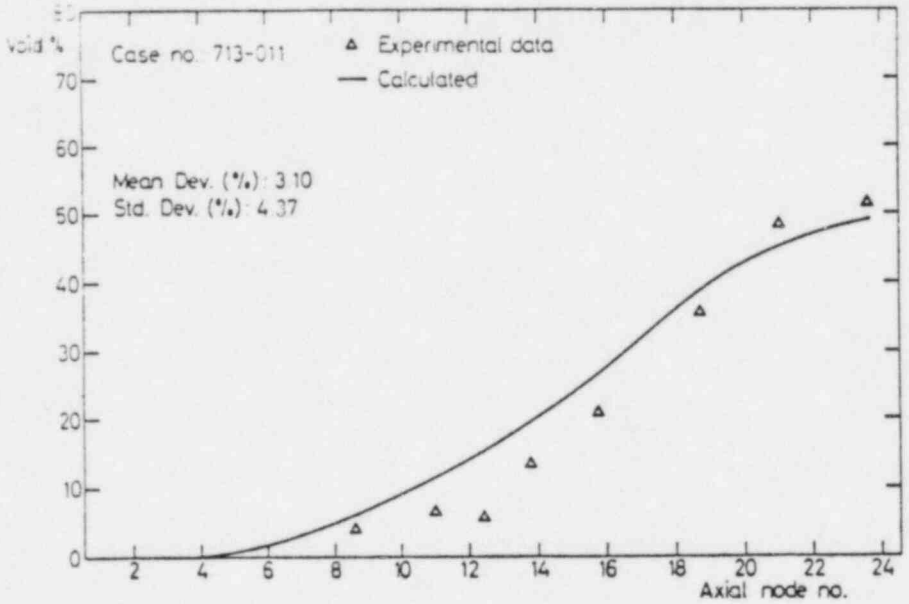

FIGURE 11.19

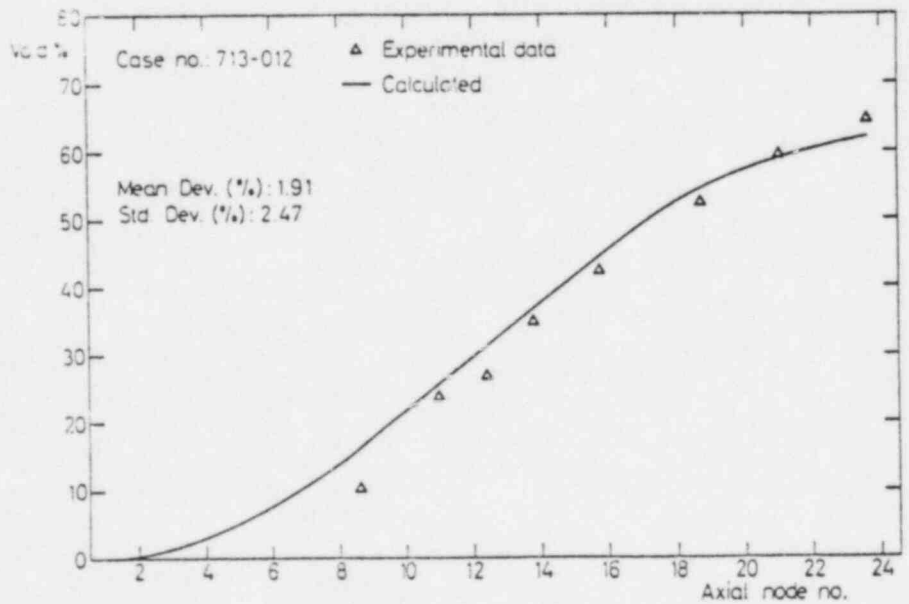

FIGURE 11.20

Comparison of Calculated and Measured Axial Void Distributions

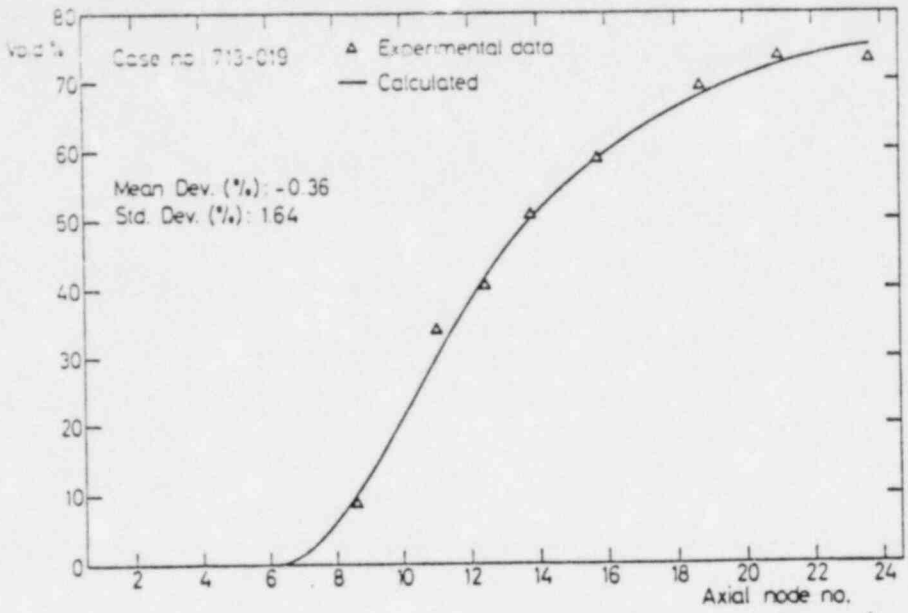

FIGURE 11.27

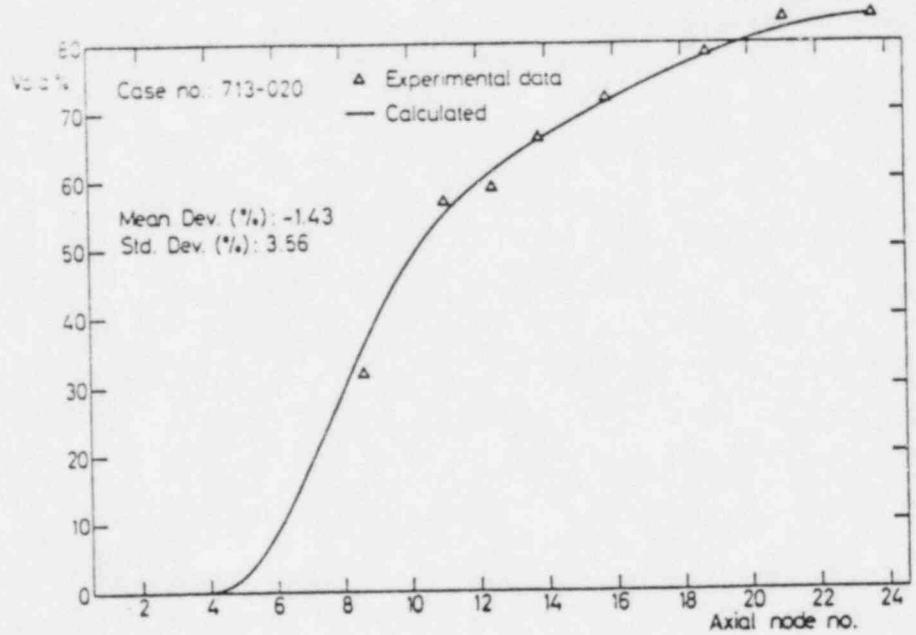

FIGURE 11.28

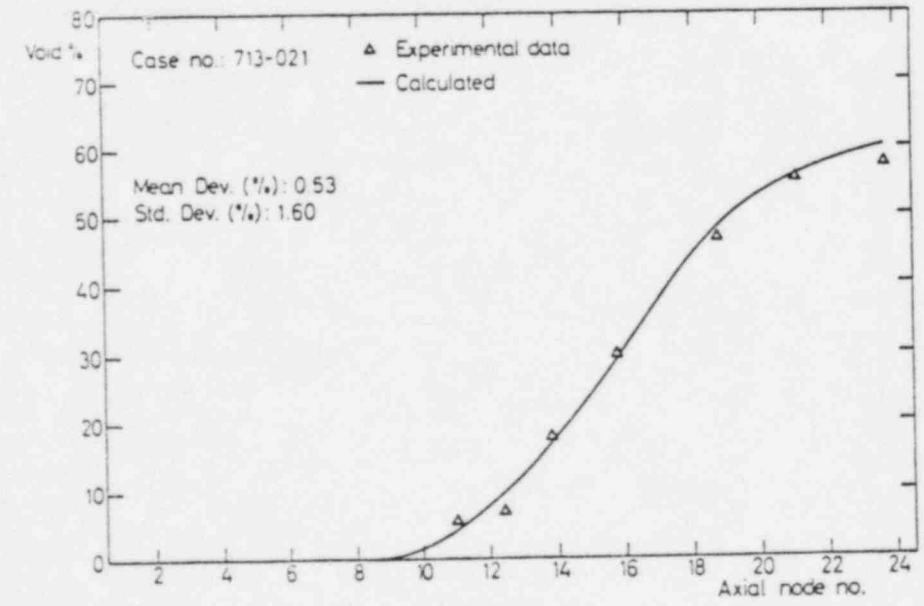

FIGURE 11.29

Comparison of Calculated and Measured Axial Void Distributions

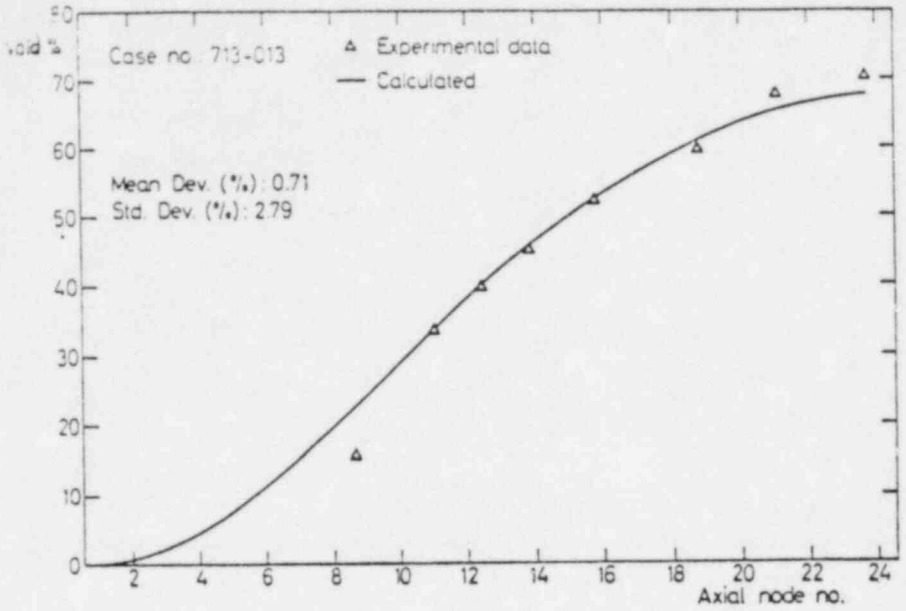

FIGURE 11.21

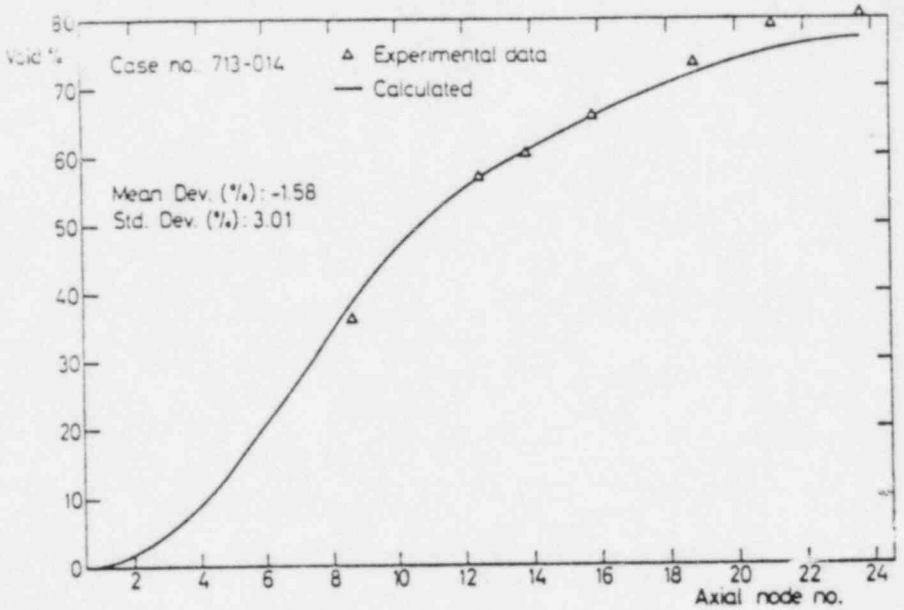

FIGURE 11.22

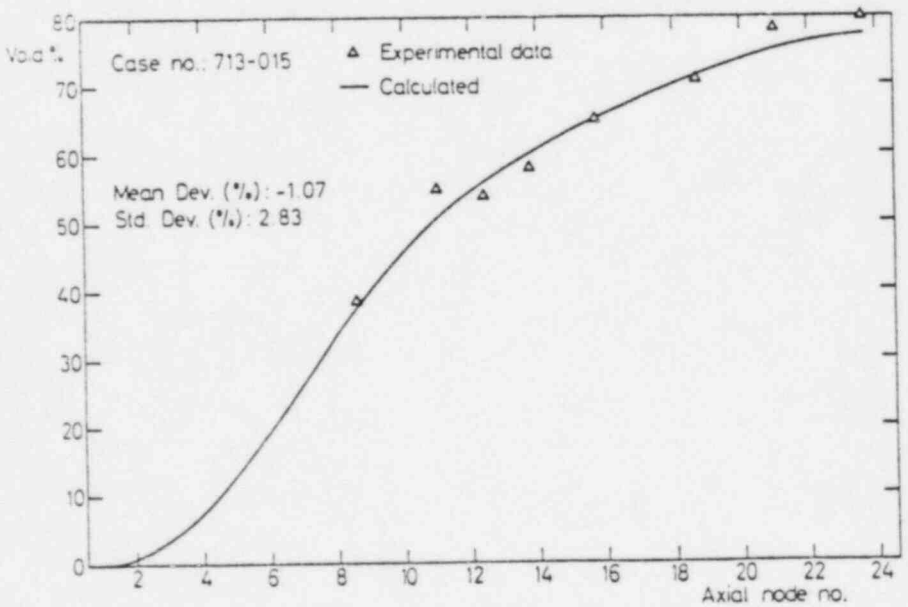

FIGURE 11.23

Comparison of Calculated and Measured Axial Void Distributions

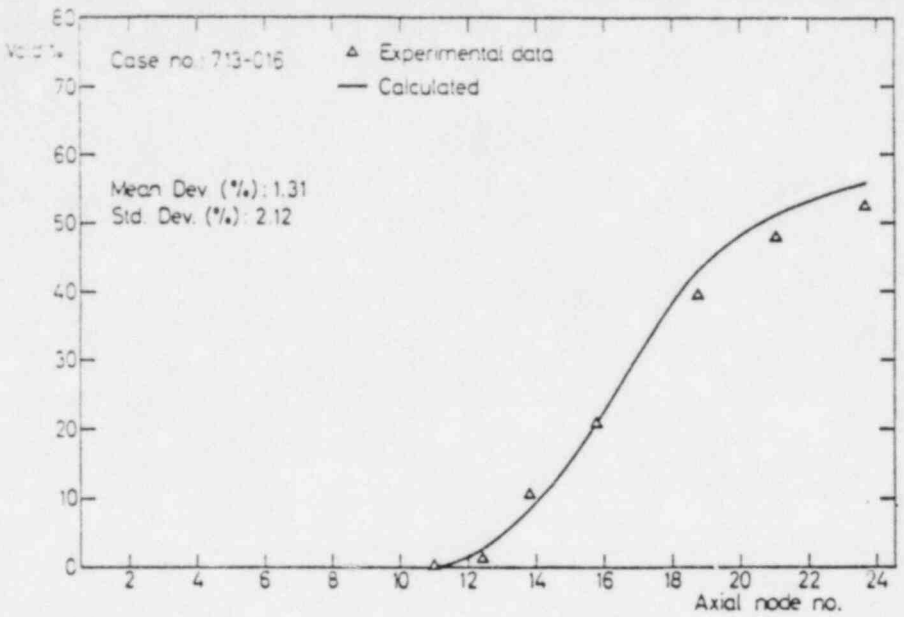

FIGURE 11.24

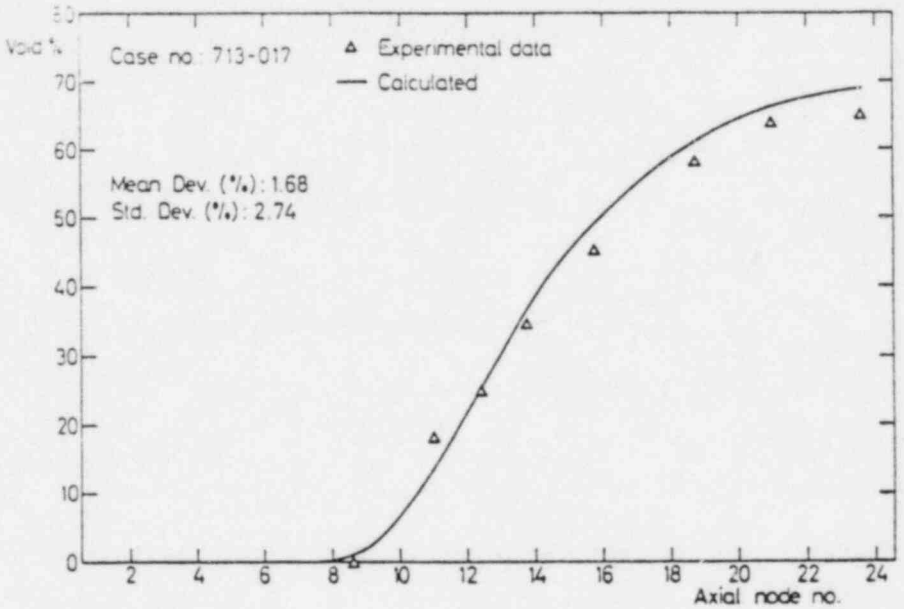

FIGURE 11.25

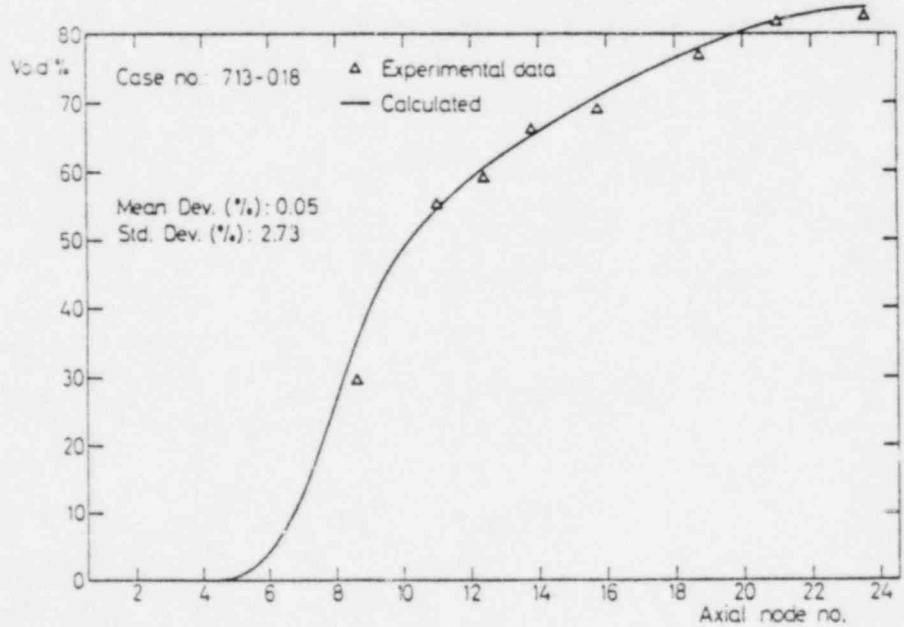

FIGURE 11.26

Comparison of Calculated and Measured Axial Void Distributions

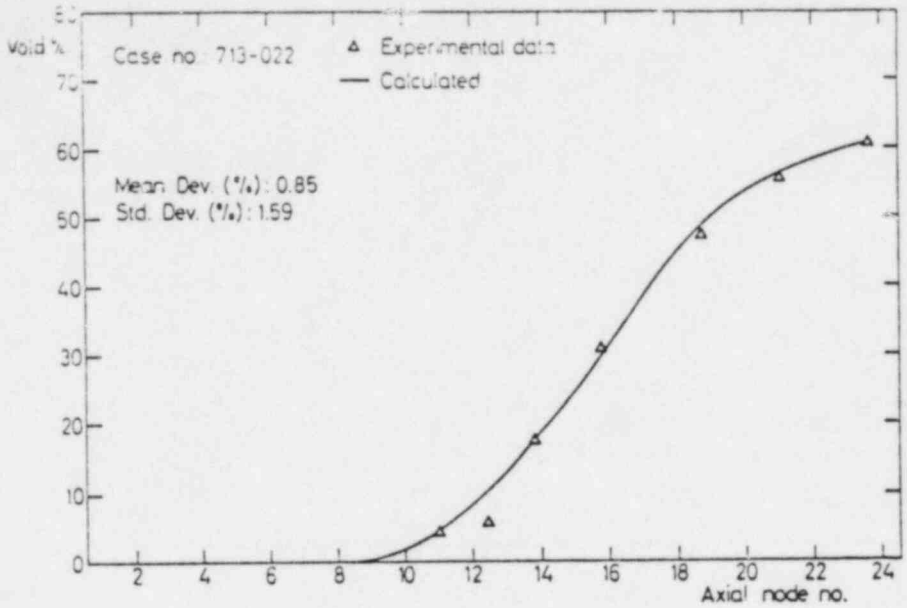

FIGURE 11.30

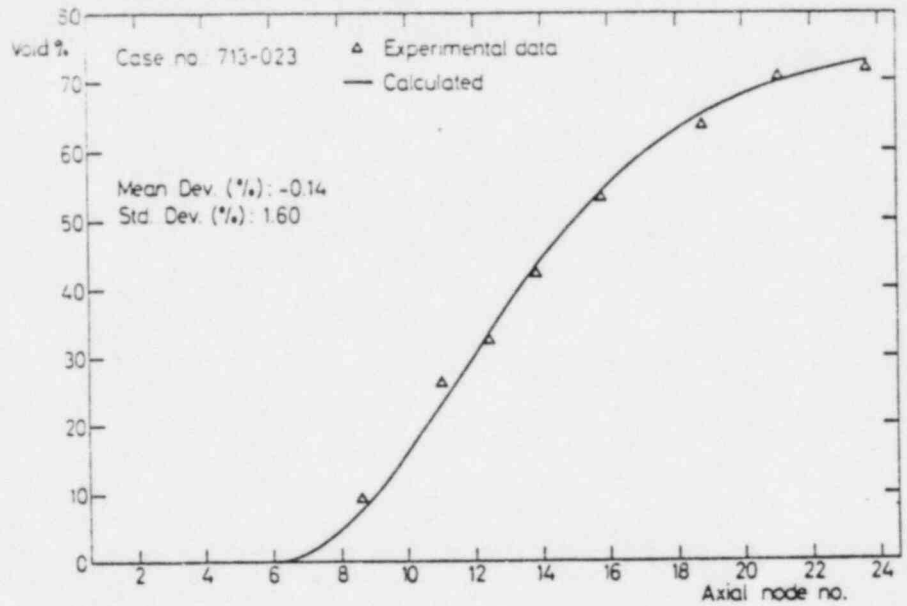

FIGURE 11.31

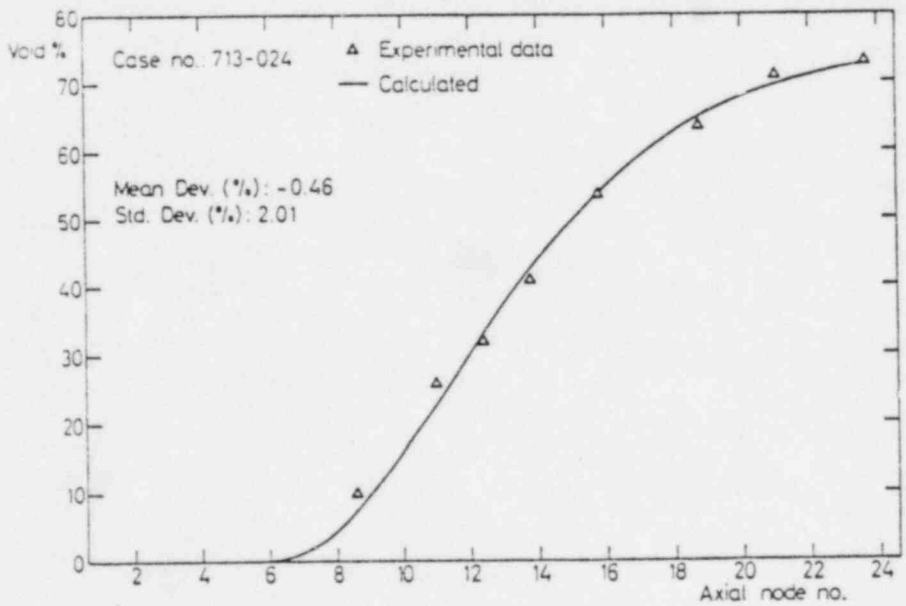

FIGURE 11.32

Comparison of Calculated and Measured Axial Void Distributions

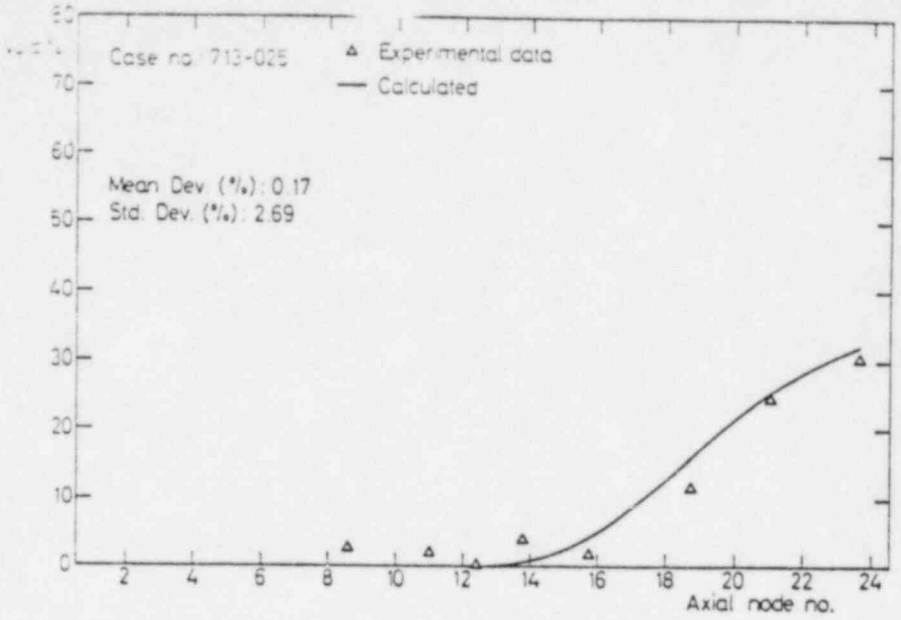

FIGURE 11.33

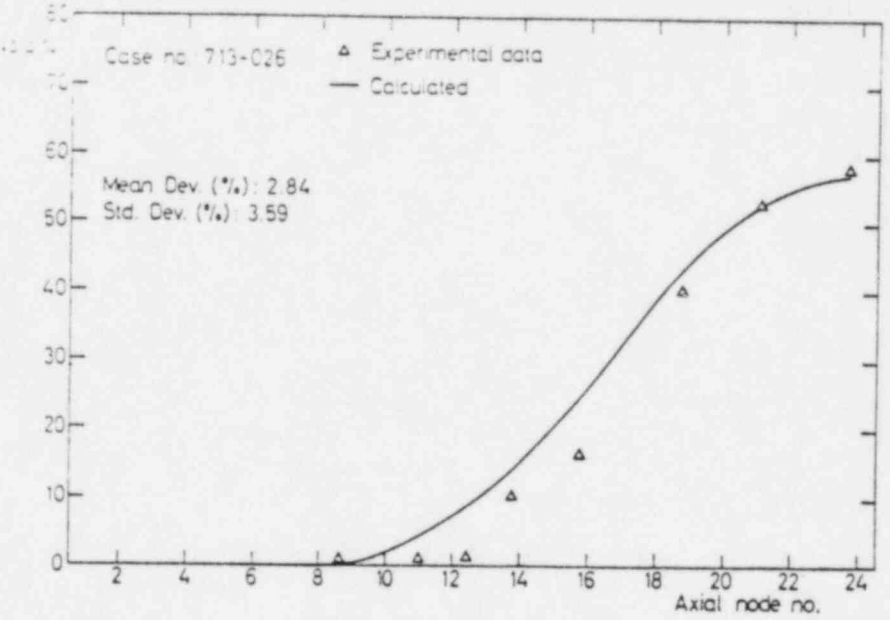

FIGURE 11.34

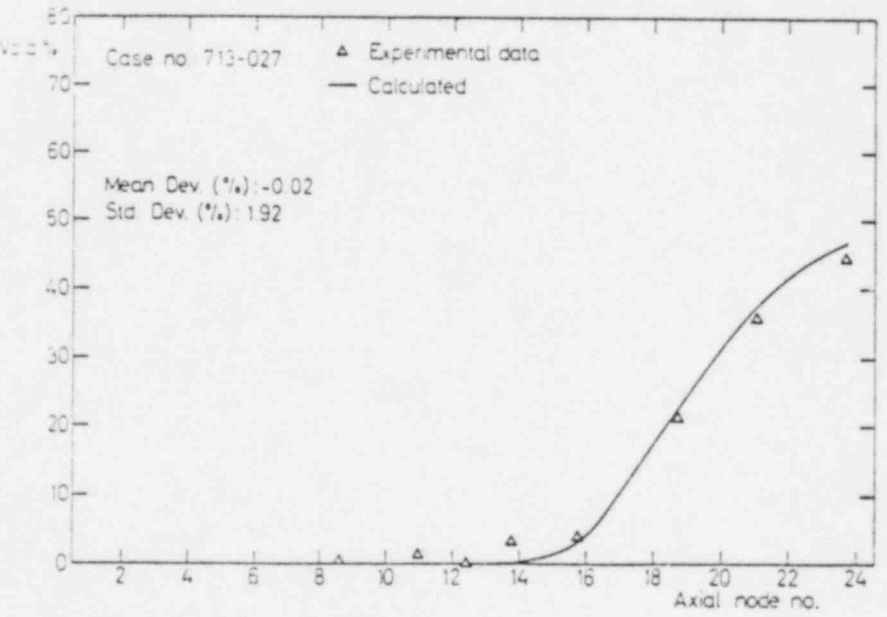

FIGURE 11.35

Comparison of Calculated and Measured Axial Void Distributions

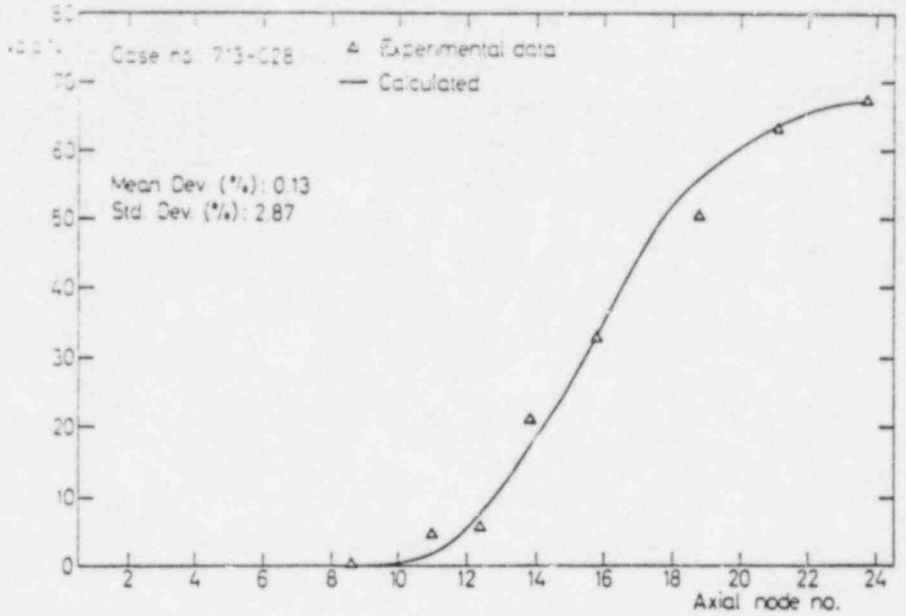

FIGURE 11.36

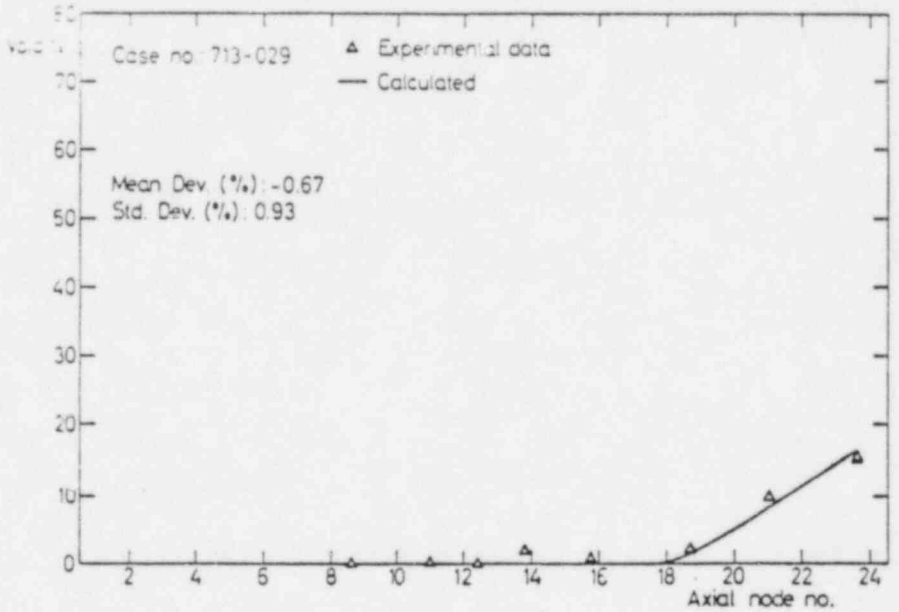

FIGURE 11.37

Comparison of Calculated and Measured Axial Void Distributions

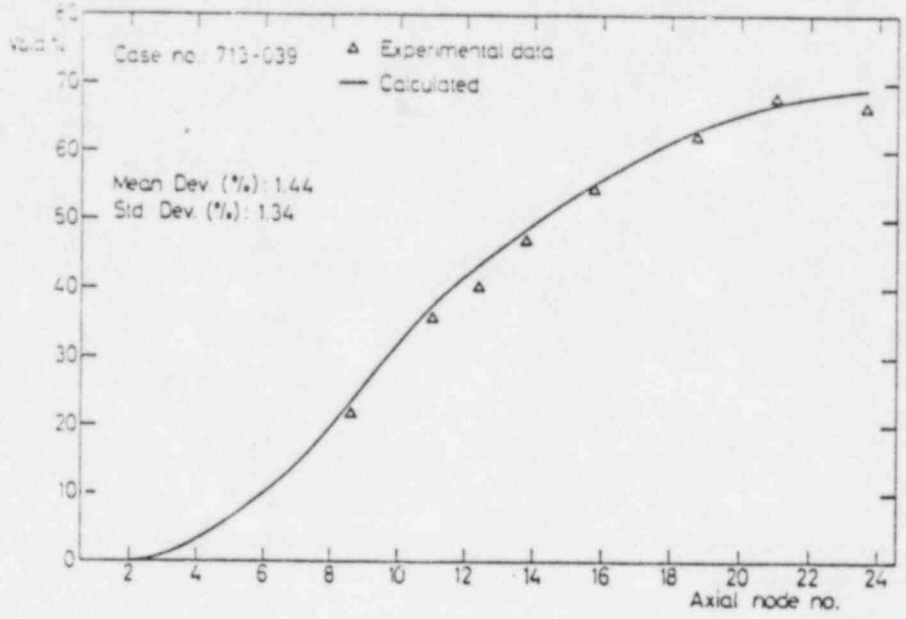

FIGURE 11.38

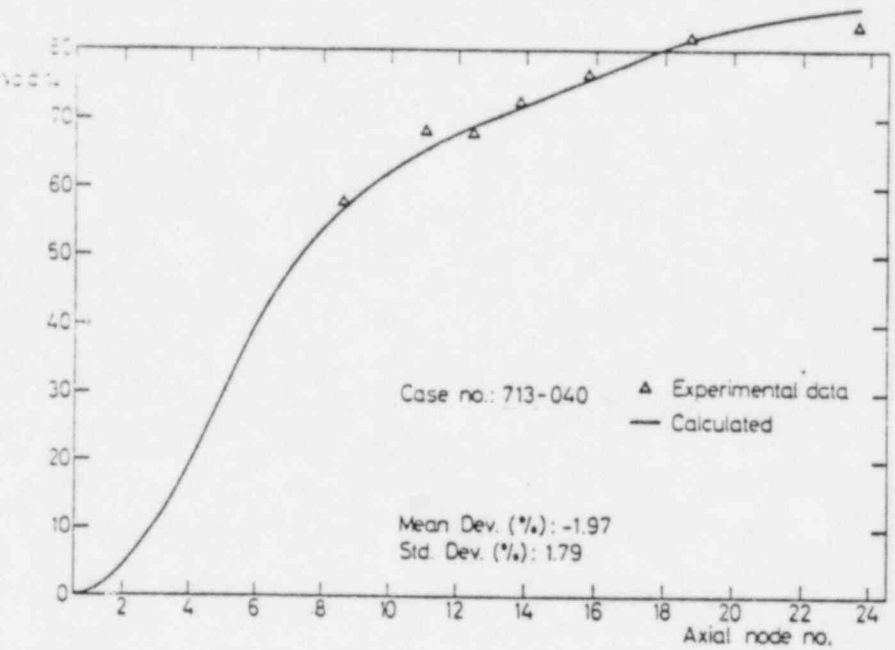

FIGURE 11.39

Comparison of Calculated and Measured Axial Void Distributions

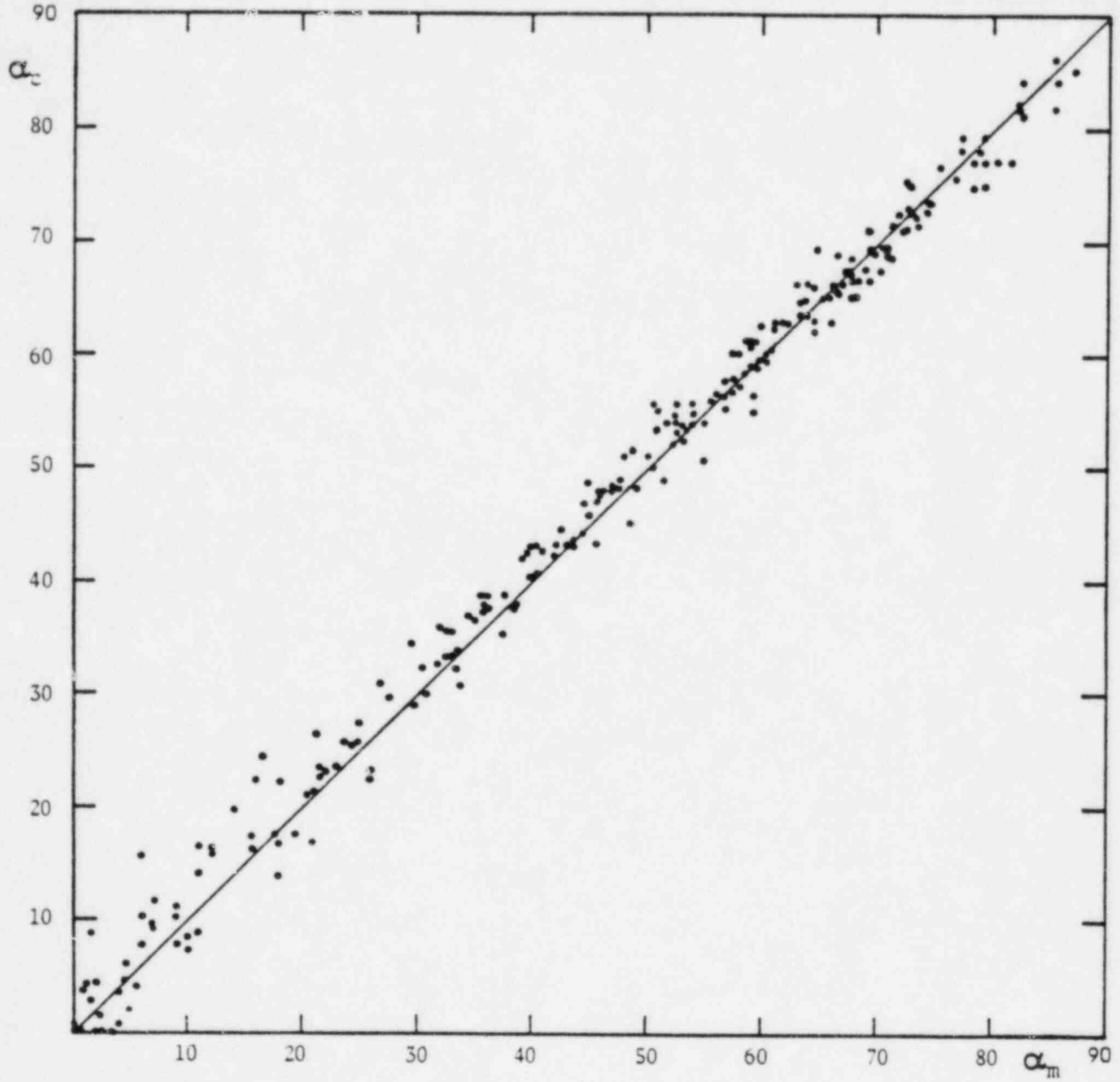

FIGURE 11.40 Correlation Between Calculated and Measured Void

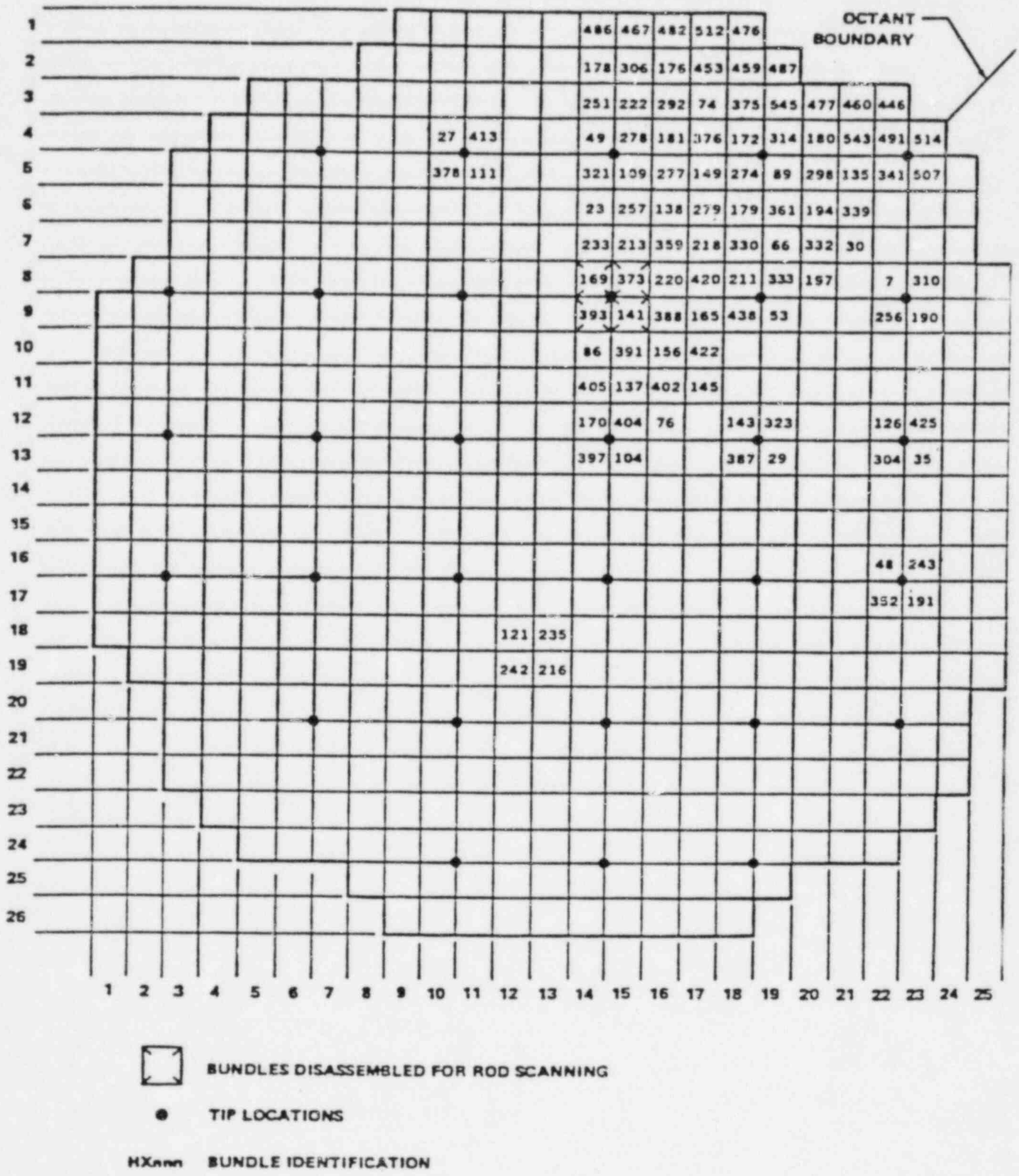

FIGURE 11.41 Gamma Scanned Bundles

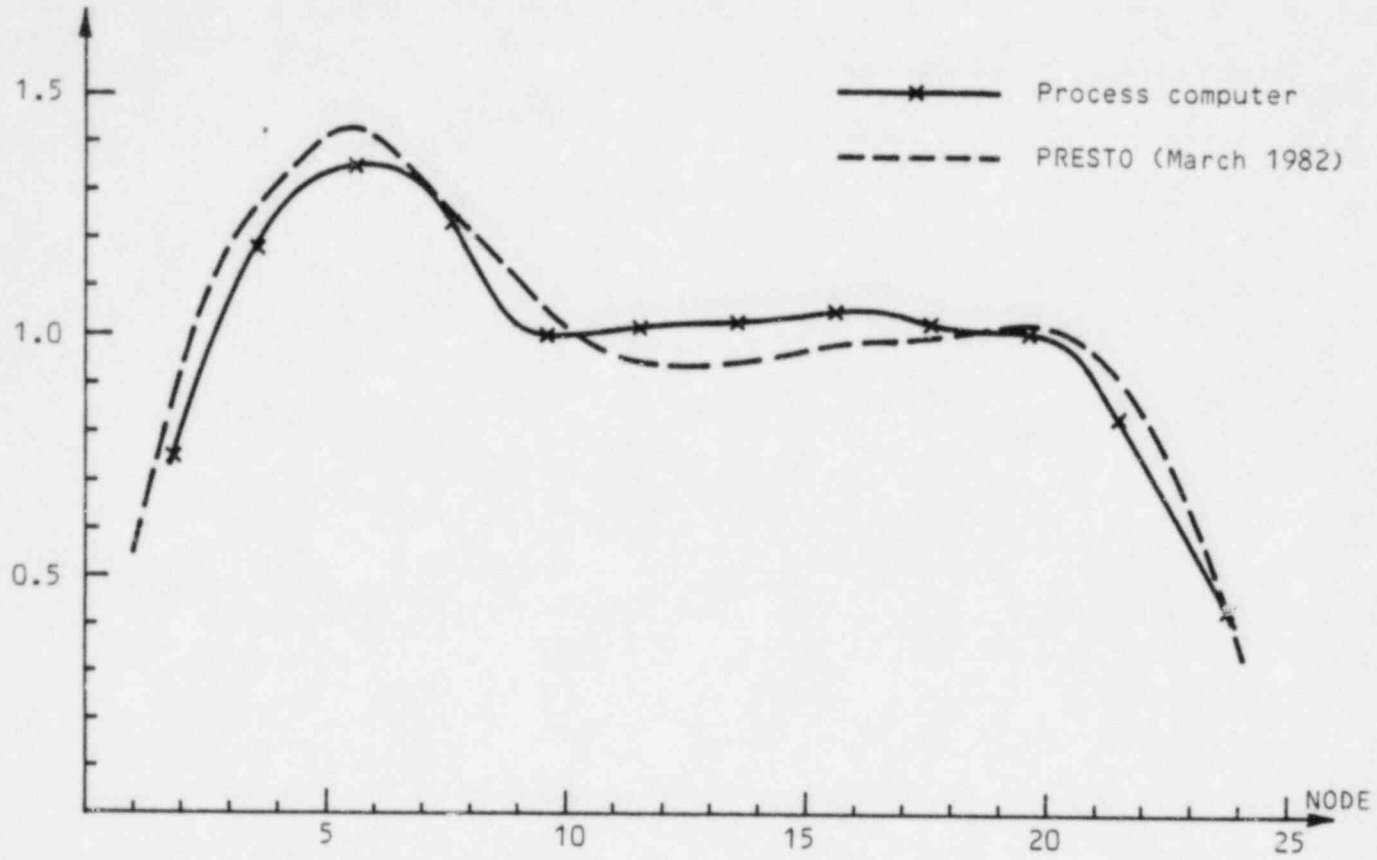

Core Average Axial Power Distribution on 4 July 1975
at 1984 MWD/TU

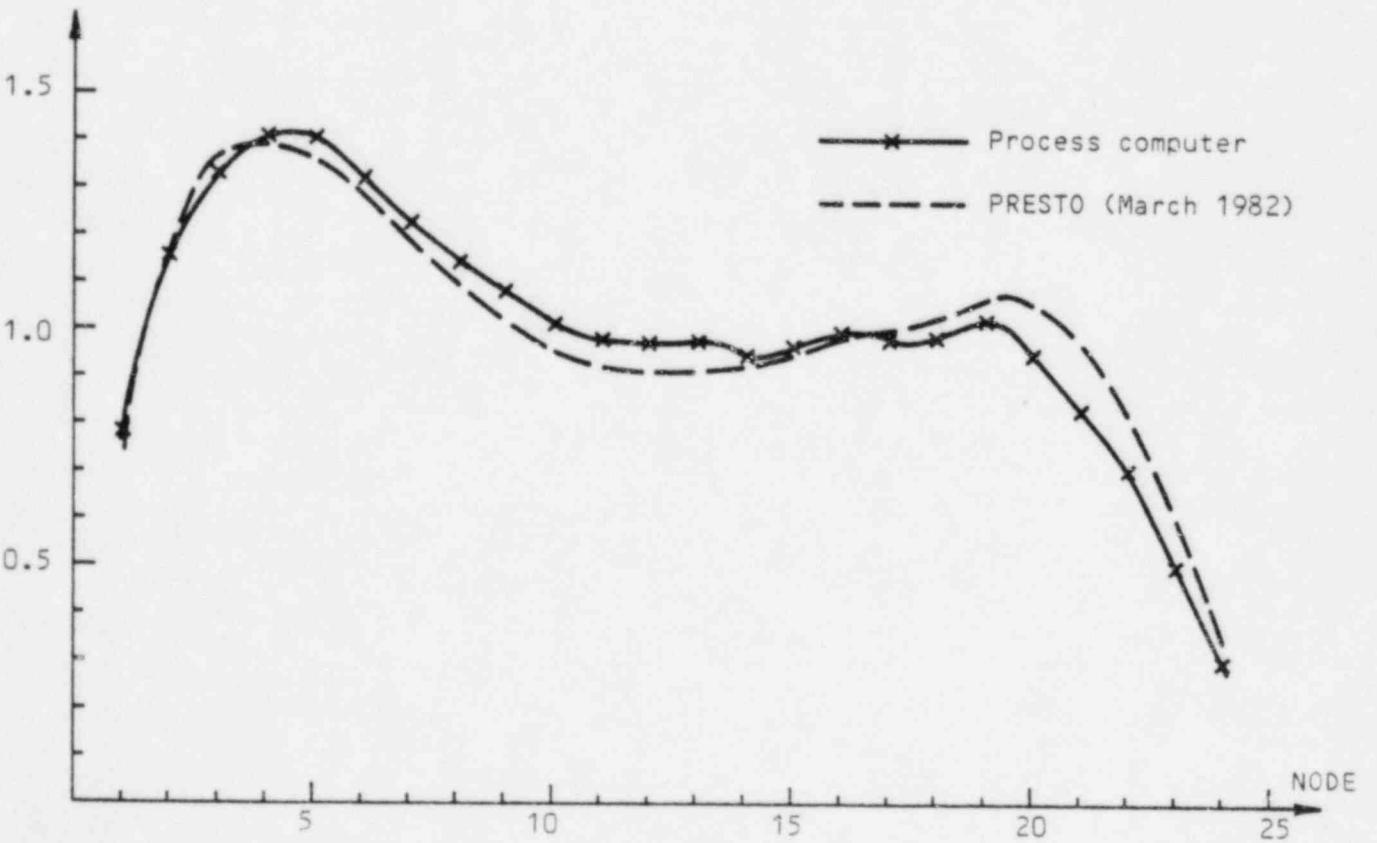

FIGURE 11.42 Core Average Axial Power Distribution on 26 August 1975
at 2584 MWD/TU

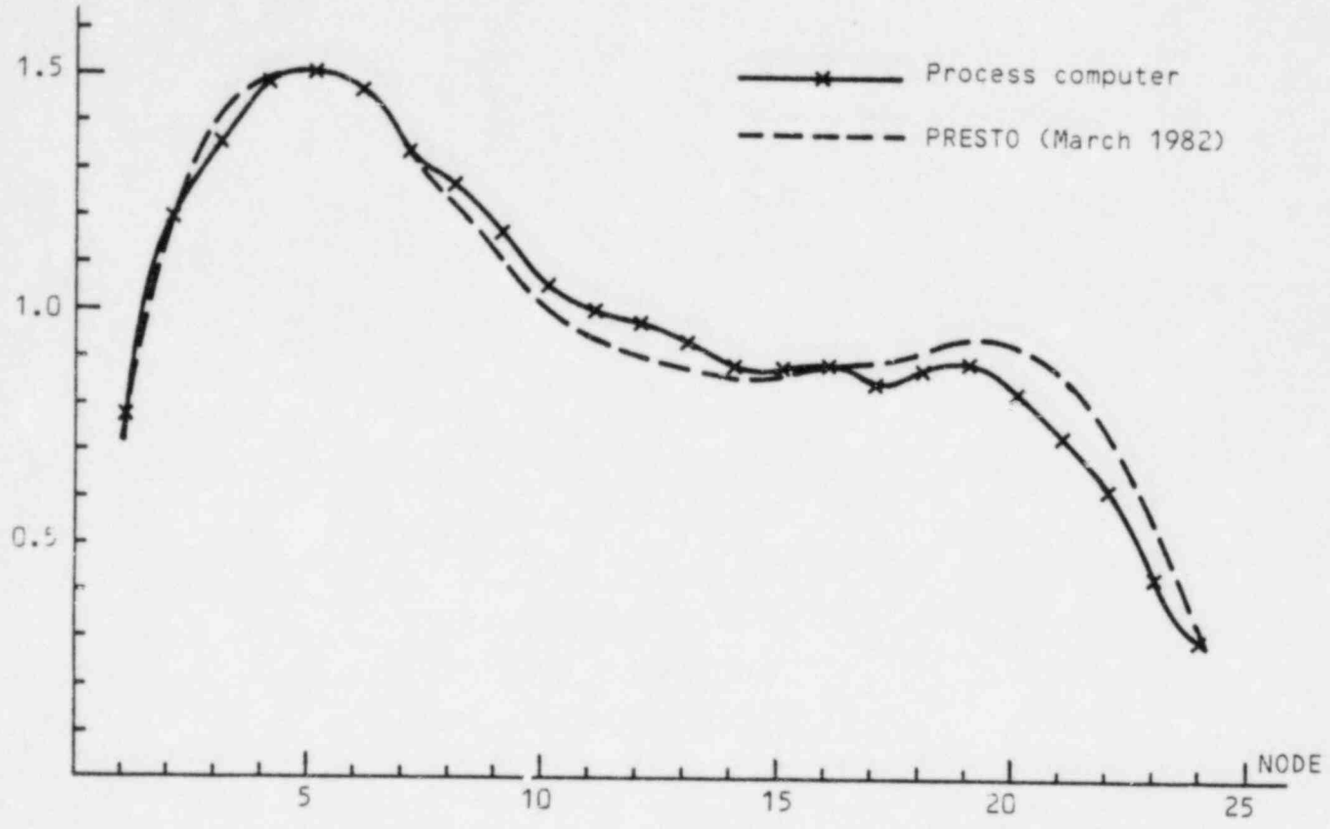

Core Average Axial Power Distribution on 24 October 1975
at 3646 MWD/TU

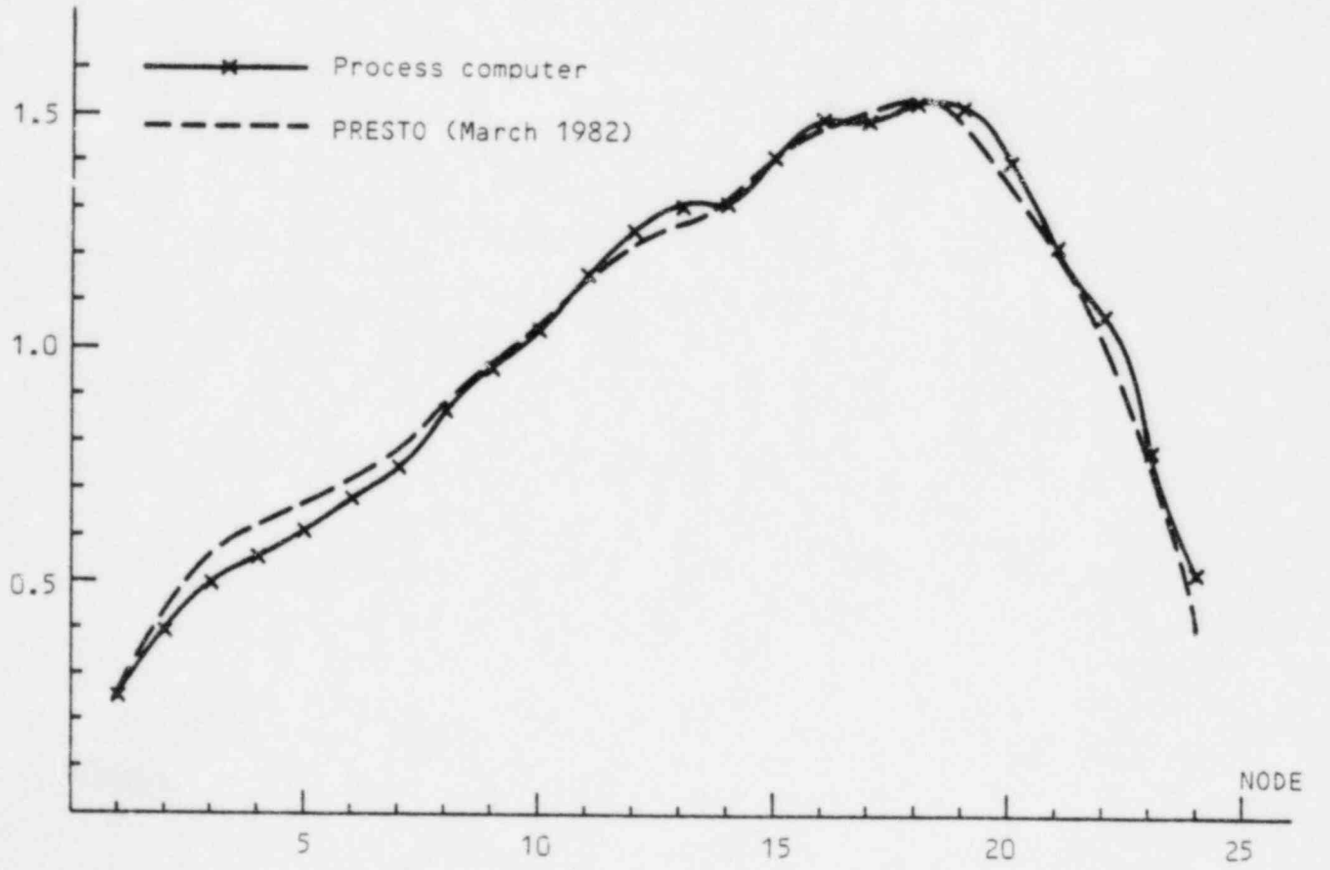

FIGURE 11.43 Core Average Axial Power Distribution on 7 March 1977
at 10 311 MWD/TU

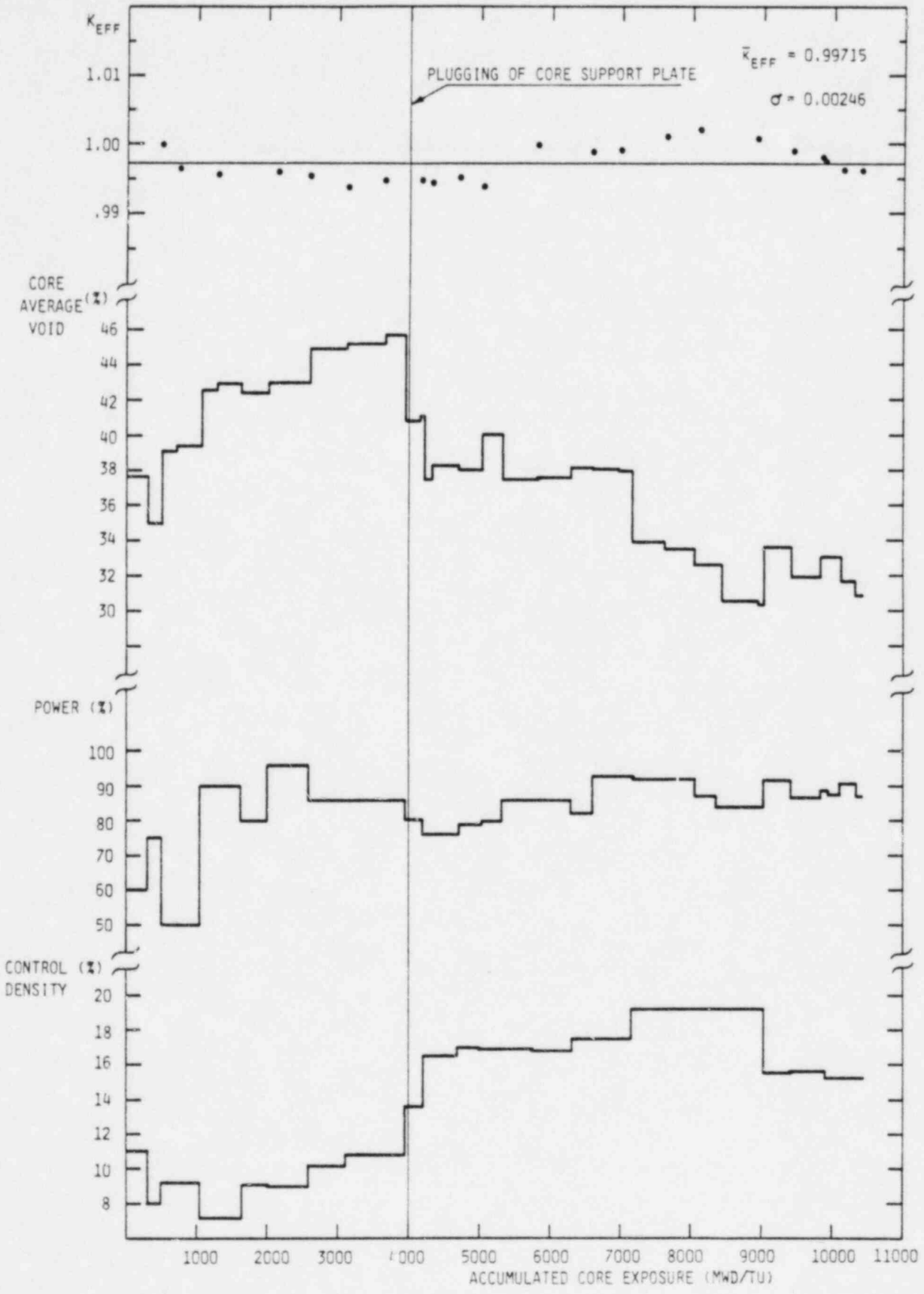

FIGURE 11.44 Calculated k_{eff} and Core Average Void Fraction vs. Core Average Exposure through Cycle 1. Power Level and Control Density also shown

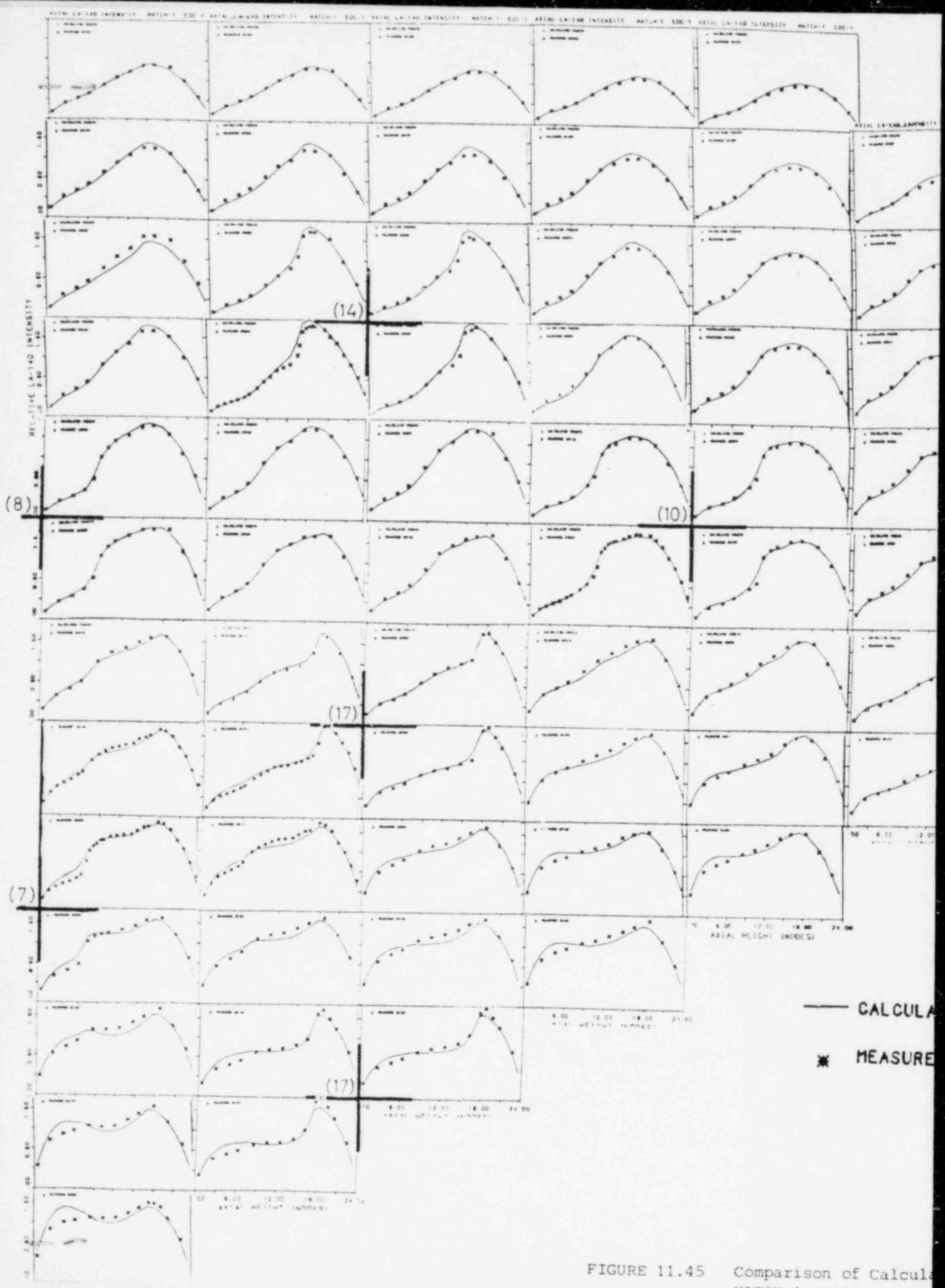

FIGURE 11.45 Comparison of Calcula
HATCH-1, EOC-1, as C

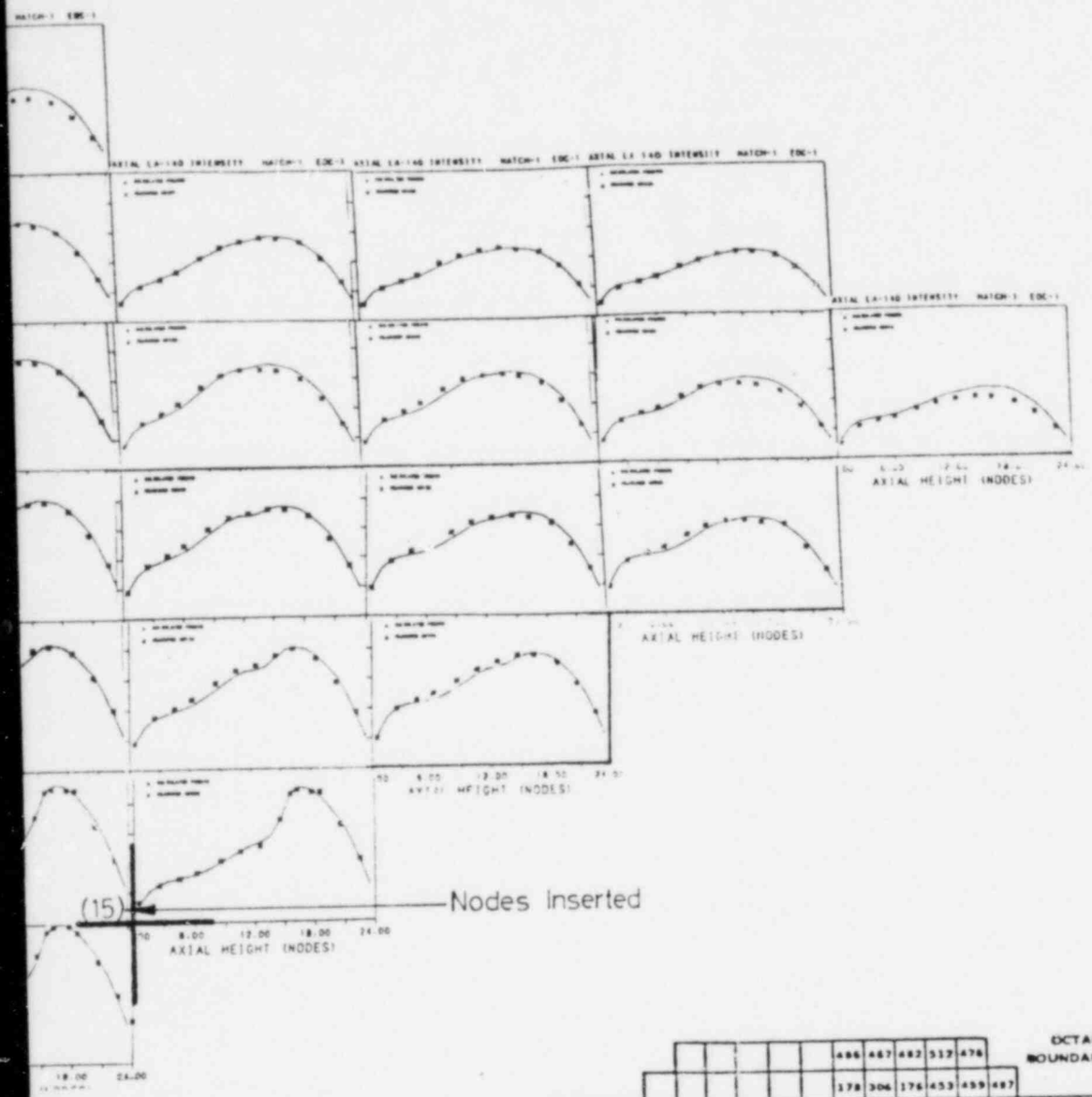

TED PRESTO

D

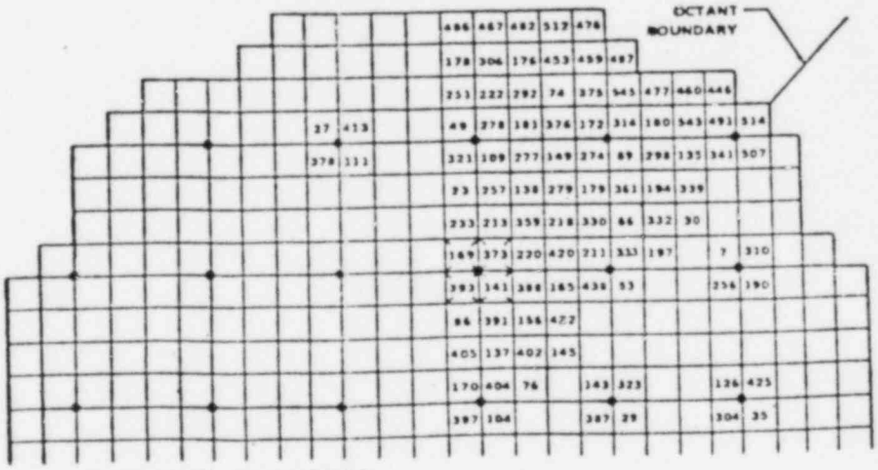

STANDARD DEVIATION

- Controlled Nodes : 6.4% (182 Points)
- Uncontrolled Nodes : 6.5% (828 Points)
- TOTAL : 6.4% (1010 Points)

ted and Measured Axial La-140 Distributions for All Bundles in Benchmark Octant,
lculated by PMS - PRESTO

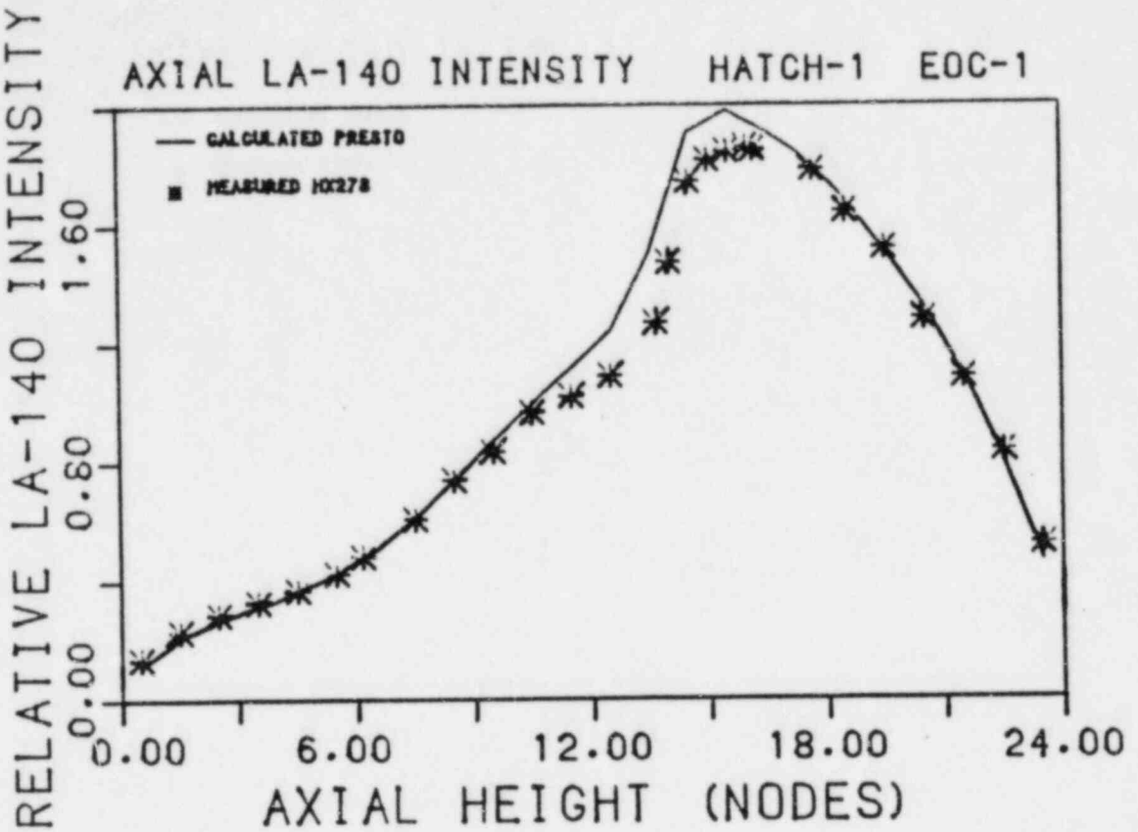

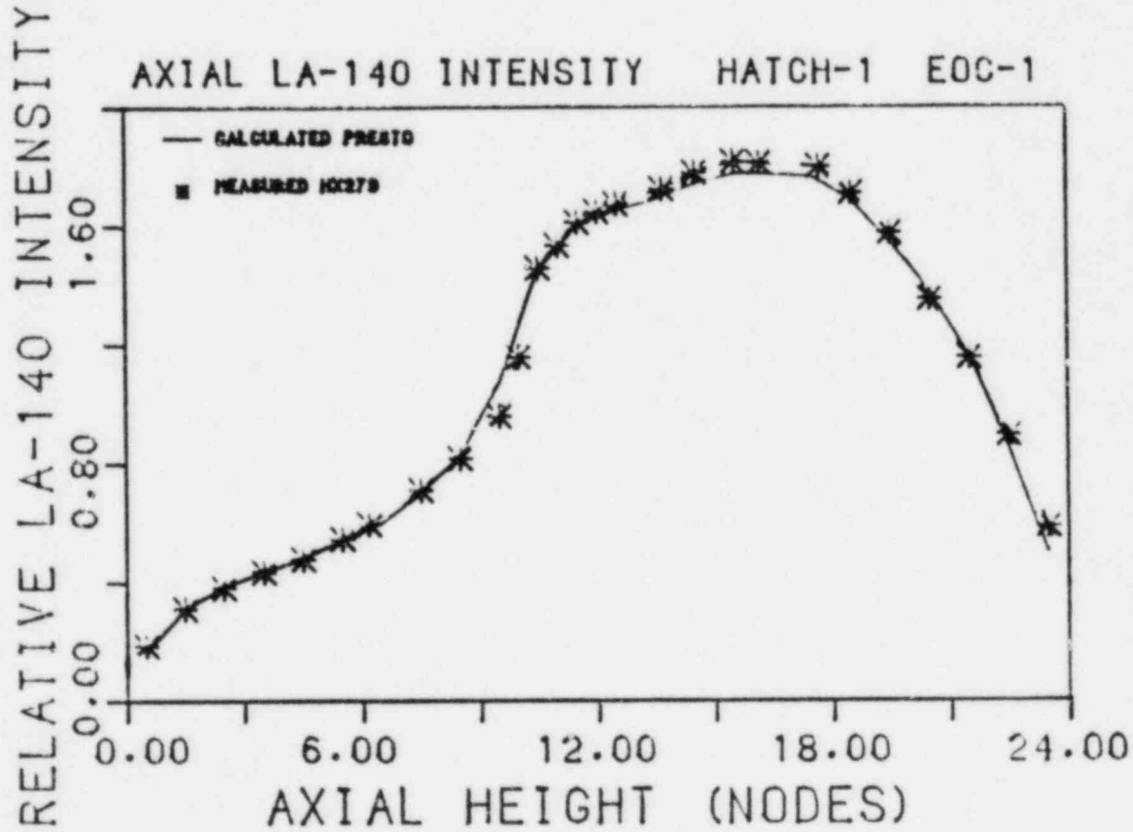

FIGURE 11.46 Comparisons for Bundles 278 and 279, both with 27 Measured Points

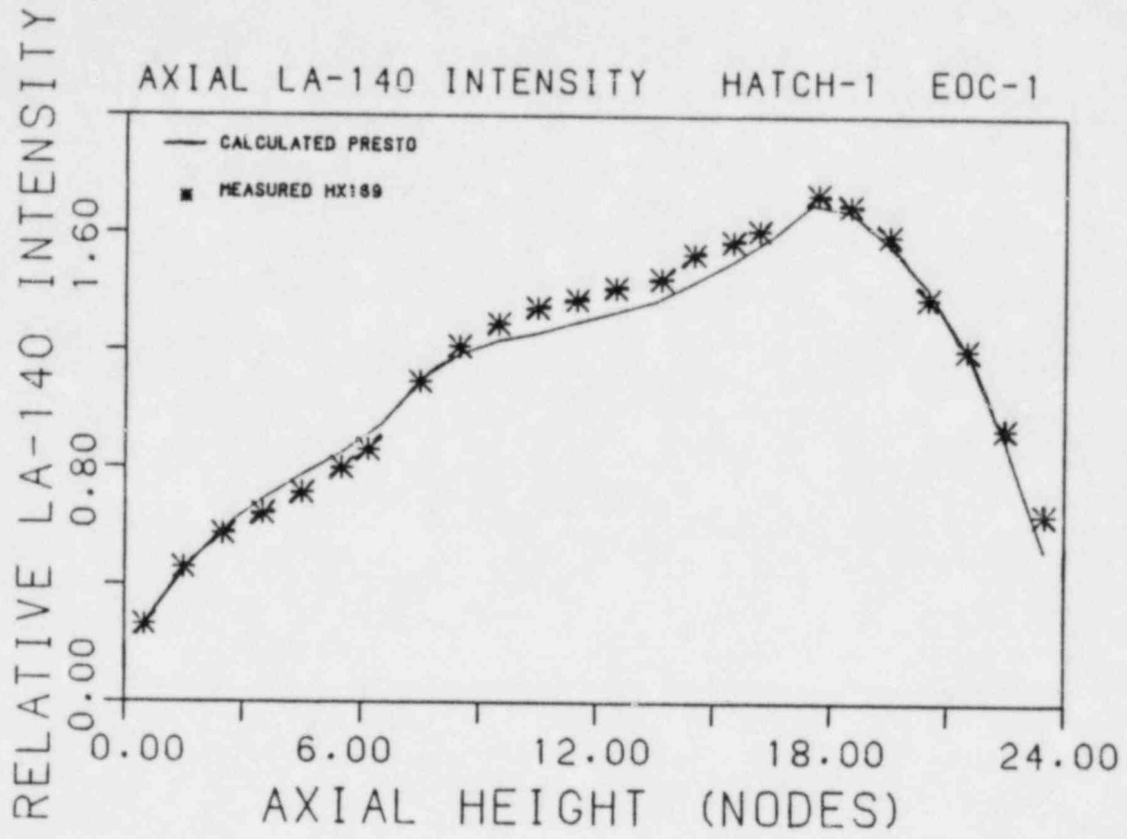

FIGURE 11.47 Comparison for Bundle 169, 24 Measured Points

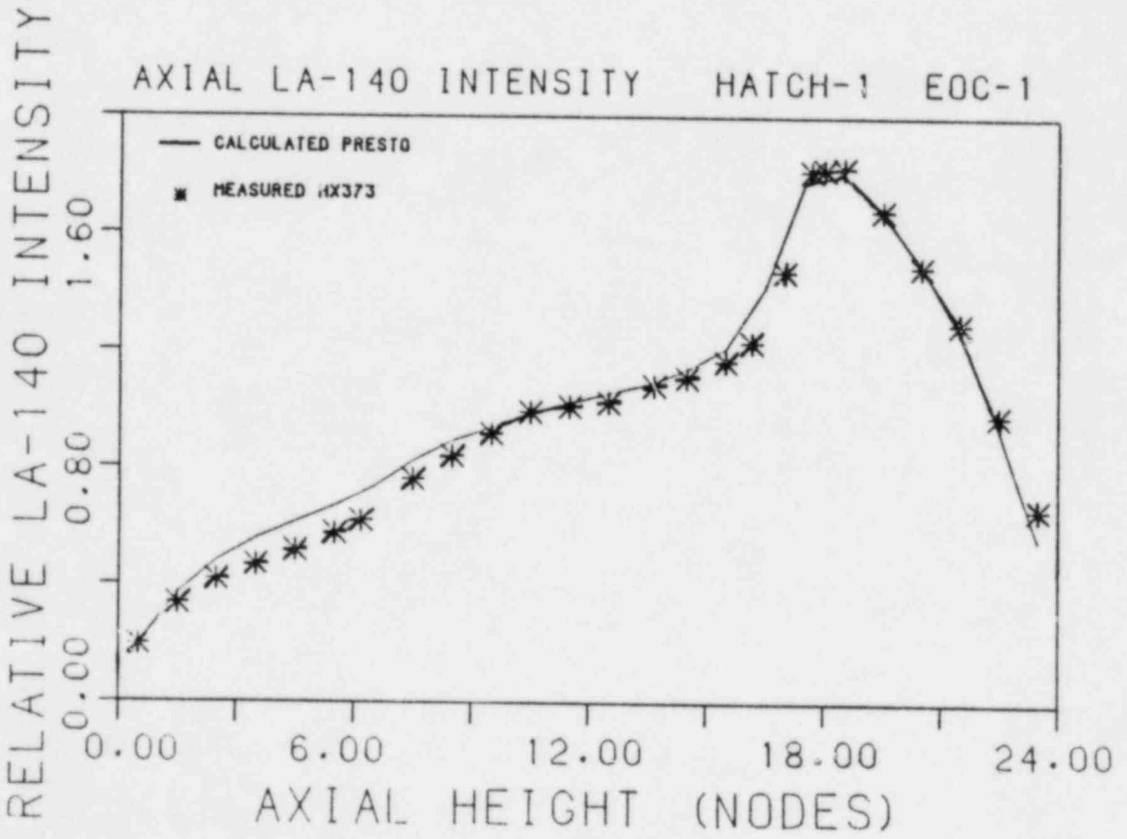

FIGURE 11.48 Comparison for Bundle 373, 27 Measured Points

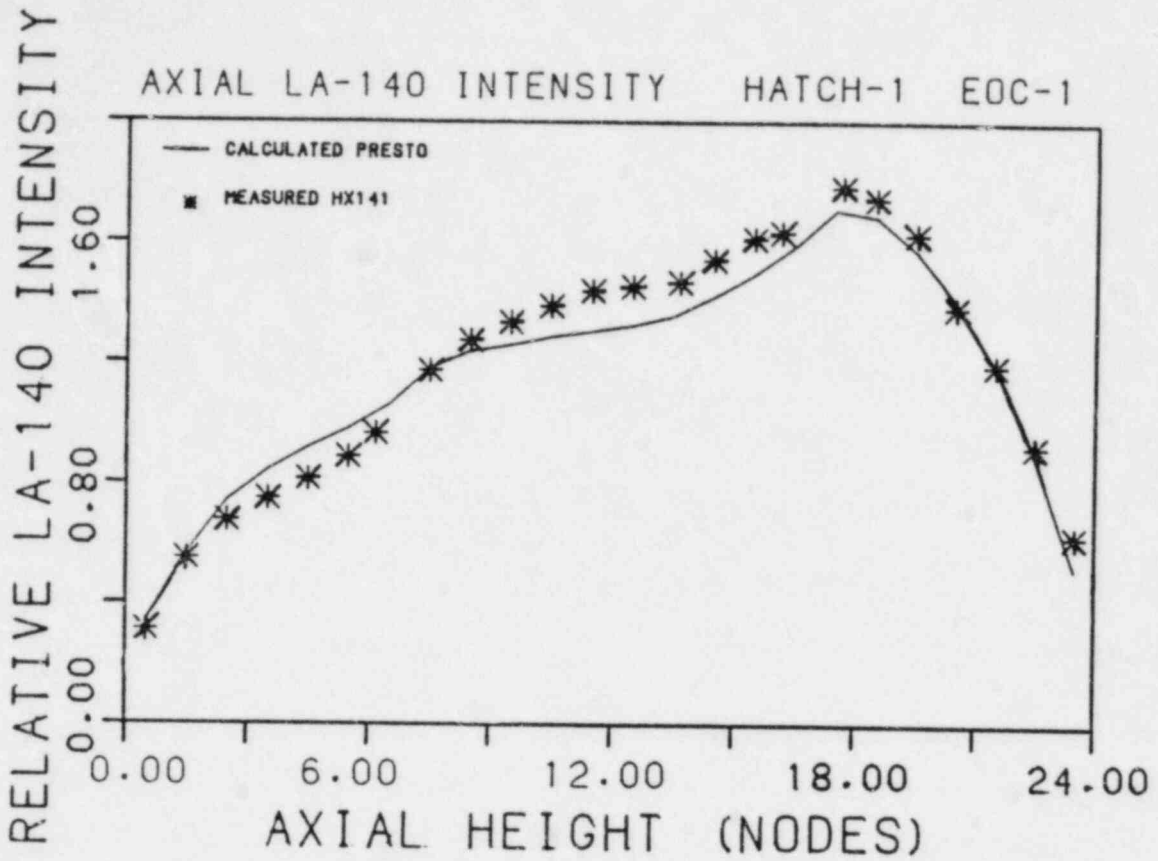

FIGURE 11.49 Comparison for Bundle 141, 24 Measured Points

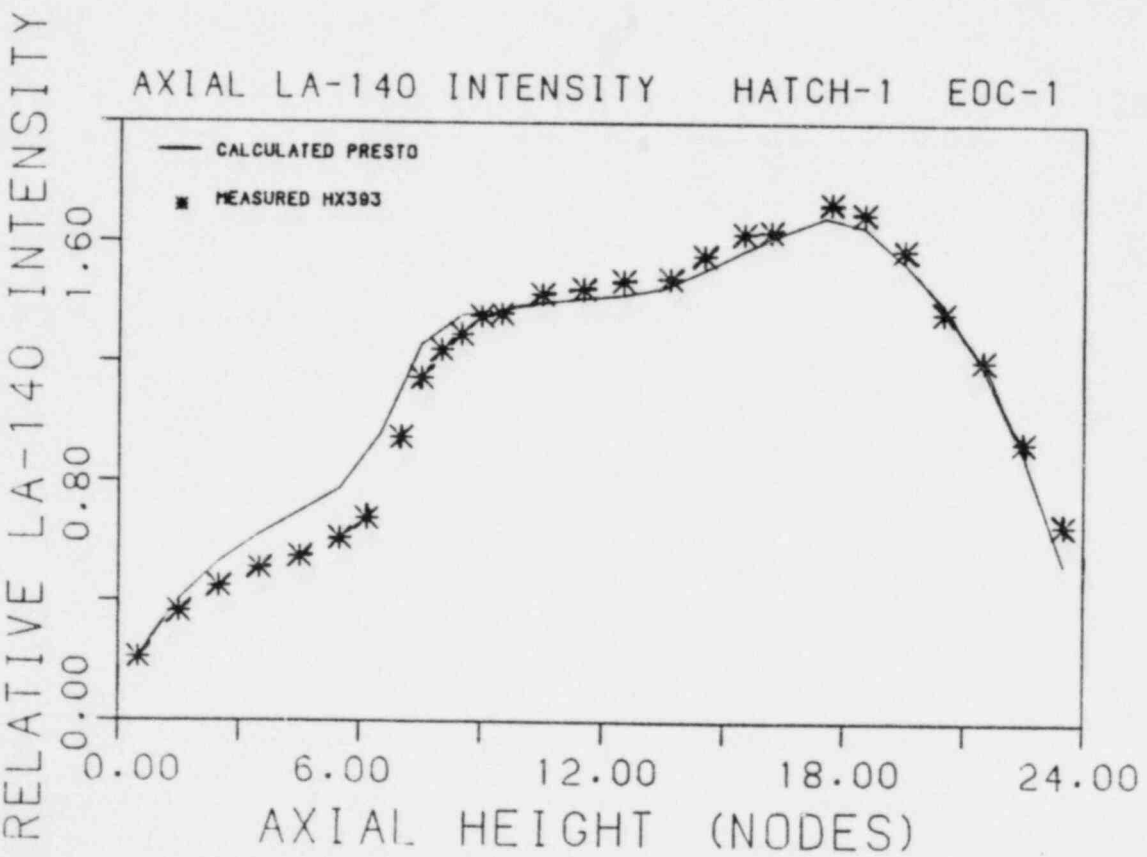

FIGURE 11.50 Comparison for Bundle 393, 27 Measured Points

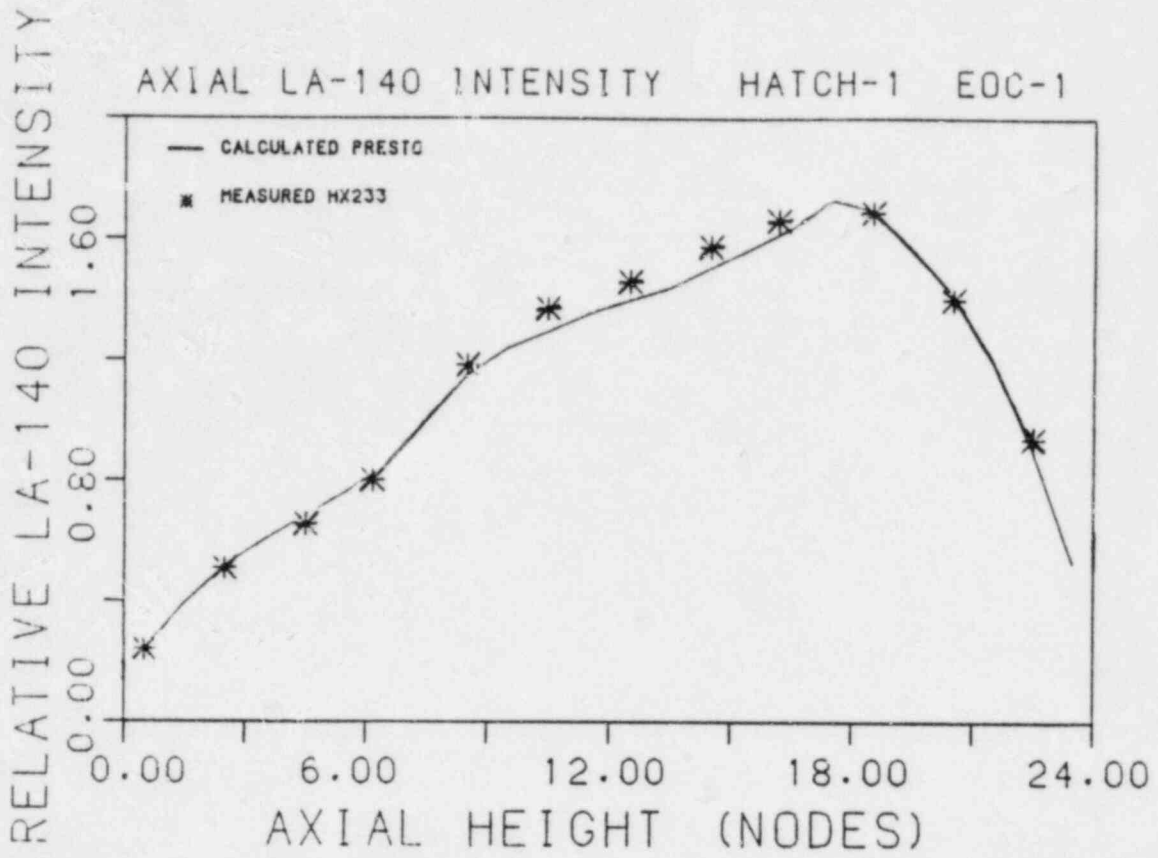

FIGURE 11.51 Example of Comparison for Unrodded Bundle

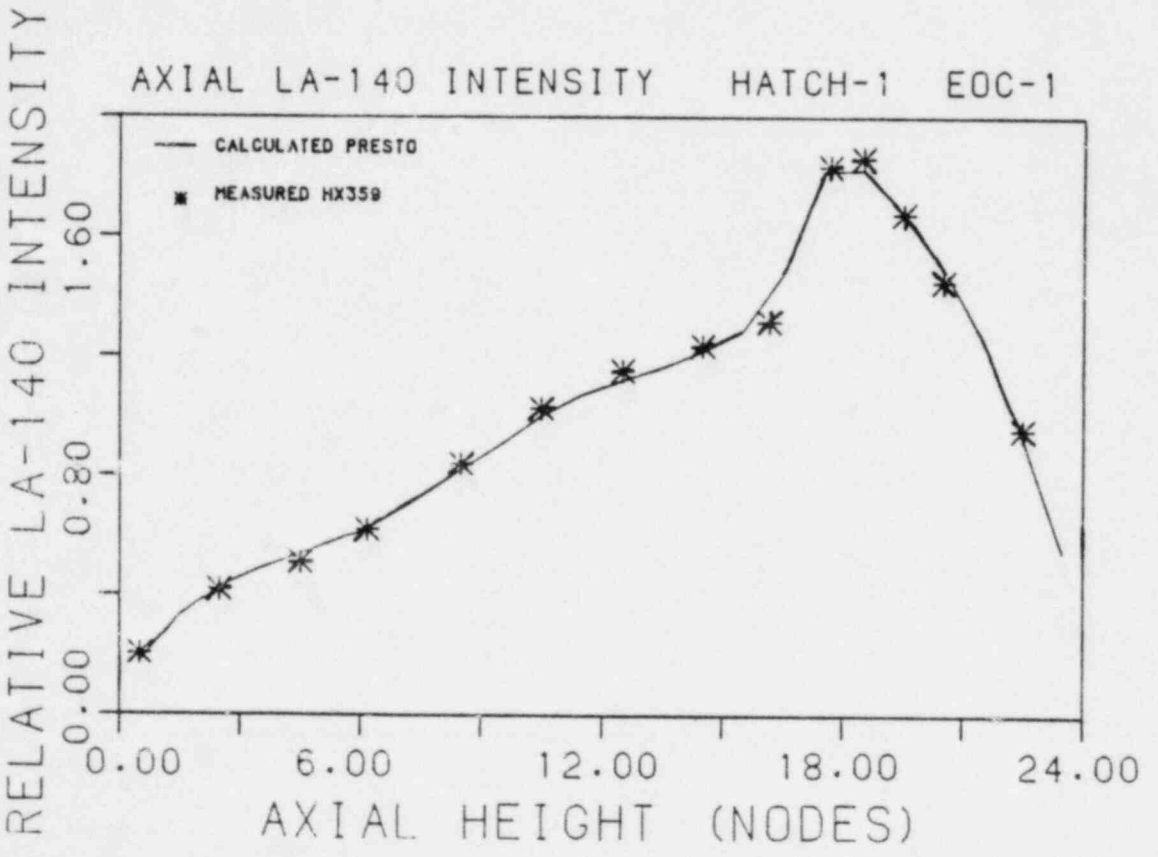

FIGURE 11.52 Example of Comparison for Bundle with Deep Control Rod (Notch 14)

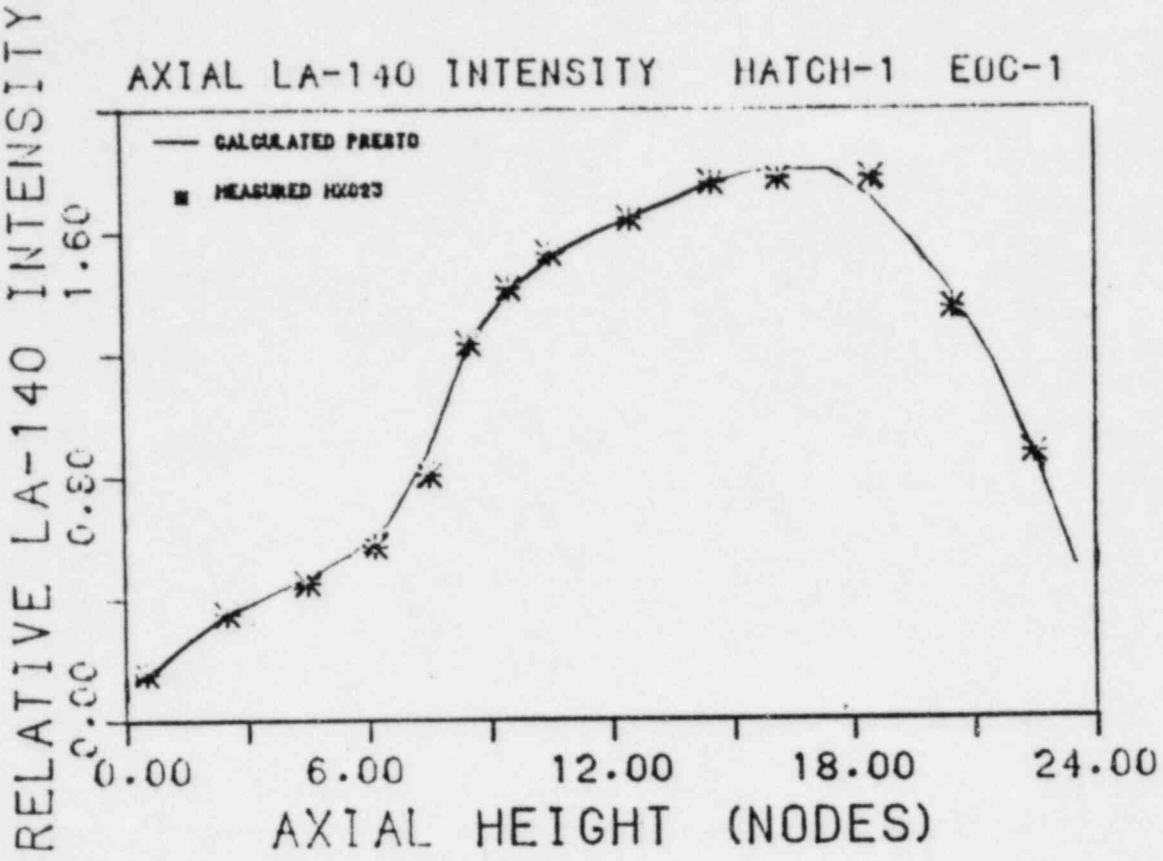

FIGURE 11.53 Example of Comparison for Bundle with Shallow Control Rod (Notch 32)

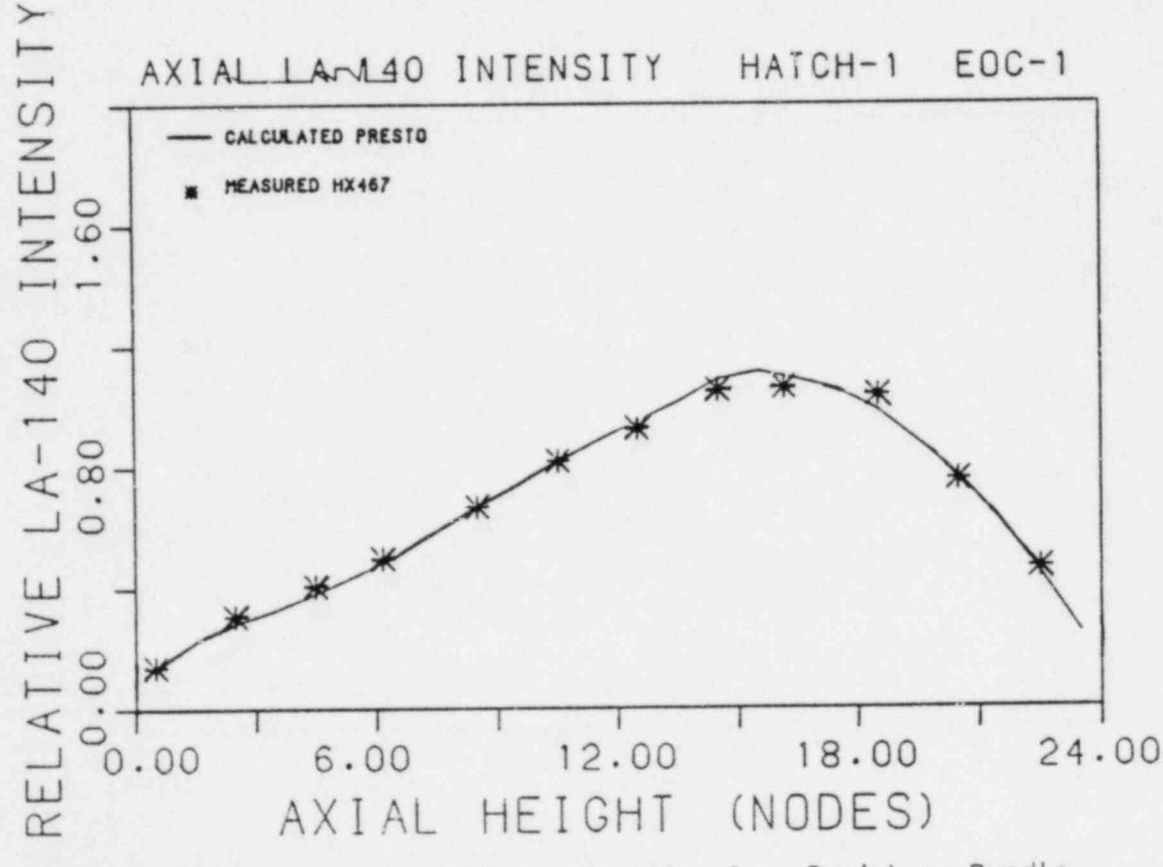

FIGURE 11.54 Example of Comparison for Core Periphery Bundle

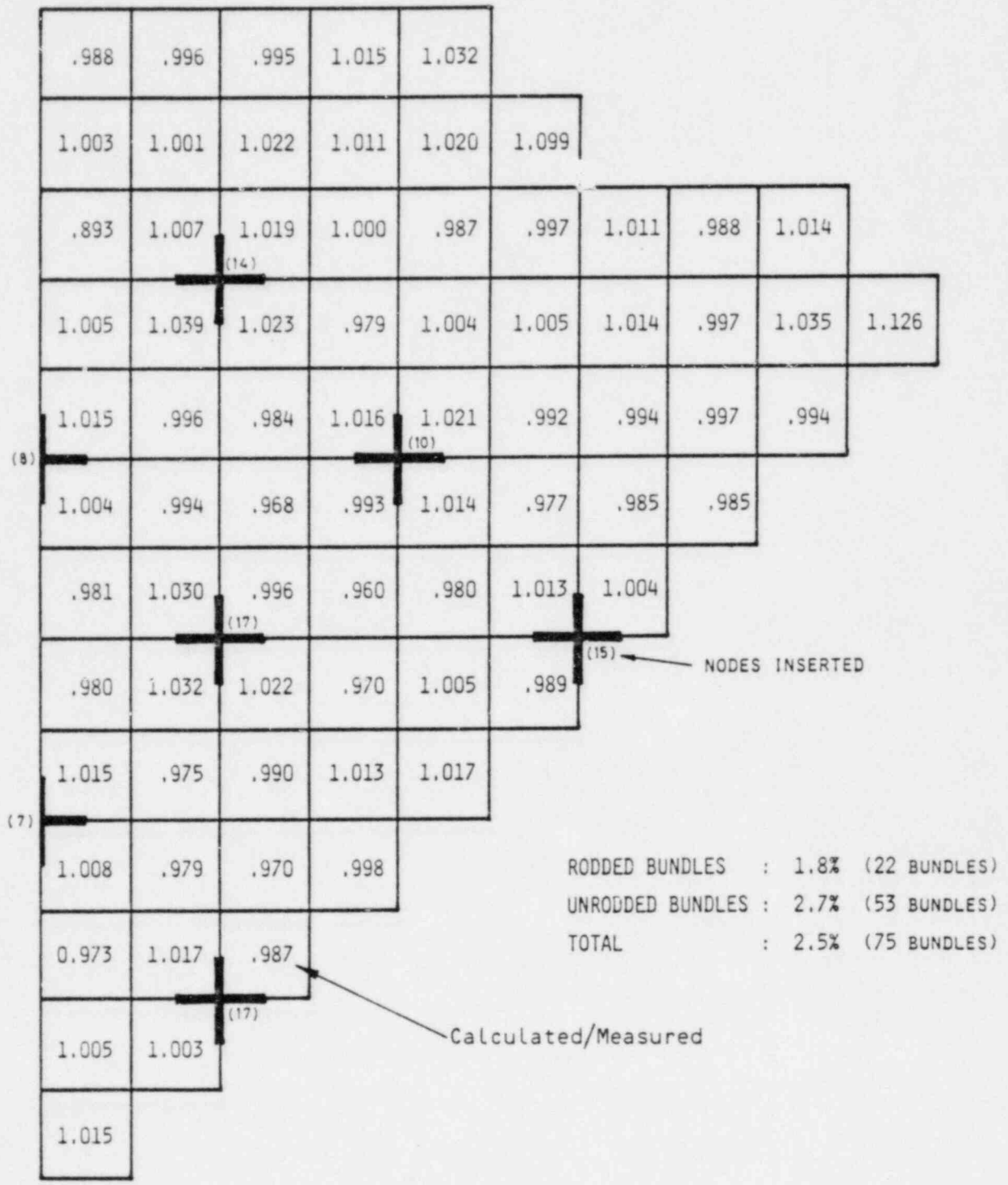

FIGURE 11.55 Bundlewise Ratios of Calculated and Measured, Axially Integrated, La-140 Distributions

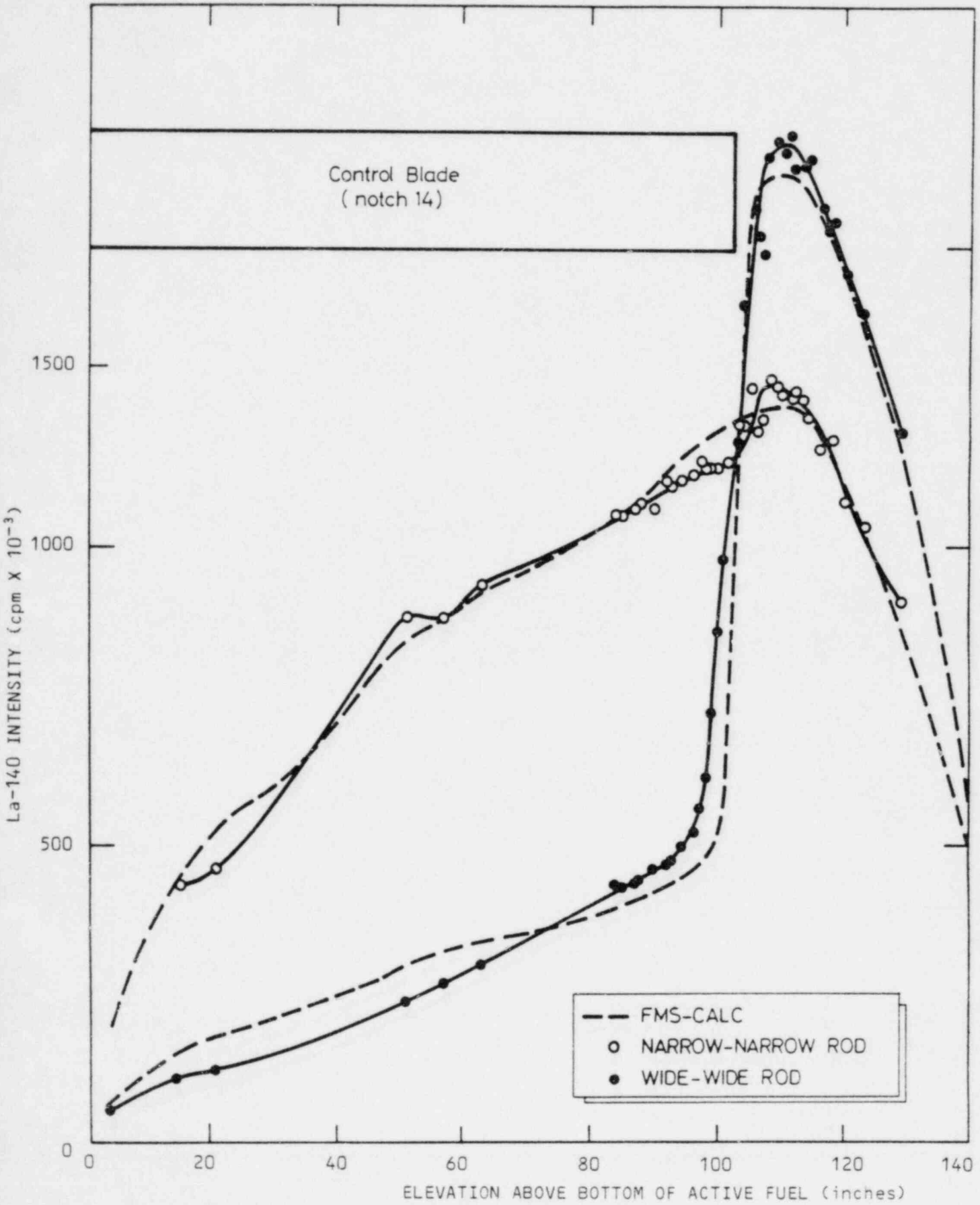

FIGURE 11.56 Calculated and Measured Axial La-140 Distributions in N-N and W-W Pins in HX-373

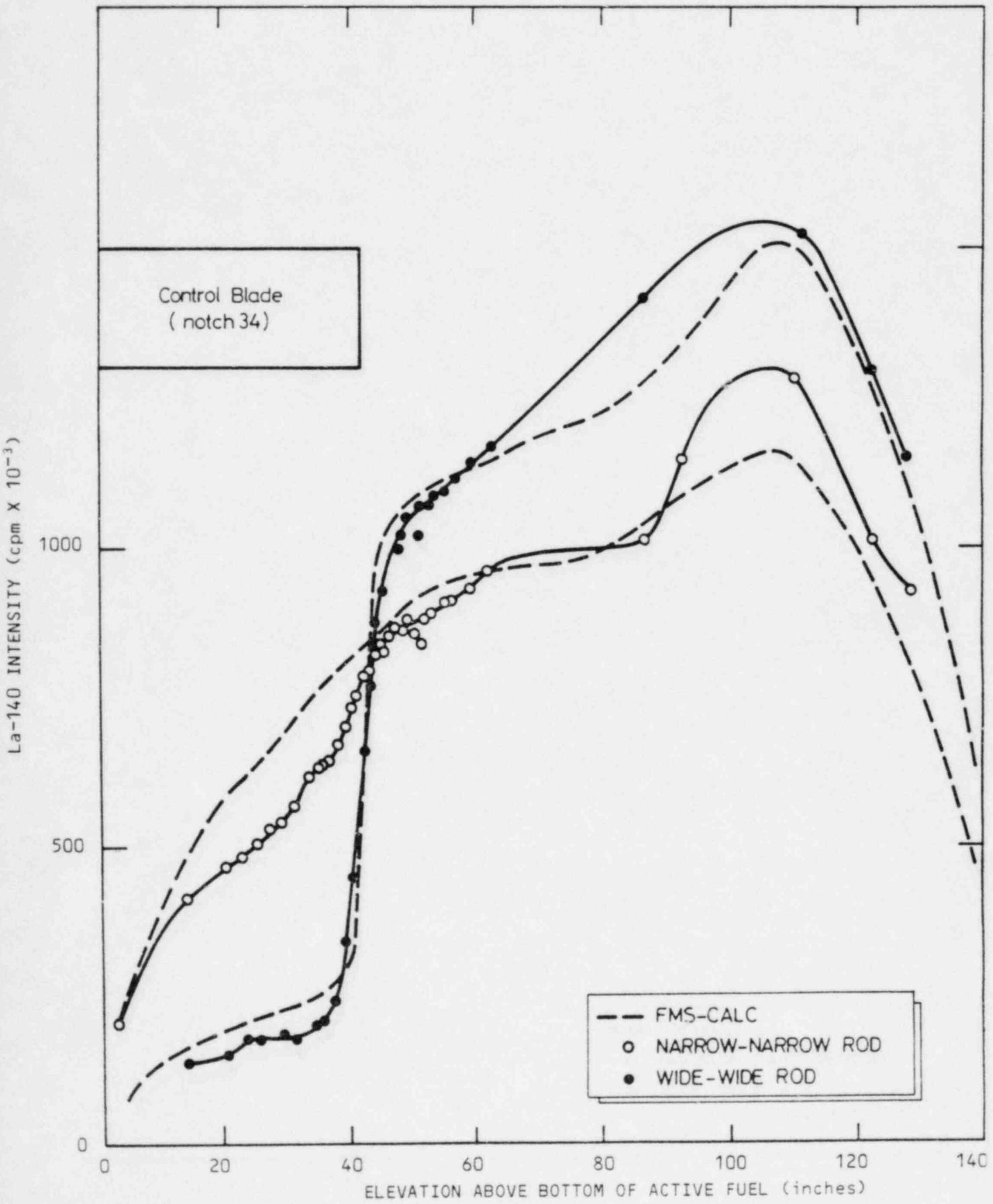

FIGURE 11.57 Calculated and Measured Axial La-140 Distributions in N-N and W-W Pins in HX-393.

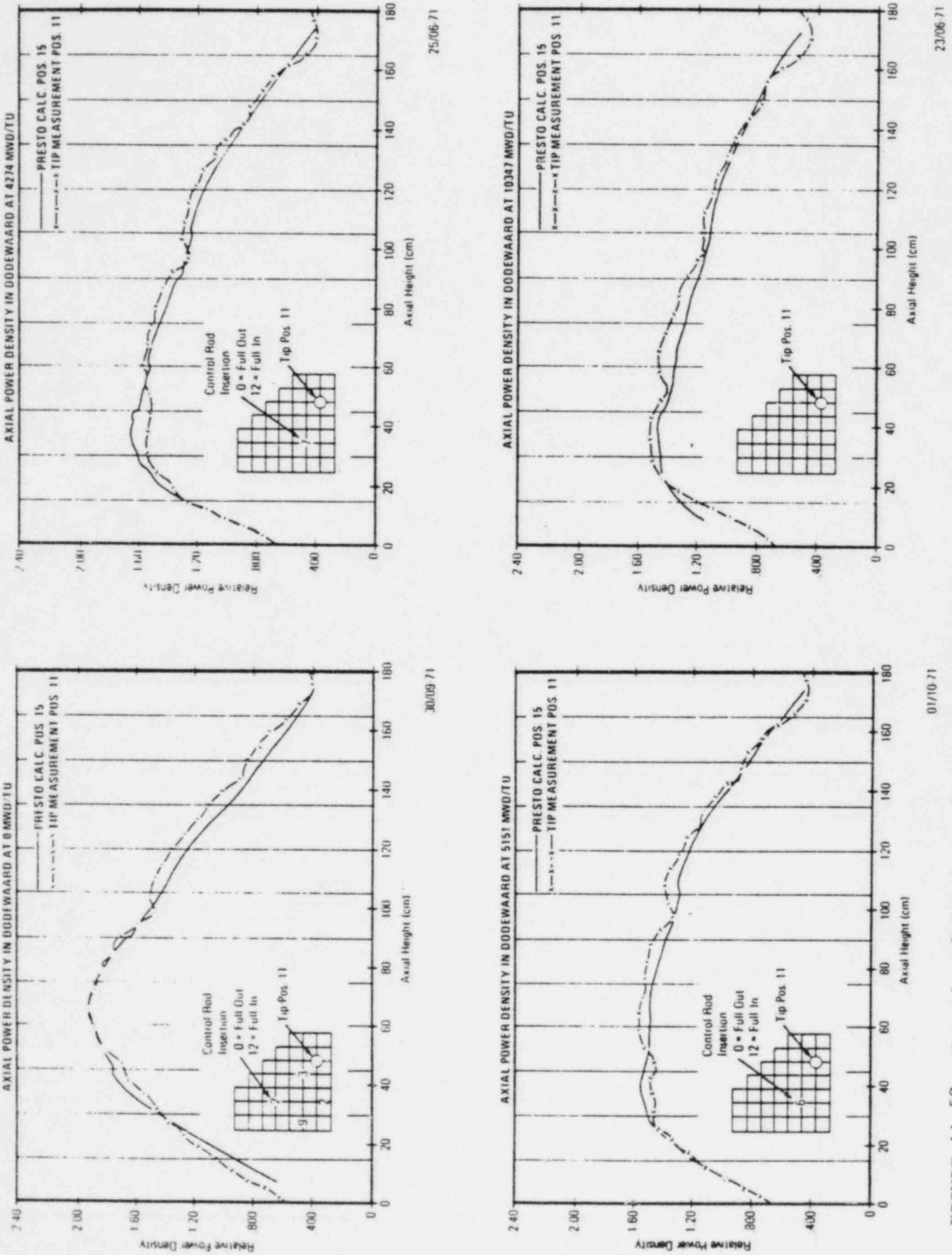

FIGURE 11.58 Example of TIP Comparison, DODEWAARD

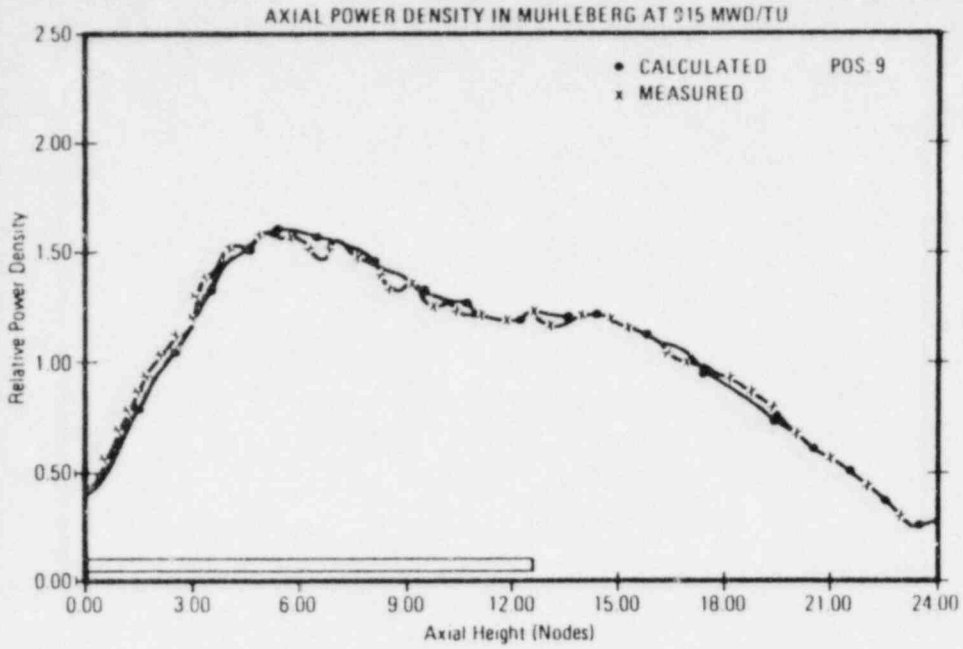

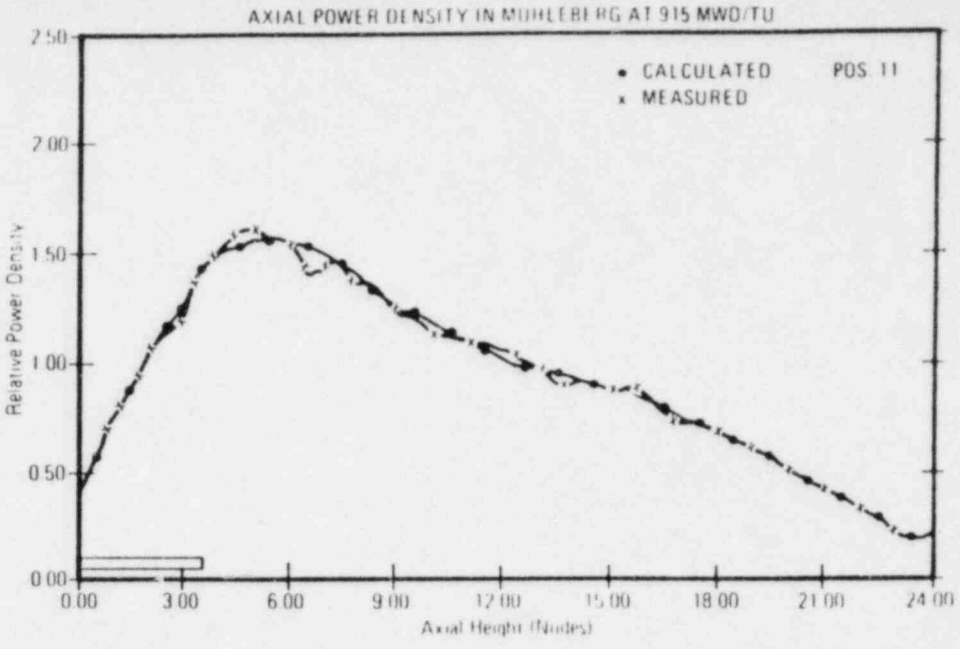

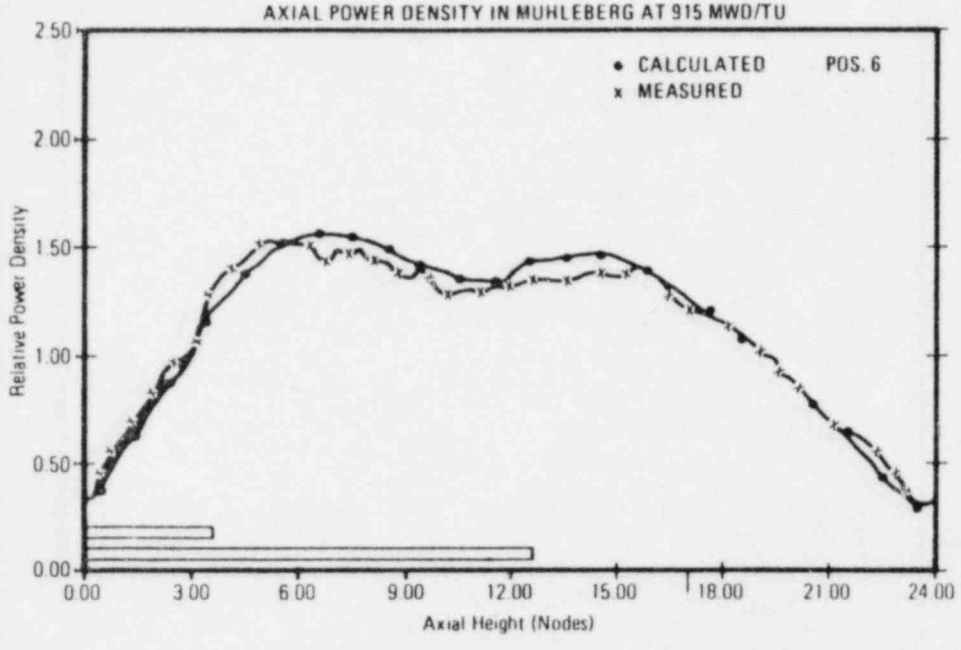

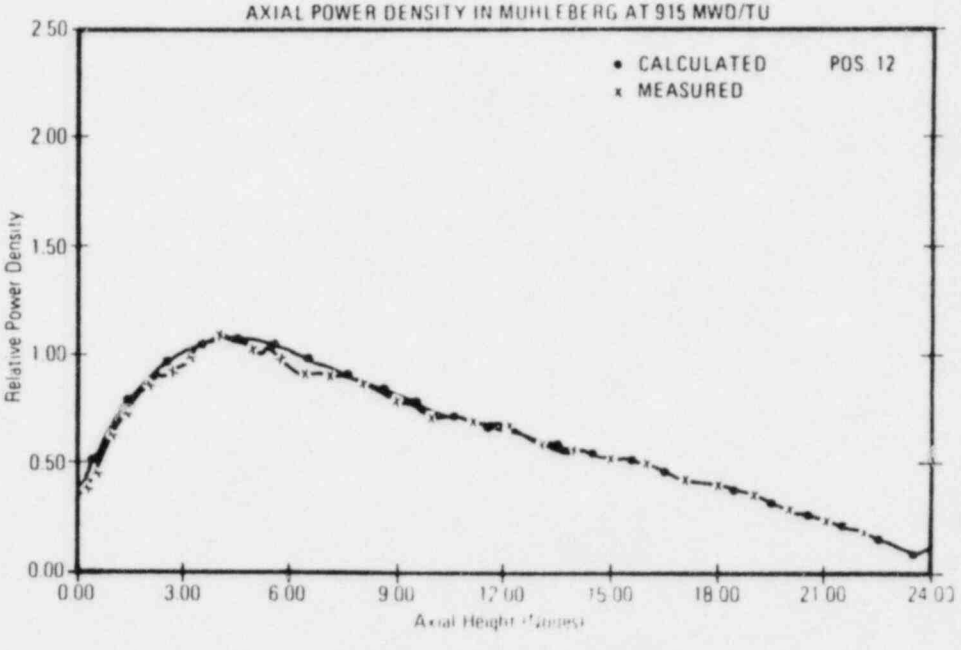

FIGURE 11.59 Examples of Comparisons of Measured and PRESTO Calculated TIP Traces (Control Rod Insertions in Adjacent Channels are Indicated.)

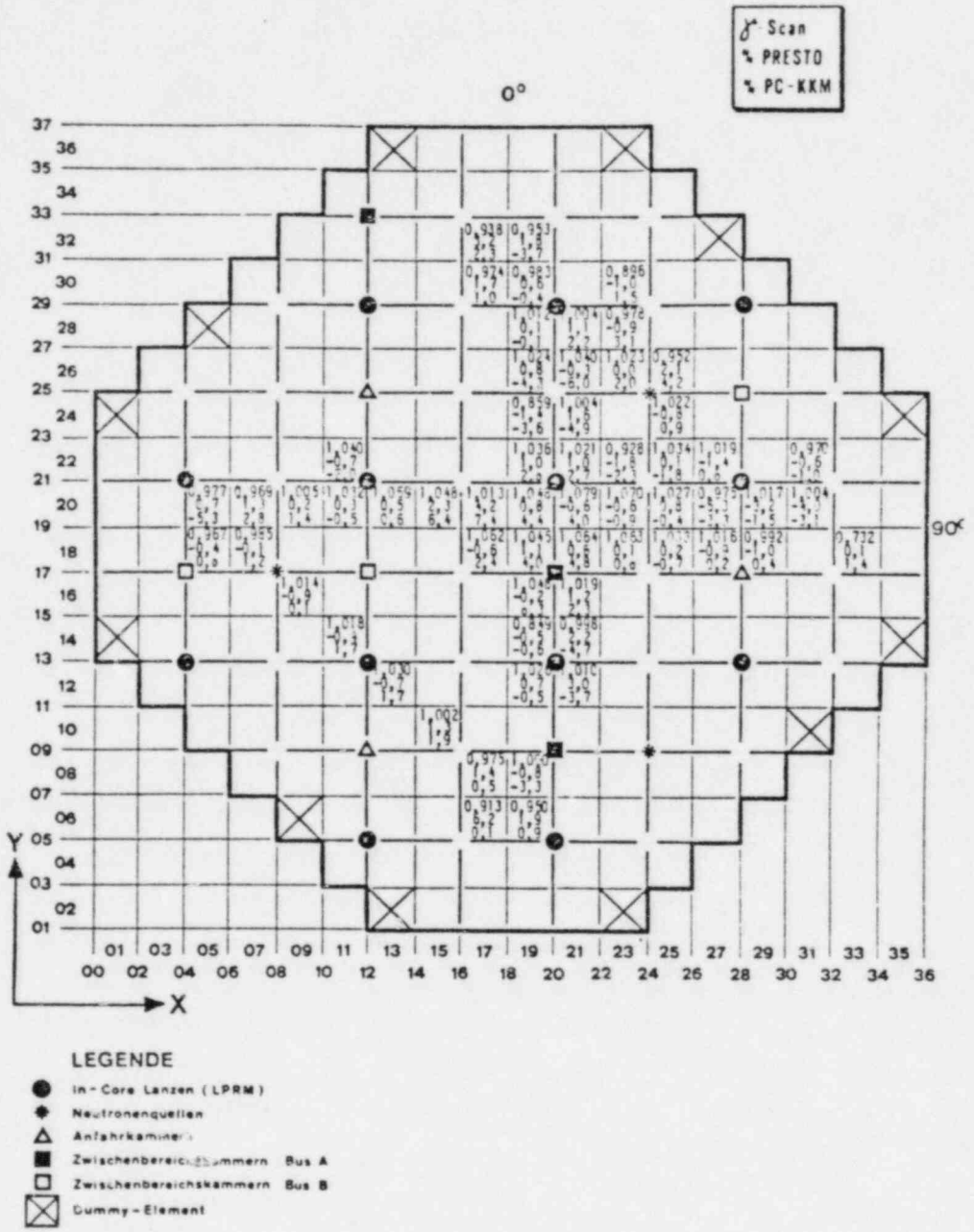

FIGURE 11.60 Relative, Assemblywise Burnup Distribution at EOC-1 of KKM, as Measured by γ-Scanning and Per cent Deviation of PRESTO Calculation and Process Computer Results

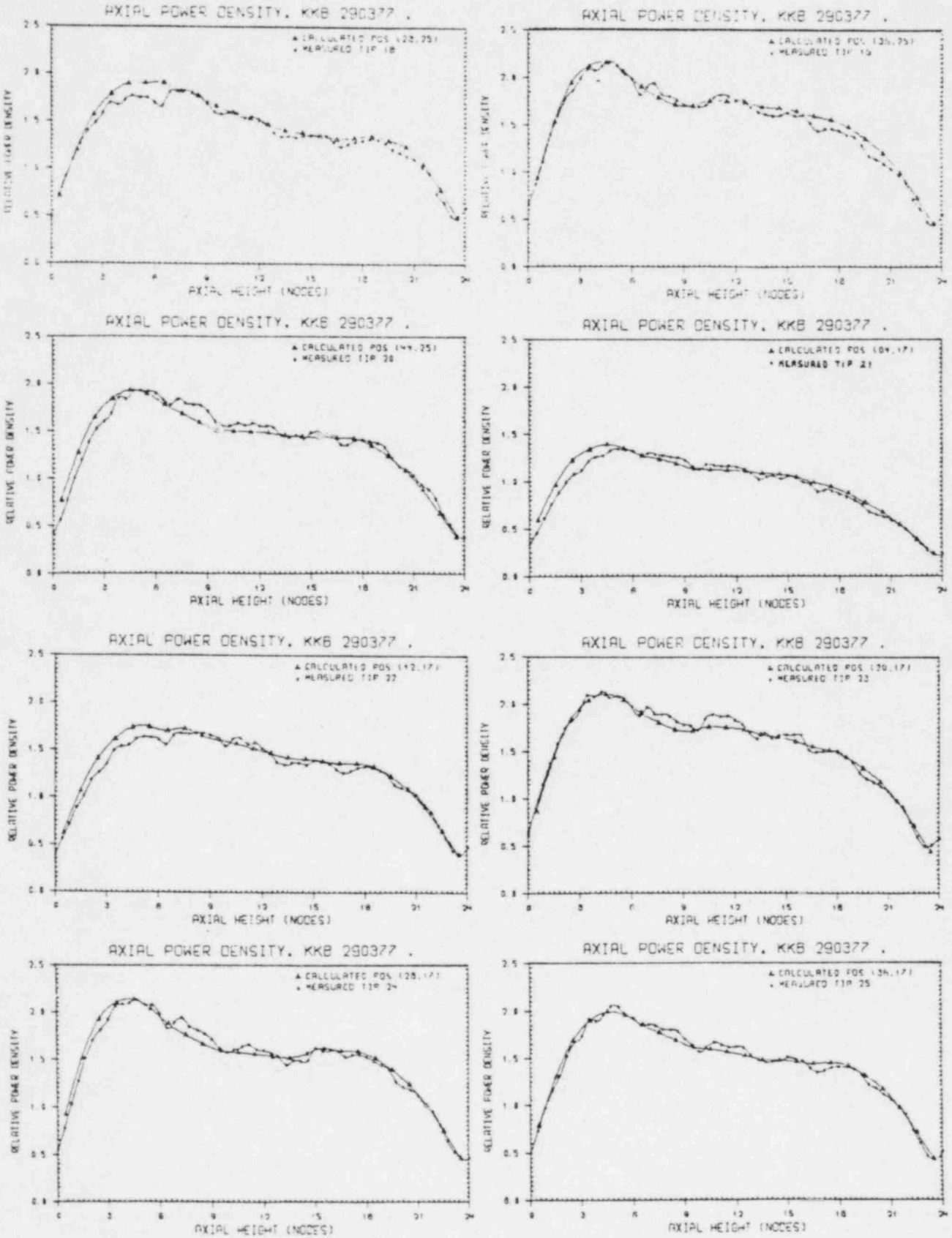

FIGURE 11.61 Example of TIP Comparison, BRUNSBÜTTEL (KKB)

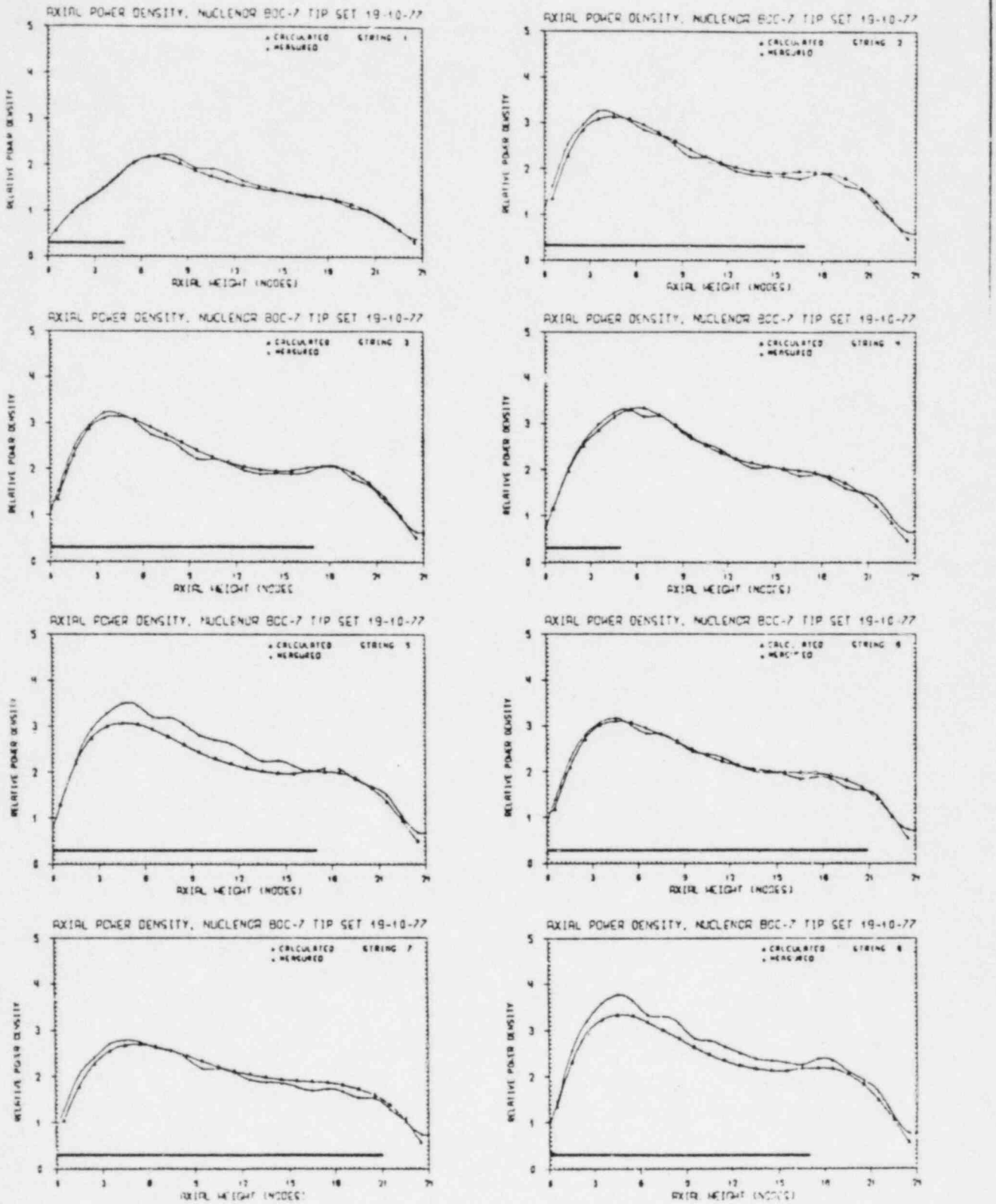

FIGURE 11.62 Example of TIP Comparisons, Santa Maria de Garoña (NUCLENOR)

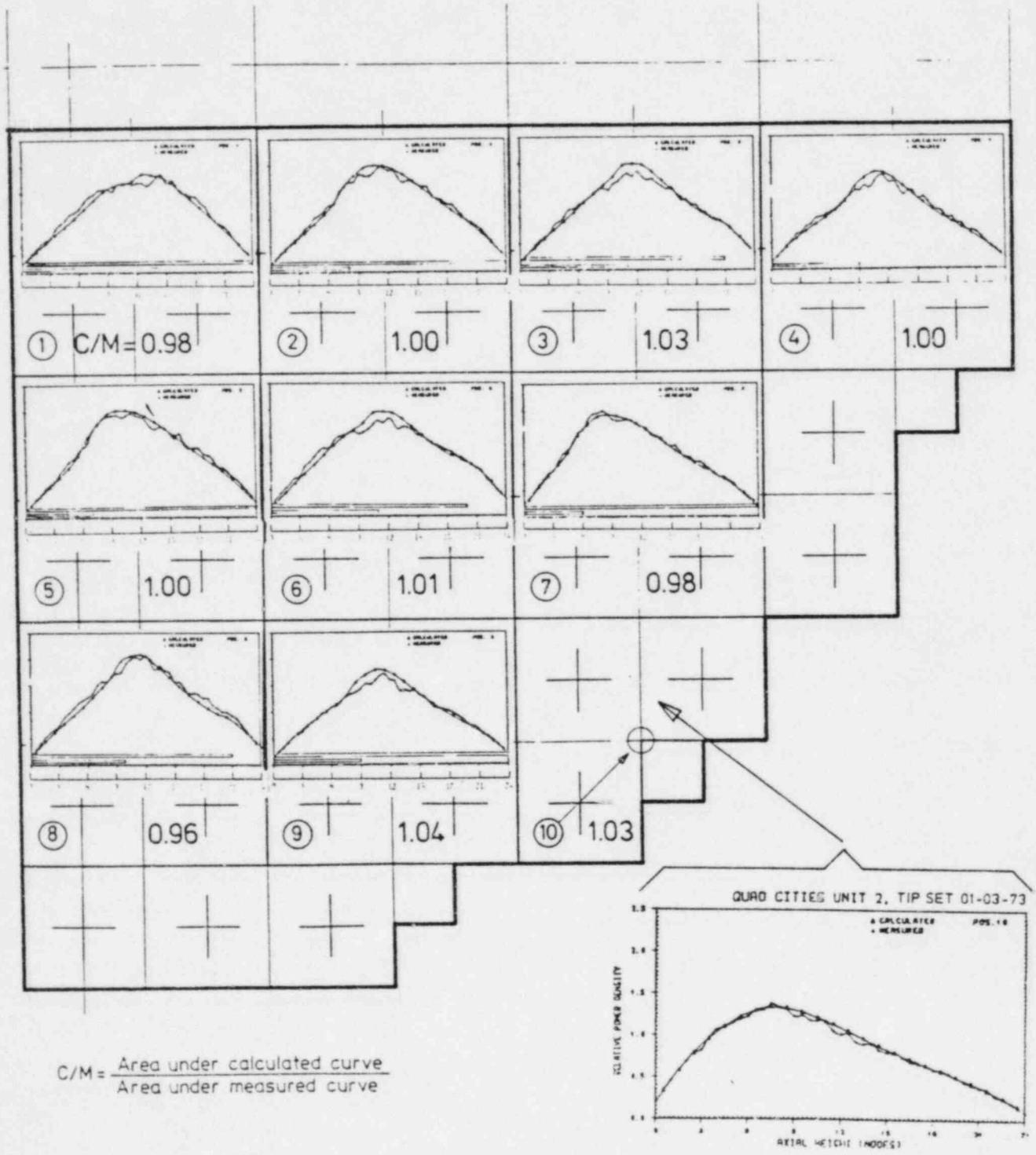

FIGURE 11.63 Evaluation of Calculated Power Distributions. Comparisons with TIP-Traces, BOC-1, Quad Cities-2

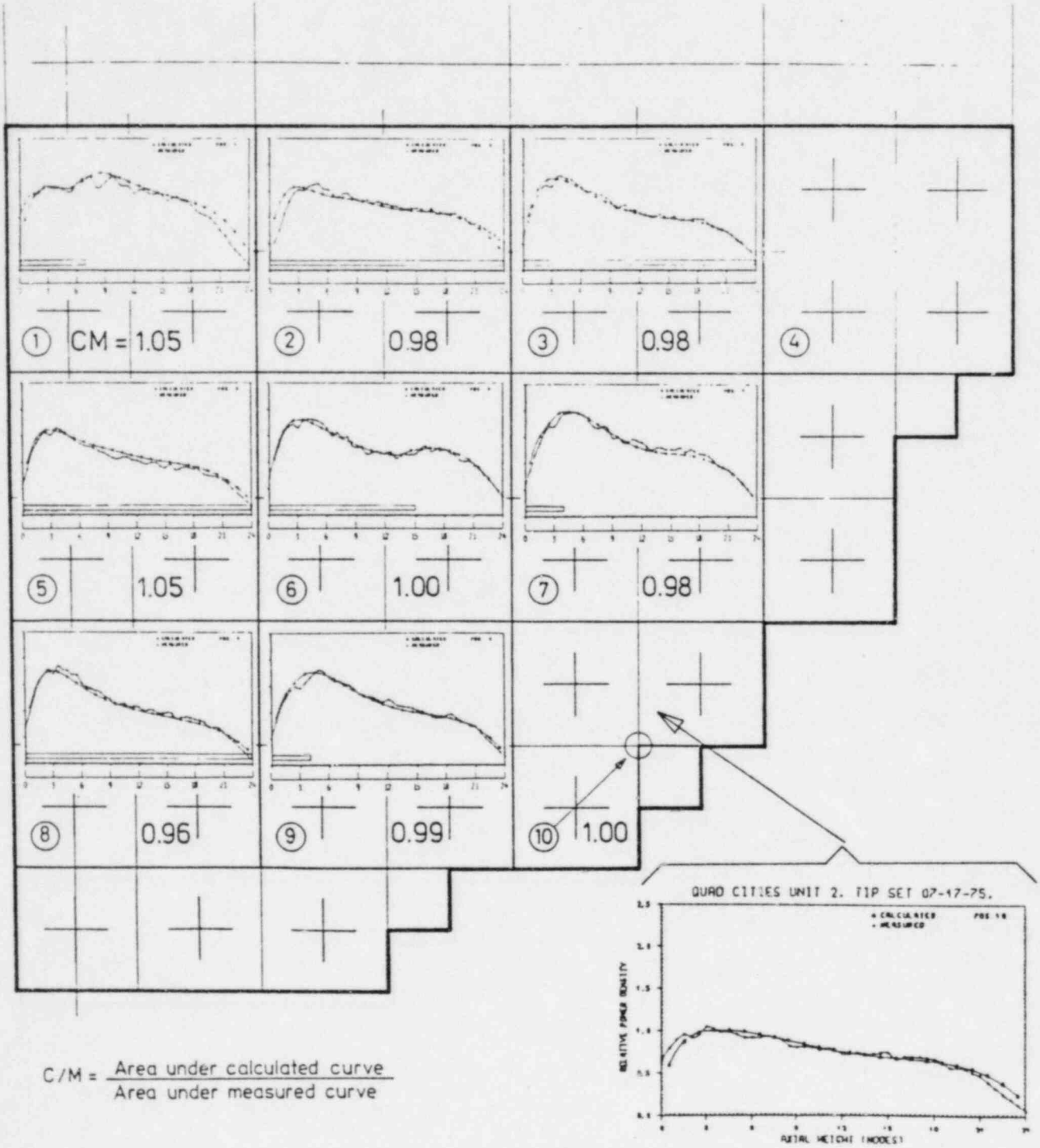

$$C/M = \frac{\text{Area under calculated curve}}{\text{Area under measured curve}}$$

FIGURE 11.64 Evaluation of Calculated Power Distributions. Comparisons with TIP-Traces, BOC-2, Quad Cities-2

12. REFERENCES

1. S. Børresen, "A Simplified, Coarse-Mesh, Three-Dimensional Diffusion Scheme for Calculating the Gross Power Distribution in a Boiling Water Reactor", NSE 44, 37-43 (1971).

2. P. Backstad, K.O. Solberg, "A Model for the Dynamics of Nuclear Reactors with Boiling Coolant with a New Approach to the Vapour Generating Process". KR-121, Kjeller, Norway, August 1967.

3. Argonne Code Center, "Benchmark Problem Book", ANL-7416, Suppl. 2, ANL (1977).

4. O. Nylund, et al, Confidential FRIGG reports on experiments and results (1969, 1970).

5. O. Nylund, K.M. Becker, et al, "FRIGG Loop Project. Hydrodynamic and Heat Transfer Measurements on a Full Scale, 36 Rod BHWR Fuel Element". Sweden 1970.

6. R. Holt, J. Rasmussen, "RAMONA-II, A FORTRAN Code for Transient Analysis of Boiling Water Reactors". KR-147, Kjeller, Norway, August 1972.

7. L. Moberg, et al, "RAMONA Analysis of the Peach Bottom-2 Turbine Trip Transients". EPRI NP-1869, June 1981.

8. K. Becker, G. Hernborg and M. Bode, "An Experimental Study of Pressure Gradients for Flow of Boiling Water in a Vertical Round Duct". Parts 1, 2 and 3, AE-69, 70 and 85, Aktiebolaget Atomenergi, Sweden, 1962.

9. R.T. Lahey, F.J. Moody, "The Thermal-Hydraulics of a Boiling Water Nuclear Reactor". Published by American Nuclear Society, 1977.

10. K.E. Karcher, "MERLIN - A Two-Group Three-Dimensional BWR Nodal Simulator with Thermal Hydraulic Feedback", Carolina Power & Light Company, Internal Report, December 1979.

11. N.H. Larsen, J.G. Goudey, "Core Design and Operating Data for Cycle 1 of HATCH-1", EPRI NP-562, 1979.

12. L.M. Shiraishi, G.R. Parkos, "Gamma Scan Measurements at Edwin I. Hatch Nuclear Plant, Unit 1, Following Cycle 1", EPRI NP-511, Research Project 130-3, Final Report, August 1978.

13. S. Børresen, T. Skardhamar, S. Wennemo-Hanssen, "Applications of FMS RECORD/PRESTO for Analysis and Simulation of Operating LWR Cores", NEA Specialists Meeting Proceedings, Paris, November 1979.

14. J. Nitteberg, J. Haugen, J. Rasmussen, T.O. Sauar, "A Core-Follow Study of the Dodewaard Reactor with the Three-Dimensional BWR Simulator PRESTO", Kjeller Report, KR-145, 1971.

15. S. Børresen, H.K. Næss, T.O. Sauar, T. Skardhamar, F. Grandchamp, J. Rognon, R. Wehrli, C. Weigel, "Core-Follow Study of the Mühleberg BWR with the Fuel Management System - FMS", ENC, Paris, April 1975.

16. W. Wiest, H. Hofner, N. Naula, C. Weigel, R. Wehrli, "Gamma-Scanning in KKM und dessen Anwendung bei der Reaktorsimulation", presented at Reaktortagung 1978, Deutsches Atomforum e.V., Hannover, 1978.

17. H. Guyer, H. von Fellenberg, W. Wiest, "Core Simulation and Its Experimental Verification of the Mühleberg BWR", ENC, 1979, Hamburg, TANSAI 31, 1979.

18. S. Børresen, D.L. Pomeroy, E. Rolstad, T.O. Sauar, "Nuclear Fuel Performance Evaluation", EPRI NP-409, Final Report, June 1977.

19. S. Børresen, "Experience, Status and Advanced Applications of PRESTO", ANS/ENS Topical Meeting Proceedings, Munich, April 1981.

A P P E N D I X A

EQUATIONS FOR INTEGRATION OF SPECIAL ISOTOPES

A1. Xe-DYNAMICS EQUATIONS

The equations used in PRESTO to calculate the nodal concentrations of I and Xe at the end of a time step t, starting from the known concentrations at the beginning of the time step, are given below :

The differential equation for the I concentration is :

$$\frac{dI}{dt} = - \lambda_I \cdot I + \gamma_I \cdot F \qquad (A.1)$$

and

$$I_{eq} = \frac{\gamma_I}{\lambda_I} \cdot F \qquad (A.2)$$

where

I = local I- concentration (cm^{-3})

λ_I = decay constant for I (sec^{-1})

γ_I = fission yield fraction for I

F = local fission rate ($sec^{-1} \cdot cm^{-3}$)

I_{eq} = local, equilibrium I- concentration (cm^{-3})

The differential equation for the Xe concentration is :

$$\frac{dX}{dt} = - \lambda_x \cdot X - \sigma_x \cdot \phi_2 \cdot X + \lambda_I \cdot I + \gamma_x \cdot F \qquad (A.3)$$

and

$$X_{eq} = \frac{(\gamma_x + \gamma_I) \cdot F}{\lambda_x + \sigma_x \phi_2} \qquad (A.4)$$

where

X = local Xe concentrations (cm^{-3})

λ_x = decay constant for Xe (sec^{-1})

σ_x = effective, local microscopic absorption cross-section for Xe (cm^2)

ϕ_2 = local average thermal flux ($cm^{-2} \cdot sec^{-1}$)

X_{eq} = local, equilibrium Xe concentration (cm^{-3})

The fission rate is obtained from the local power density

$$F = \frac{1}{E_f} \cdot P \tag{A.5}$$

where

P = local power density ($w \cdot cm^{-3}$)

E_f = energy release per fission (wsec)

Equations A.1 and A.3 are integrated analytically through a time step Δt, assuming constant fission rate (F), thermal flux (ϕ_2) and Xe cross-section (σ_x) through the time step :

$$I(t+\Delta t) = \left[I(t) - \frac{\gamma_I}{\lambda_I} \cdot F \right] e^{-\lambda_I \cdot \Delta t} + \frac{\gamma_I}{\lambda_I} \cdot F \tag{A.6}$$

$$X(t+\Delta t) = \left[X(t) - R_1 - R_2 \right] e^{-(\lambda_x + \sigma_x \phi_2)\Delta t} + R_1 \cdot e^{-\lambda_I \Delta t} + R_2 \tag{A.7}$$

where

$$R_1 = \frac{\lambda_I \cdot I(t) - {}_I \cdot F}{\lambda_x - \lambda_I + \sigma_x \phi_2} \tag{A.8}$$

$$R_2 = \frac{\gamma_x + \gamma_I}{\lambda_x + \sigma_x \phi_2} \cdot F \tag{A.9}$$

A2. EQUATIONS FOR INTEGRATION OF THE Pr - Sm CHAIN

The Pr-149 → Sm-149 chain is integrated through each time step under the assumption of constant power and thermal flux through the step :

$$Pr^{n+1} = \left[Pr^{n} - \frac{\gamma_{Pr}}{\lambda_{Pr}} \cdot \frac{P}{E_f} \right] e^{-\lambda_{Pr} \cdot \Delta t^{n}} + \frac{\gamma_{Pr}}{\lambda_{Pr}} \cdot \frac{P}{E_f} \qquad \text{(A-10)}$$

$$Sm^{n+1} = \left[Sm^{n} - R_1 - R_2 \right] e^{-(\sigma_{Sm}\phi_2)\Delta t^{n}} + R_1 \, e^{-\lambda_{Pr}\Delta t^{n}} + R_2 \, , \qquad \text{(A-11)}$$

$$R_1 = \frac{\lambda_{Pr} \cdot Pr^{n} - \gamma_{Pr}\left(\frac{P}{E_f}\right)}{\sigma_{Sm} \cdot \phi_2 - \lambda_{Pr}} \qquad \text{(A-12)}$$

$$R_2 = \frac{\gamma_{Pr}}{\sigma_{Sm} \cdot \phi_2} \cdot \frac{P}{E_f} \qquad \text{(A-13)}$$

where

Pr^{n} = Average concentration per fuel type of Pr-149 at the beginning of time step n

Sm^{n} = Corresponding for Sm-149

γ_{Pr} = Fission yield of Pr-149

λ_{Pr} = Decay constant of Pr-149

σ_{Sm} = Effective thermal group microscopic absorption cross-section for Sm-149

E_f = Energy release per fission

P = Average power density for fuel type

ϕ_2 = Average thermal flux per fuel type

The equilibrium concentration of Sm-149 ($\Delta t \to \infty$) is :

$$Sm^{equi} = R_2 \qquad \text{(A-14)}$$

If power is zero through the time step Δt^n, the following relations are used :

$$Sm^{n+1} = Sm^n + Pr^n\left(1 - e^{-\lambda_{Pr}\cdot\Delta t^n}\right) \qquad \text{(A-15)}$$

$$Sm^{equi} = Sm^n + Pr^n \qquad \text{(A-16)}$$

The influence of the Sm-149 concentration on the nodal cross-sections is described in §4.4.

A3. EQUATIONS FOR INTEGRATION OF γ-SCAN ISOTOPES

The γ-scan isotopes are integrated as follows :

$$N^{n+1} = \frac{Y(E)}{\lambda} P^n + \left[N^n - \frac{Y(E)}{\lambda} \cdot P^n \right] e^{-\lambda \Delta t_n} \qquad \text{(A-17)}$$

where

$$P^n = \frac{Q^n}{Q^r} \cdot P^{rel} \qquad \text{(A-18)}$$

N^{n+1} = Isotope concentration (arbitrary units) at end of time step n

N^n = Isotope concentration at beginning of time step n

Q^n = Reactor thermal power (w) through time step n

Q^r = Reactor thermal power - rated condition

P^{rel} = Nodal relative power

$Y(E)$ = Effective fission yield at the nodal burnup E, calculated from polynomial expansions of tabular data

λ = Decay constant of isotope considered (day^{-1})

Δt_n = Length of time step n, (days)